Role of Prickle1 in Ciliogenesis and Localization of Sonic Hedgehog Components

by

Nadine Robert

Bachelor in Dentistry, State University of Haiti, 2012

Submitted to the Graduate Faculty of the

School of Dental Medicine in partial fulfillment

of the requirements for the degree of

Master of Science

University of Pittsburgh

2020

UNIVERSITY OF PITTSBURGH

SCHOOL OF DENTAL MEDICINE

This thesis was presented

by

Nadine Robert

It was defended on

July 31, 2020

and approved by

Heather Szabo-Rogers, PhD, Oral Biology Department

Dobrawa Napierala, PhD, Oral Biology Department

Elia Beniash, PhD, Oral Biology Department

Thesis Advisor: Heather Szabo-Rogers, PhD, Department Affiliation

Role of Prickle1 in Ciliogenesis and Localization of Sonic Hedgehog Components

Nadine Robert, MA

University of Pittsburgh, 2020

Robinow Syndrome (RS) is a rare genetic disorder characterized by dwarfism, craniofacial dysmorphology, vertebral and gonadal dystrophy. RS is caused by mutations in members of the Wnt/Planar Cell Polarity pathway. In addition, patients with RS have phenotypic features of ciliopathies. To model RS, we have chosen *Prickle1*$^{Bj/Bj}$ mice. The *Prickle1*$^{Bj/Bj}$ develop wider faces and shorter limbs similar to many mouse models of RS and ciliopathies. During facial development, I observed swollen primary cilia and increased Hedgehog (HH) signaling. Importantly, I localized Prickle1 protein in the nucleus and cilia of cells in the *Prickle1*$^{+/+}$ and *Prickle1*$^{Bj/Bj}$ embryonic faces. The primary cilium is a microtubule-based organelle that perceives and executes mechanical and chemical signaling transduction for the HH pathway. Mediating the normal activity of HH requires an intact ciliary axoneme and appropriate localization of HH components by intraflagellar transport (IFT) in the cilium. In *Prickle1*$^{Bj/Bj}$ mutants, I observed widening of the ciliary pockets with Transmission Electron Microscopy. Immunofluorescence staining revealed defective anterograde (IFT-88, IFT-52) and retrograde (IFT-122, IFT-140) intraflagellar trafficking in addition to the mislocalization of a ciliary membrane component (ARL13B) in the *Prickle1*$^{Bj/Bj}$ face compared to controls. I observed increased staining of SMO and Gli2, in the *Prickle1*$^{Bj/Bj}$ nucleus and ciliary axoneme. In agreement with these results, I observed defective Gli processing by Western Blot in the *Prickle1*$^{Bj/Bj}$ face and limbs. We attempted to rescue the *Prickle1*$^{Bj/Bj}$ phenotype by dampening HH signaling with Vismodegib, an FDA-approved HH antagonist, and observed tissue specific responses in the skeleton, and ciliary morphology. We

directly tested if HH signaling is contributing to the etiology of RS using primary RS fibroblast cells. In RS fibroblasts Prickle1 and SMO proteins are localized to the ciliary axoneme. We modulated HH signaling in the RS-fibroblasts using Vismodegib, and purmorphamine (agonist) which resulted in shortened cilia enriched in SMO. I observed reduced Gli processing in response to SHH treatment in the RS fibroblasts. In conclusion, my data suggests that the *Prickle1*$^{Bj/Bj}$ facial phenotype arises from increased HH signaling resulting from defective intraflagellar transport, and defective Gli processing and this mechanism contributes to the etiology of RS.

Table of Contents

List of Tables

List of Figures

Acknowledgements

When I was applying to my Fulbright Scholarship, one of the required steps was to contact a mentor to secure a position in the program. I started an incredible journey when I contacted Dr. Mooney who recommended Dr. Heather Szabo-Rogers as he was going to retire. With Luis Guillermo Vanfossen Bravo, Dr. Mooney worked with Fulbright Laspau to offer me the admission. Since my first interview with Dr Szabo-Rogers, I knew that she would be a great mentor to guide me through the start of my research career. During the two years that I have spent working with her, she patiently taught me all the research skills that I needed and helped me develop the critical thinking necessary to work in biological research. I want to thank her for this continued support, guidance, and mentorship throughout my masters training that made me stronger and more confident when I still doubted myself. This thesis would not have been possible without her encouragement, advice, and motivation. Whenever needed, I knew I could always count on her support.

I want also to thank Dr. Elia Beniash and Dr. Dobrawa Napierala for responding positively to be part of my Thesis Committee. Thank you for the constructive and valuable feedback, and all technical support that contributed to improve my work and achieve this research project. Thank you for your time. I am grateful that you were always open to talk about any concern particularly when I struggled with my experiments. I am also grateful to Roy (Yong) Wan, who taught me patiently the research techniques and prepared me to work independently before moving to another research position. Thank you to Hajime Yamazaki for helping with the TEM procedures. Thank you for the time spending preparing the samples, sectioning, and imaging. Thank you to Casey

White who contributed in data analysis. Without their collaboration, I would not be able to accomplish this research project.

I would like to thank my Center for Latin American Studies (CLAS) advisor, Luis Guillermo Vanfossen Bravo, who supported me a lot during these two years. Thank you to Dr. Martha Terry who is an inspiring professor at the School of Public Health and CLAS. Thank you to all staff from the Oral Biology Department: Michele, Deb, and Elaine who work hard to help us with any request. Thank you to the CLAS staff, particularly Luz. I always felt welcomed and home whenever I visited her.

I would like to thank all the Oral Biology students, specially Parul Ahuja and Nadeen Meshry for their friendship and valuable feedback. My experience in Pittsburgh would not have been great without some friends that were always present and support me throughout these two years. Thank you to my best friend Anne Caroline Silva Barbosa who met me since the first day I arrived in Pittsburgh. I appreciate her friendship, her empathy, and all the Brazilian friends that she shared with me. Thank you to Dr. Berthony Deslouches and his wife Sandra who supported me since my academic advisor introduced me to them. Thank you to Vania, Moise, Tshianda, Kayowa, my Haitian friends who welcomed me, looked over me, and helped me throughout these two years. I am grateful to Jacob, Felicia, Rafael, and Saw Tha who built a true friendship at the residence and provided me company and more.

I would certainly not be able to come here without the incredible work of Dean Samuel Prophete, Dr. Christina Hyppolite, Dr. Lesly Joseph, and Dr. Benedict Larose who coached me during my Fulbright scholarship application. Thank you to Romuald Zamy, Megan Goold, and Derek V. Tavares from Fulbright Haiti and Fulbright LASPAU. Thank you to my family, particularly my grandmother Viergina Pierre-Saint Lamothe, my mom Helene Lamothe, my

godmother Emilienne, my adoptive fathers Father Godefroy Midy, and Father Miller Lamothe, who provided me education, inspiration, and means to achieve all my plans and dreams. Thank you to my sisters Carine and Elizabeth Robert, my cousins Lisa, Katia, Ruth-Sheena, Jonathan, Anaelle, Assael, Jovaneka, Reephaella, and Gina. To my aunts Rose, Nelas, Virgina, Nancy, and uncle Vincent. To my friends from high school Lavictoire, Belinda, Maudeline, Sofia, Cassandra, Ariel, Eunice, Jeanicie, Marie-Mica, Wendy, Rolanda. To my colleagues Mickerline, Ruthza, Serge, Fedeline, Geralda, Jakim. Thank you to Father Paul-Fils, Father Germain, and Andreciane. Special thanks to the unconditional support from Brother Augustin Nelson and Lovely Reina Feuillé who were always present for me from Haiti.

Thank you to Fulbright that made my dream of seeking higher education possible and for providing me many friends from different countries. Thank you to the Fulbright friends from Haiti: Danta, Bens, Ricard, Marc-Ansy; from Dominican Republic: Luis; Indonesia: Satria; and Colombia: Natalia and Grace. I enjoyed all the moments shared with them. Above all I want to express my gratitute to God, Who provided me health, strength, and skills to work toward my dream.

1.0 Introduction 1

1.1 The Prickle1 mouse model

The *Prickle1*^{Beetlejuice} (*Prickle1*^{Bj}) is a mouse line with a missense homozygous mutation in the LIM1 domain of Prickle1 at c.G482T:p.C161F (Gibbs et al., 2016) (Figure 1). This mouse line was recovered from ethylnitrosourea-induced mutational screen of C57BL/6J mice to generate a model to study human congenital heart disease (Gibbs et al., 2016). The homozygous *Prickle1*$^{Bj/Bj}$ mutants' fetuses survive to term but die neonatally as they present outflow tract misalignment due to valvular morphogenesis deficiencies, and ventricular septum defect (Gibbs et al., 2016). Besides the cardiac defects, the *Prickle1*$^{Bj/Bj}$ mutants exhibit a specific phenotype with skeletal defects resulting in shorter stature, limbs, and tail (Gibbs et al., 2016). They also develop some craniofacial abnormalities which include a small head, snout and mandible, and cochlear defects (Wan et al., 2018). Wan et al. (2018) performed further analysis to describe the *Prickle1*$^{Bj/Bj}$ mutants microcephalic skull (Figure 2). Compared to wild-type littermates, the mutants have a length reduction in the proximal-distal axis of the skull while an increase in the medial-lateral axis. The craniofacial structures affected are mostly those derived from the neural crest cells rather than those from the mesoderm. The skull structures in the *Beetlejuice* mutants have a normal morphology but they present a reduction in the medial-proximal direction. They also observed enlarged fontanelles, a decrease contribution of the nasal septum in the skull length, and the frontal bone length is reduced. In addition, all the *Prickle1*$^{Bj/Bj}$ late stage fetuses developed a midfacial cleft lip, and 52% of them developed cleft palate located between the palatine processes of the maxillary bones (Wan et al., 2018). Cell proliferation and cell death in the frontal bone of the

mutants were unaffected; however, decreased Hedgehog and Wnt/β-catenin signaling were observed in the frontal bones. In the *Prickle1*$^{Bj/Bj}$ mutant , the expression of *Wnt5a* mRNA in the developing heart was reduced, and the embryos were unable to establish cell polarity mediating cell migration, which suggest a planar cell polarity (PCP) defect (Gibbs et al., 2016). Whole mount *in situ* hybridization showed an increased expression of *Patched1* (*Ptc1)* mRNA in the medial nasal prominences and cranial base of embryos at developmental stage E 10.5 (Wan et al., unpublished data) (Figure 2, E-F). Hedgehog signaling is increased in the presphenoid synchondrosis through *in situ* hybridization for *Ptc1* and *Gli1*, two key components of the Hedgehog signaling pathway (Wan et al., unpublished data). These observations of the *Prickle1*$^{Bj/Bj}$ mutants phenotypes suggest that Prickle1 protein functions during all stages of embryonic development (Wan et al., 2018). They are also consistent with the phenotypic findings in other mice models exhibiting a *Prickle1* mutation (Gibbs et al., 2016; Liu et al., 2013).

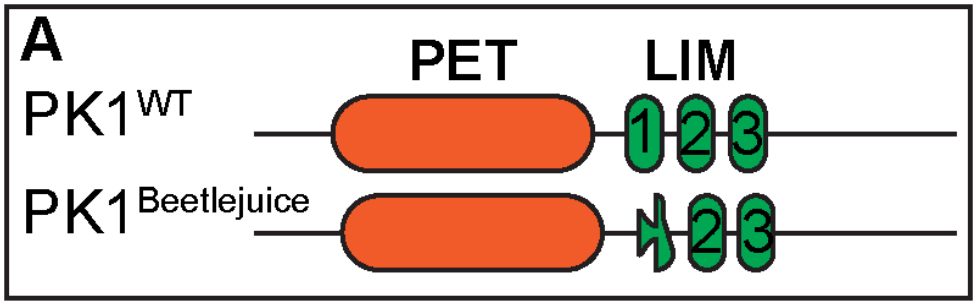

Figure 1: Prickle1 protein structure.

Prickle1 wildtype protein contains a PET, 3 LIM domains. Prickle1^{Beetlejuice} is c: G482T, p:Cys161Phe which only disrupts the LIM1 domain and leaves the transcriptional and translational control of the wildtype Prickle1 locus. PK1, Prickle1; PET, Prickle, Espinas and Testin domain; LIM, Lin 11, Isl-1 and Mec-3 domains

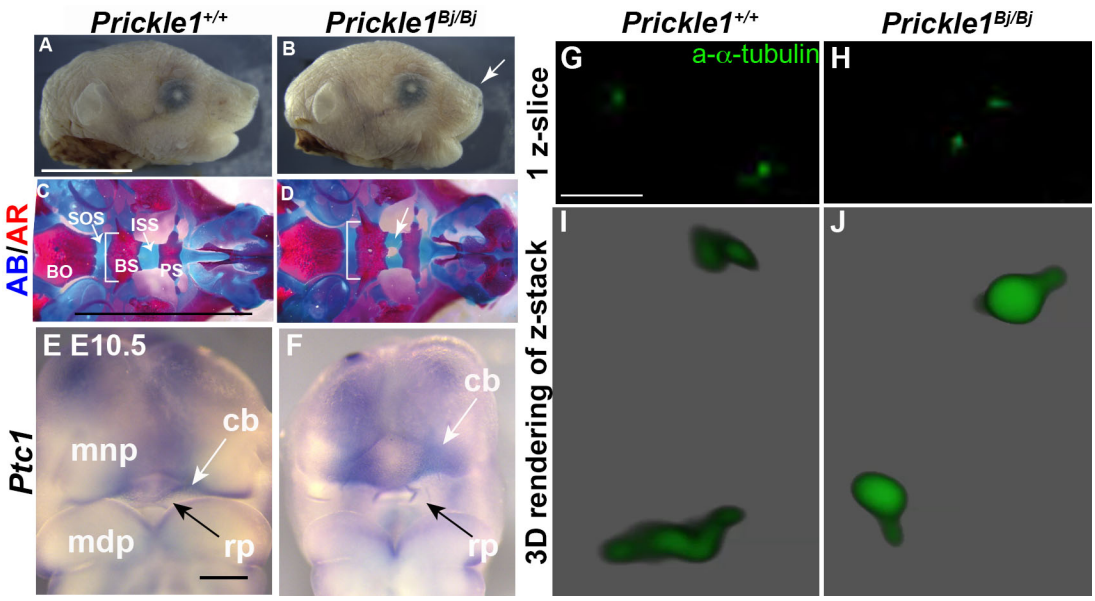

Figure 2: Skull morphology, expression of Patched1, and ciliary phenotype of Prickle1 Beetlejuice litter. At P0, the Prickle1$^{BJ/Bj}$ mutants are microcephalic with shorter snout and frontal bossing (A-B);. Alcian Blue and Alizarin Red whole-mount stained skull base showing length reduction in the proximal-distal axis whereas the medial-lateral axis of the cranial base remained wider compared to control littermate (C-D). The expression of Patched1 increased in the medial nasal prominences and the cranial base of the mutants (E-F). E11.5 craniofacial mesenchymal cells stained with the ciliary axenome labelled with acetylated α-tubulin and imaged using STED microscopy of demonstrating swollen cilia in the mutants (G-J). AB/AR, alcian blue/ alizarin red; BO, basioccipital; BS, basisphenoid; cb, cranial base; ISS, intersphenoid synchondrosis; mdp, mandibular prominence; mnp, medial nasal prominence; PS, presphenoid; rp, Rathke'SOS, spheno occipital synchondroses; Scale bar A = 5 mm, applies to B; C =5 mm, applies to D; E=1 mm applies to F; G=3 μm applies to G-J.

1.1.1 Prickle1 homology, and protein structure

The *Prickle1* is a highly conserved gene across different species that transcripts the Prickle1 or Prickle planar cell polarity 1 or Prickle homolog 1 protein. In Drosophila, there is one *Prickle1* gene in chromosome15 that encodes three isoforms: *Prickle^{Prickle}, (Prickle^{PK}), Prickle$^{Spiny\text{-}legs}$ (Prickle^{Spl})* and *PrickleM (PK^{M})* (Gubb et al., 1999). While the *PK^{M}* transcripts seems to not

have any role during adult age, *Prickle*^{PK} and *Prickle*^{Spl} isoforms need to be balanced to control planar polarity in the Drosophila hair cells and wings (Ayukawa et al., 2014; Gubb et al., 1999). Four Prickle proteins had been identified in mammals (Liu et al., 2013). In mouse, the *Prickle1-like* gene is localized in chromosome 15 and encodes *Prickle1 (mPk1)*, and the gene for *Prickle2 (mPk2)* protein homologs on chromosome 6 (Katoh and Katoh, 2003; Tao et al., 2009). In humans, the *PRICKLE1* gene is situated at the longer arm of chromosome 12 at position 12p11- q12 (Katoh and Katoh, 2003). *PRICKLE2* is a pseudogene found in chromosome 3 at position 3p14, has 51.9% total amino-acid identity with human *PRICKLE1* gene (Katoh & Katoh, 2003).

The Prickle1 protein has several conserved domains across species. It contains a N terminal, one PET (Prickle, Espinas and Testin) domain, and three LIM (Lin 11, Isl-1 and Mec-3) domains, a C-terminal Prickle homologous (PKH) domain with a CAAX prenylation motif (Figure 1)(Lin and Gubb, 2009). *PK1* protein shares similarities with other proteins like *Testin* and *LIM domain only 6 (LMO6)* in the LIM and the PET domains while the C-terminal region remains unique to proteins of the *PRICKLE* family (Katoh and Katoh, 2003).

Each LIM domain consists of approximately 55 amino acids each, eight of them are highly conserved and are mostly cysteines and histidines positioned at specific intervals (Kadrmas and Beckerle, 2004). The cysteines and histidines within the LIM domain form a double zinc-finger domain organized from 4 β-hairpins orthogonally disposed and two α-helix strands (Kadrmas and Beckerle, 2004). Although absent in prokaryotes, LIM domains have been identified in the cytoplasm or nuclear membrane of many eukaryotic organisms. LIM domains are responsible for facilitating protein dimerization by providing a stable structural framework that allows a wide variety of protein interactions (Feuerstein et al., 1994). LIM-containing proteins may function in

different biological processes to control many aspects related to the cytoskeleton or by controlling gene expression (Kadrmas and Beckerle, 2004).

The PET domain is monomeric with a nonglobular conformation; the PET domain may play a role in Prickle membrane targeting for protein binding (Bassuk et al., 2008; Gubb et al., 1999; Sweede et al., 2008). Sweede et al. (2008) also reported that *PK* LIM domains may protect the PET domain by guiding, in the presence of zinc, a folded and stable region that decreases trypsin access and thus, limiting the degradation of this disordered region. The PET and LIM domain of PK are necessary and sufficient for Dishevelled recognition and participation into a cascade of signaling pathway among other functions.

1.1.2 Prickle1 reported function during embryonic development

1.1.2.1 Prickle1 and brain development:

During human embryonic development, Prickle1 is reported to be necessary for proper brain development where it controls neuronal cells movement aided from its interaction with *RE1-SILENCING TRANSCRIPTION FACTOR (REST)* (Bassuk et al., 2008). *Prickle1* expression is found in mouse forming brain before gastrulation and through all stages of development (Liu et al., 2013; Tissir and Goffinet, 2006). They have also suggested that Prickle1 is required for maturation of the central nervous system particularly for axonal and dendritic configuration. mprickle1 and mprickle2 may play important roles in positive regulation of neurite extension during embryonic brain development (Okuda et al., 2007). They had also revealed that mPrickle1 expression was higher and is important for the proper growth of the cerebral cortex and the hippocampus. The role of Prickle1 in the brain goes beyond embryonic development as the protein

has been reported to be a positive regulator of oligodendrocytes differentiation and maturation during central nervous system injury specifically during demyelinating disease (Zilkha-Falb et al., 2017). In zebrafish, Prickle1 paralogs Prickle1b and Prickle1a are required for NCCs migration in ventrolateral direction, and regulation of changes in the level of E-cadherin and N-cadherin to prepare for regulatory cells migration (Ahsan et al., 2019).

1.1.2.2 Prickle1 and craniofacial development:

Mice models with mutation in *Prickle1* present defects in palatogenesis and develop cleft lip and/or cleft palate (Figure 2) (Gibbs et al., 2016; Liu et al., 2014; Yang et al., 2014). In human, *Prickle1* contribute to palatal development by controlling cells migration independently to Vangl2 function (Yang et al., 2014). Yang et al. (2014) reported two rare coding variants and some more common noncoding *PRICKLE1* SNPs in the human genome in familial cleft palate. *Prickle1* also functions in ocular and eyelid development and mediates the PCP pathway (Guo et al., 2019). Loss of *Prickle1* altered cell polarity, expression of β-catenin, and phosphorylated c-Jun leading to delayed embryonic eyelid closure (Guo et al., 2019). In addition, *mPrickle1* is responsible for cochlea development (Gibbs et al., 2016).

1.1.2.3 Prickle1 and skeleton:

Prickle1 is also involved in skeletal growth where it is important for modulating chondrocytes resting and proliferative zones in endochondral derived bones (Wan et al., 2018); (Wan et al., unpublished). Moreover, Prickle1 influences limb development through controlled apoptosis, changes in Wnt5a and BMP4 expressions, an action that has been attributing to its role in the non-canonical Wnt/ PCP pathway (Yang et al., 2013).

1.1.3 Wnt signaling and Prickle1

1.1.3.1 Introduction to Wnt Signaling:

Wnt signaling is named for the Wingless and Int-1 locus that was identified in development and carcinogenesis originally. Wnt signaling consists of 3 interdependent but highly conserved signaling pathways: Wnt/PCP (Wingless-Integrated*)*/Planar Cell Polarity), Wnt/ β-catenin (Wnt/β-cat) and Wnt/Calcium (Wnt/Ca^{2+}) signaling pathway. In general, the Wnt/PCP pathway functions to ensure that individual cells are able to understand neighbor relationships and manage shape changes that contribute to morphogenesis. Wnt/PCP signaling requires the function of seven core components of the pathway: *Prickle, Dishevelled, Vangl2*, *Diego, Flamingo, and Frizzled*, and does not require β-catenin function. The Wnt/ β-cat pathway is known as the canonical Wnt pathway and is critical for cell proliferation, cell fate decisions and tumorogenesis, it requires β-catenin for its function. The Wnt/Ca^{2+} signaling controls calcium release from the endoplasmic reticulum.

The Wnt pathways were uncovered first from genetic studies in *Drosophila melanogaster* wing, eye, abdomen, and notum, and later in vertebrates (Mlodzik, 2002; Simons and Mlodzik, 2008). Wnt ligands are secreted glycoproteins and are responsible for numerous cellular processes determining cell fate, motility, apical-basolateral polarity, primary axis formation, organogenesis, and stem cell renewal (reviewed in (Komiya and Habas, 2008)). The extracellular Wnt ligands stimulate intracellular signaling transduction via different pathways which are the canonical Wnt, the non-canonical Wnt that further divides into the PCP pathway and the Wnt/Ca^{2+} pathway.

1.1.3.2 Wnt/PCP signaling

From the numerous identified Wnt ligands, only Wnt4, Wnt5a and Wnt11 are known to participate in the non-canonical Wnt/PCP pathway, although they can also act in the Wnt/β-catenin pathway (Simons and Mlodzik, 2008). The PCP pathway is important for organizing cell orientation within layer, remodeling the cytoskeleton, and coordinating convergent extension during gastrulation and neurulation (Simons and Mlodzik, 2008). The PCP pathway acts via a core component consisting of six proteins, including Frizzled (Patton and Afzal) homolog of human FZD1- FZD10; Disheveled (Dsh in *Drosophila*, Dvl in mammals, or DVL1-DVL3 in human), Van Gogh-like / Strabismus (Vangl / Stbm, VANGL1/2 homologs in human), Prickle (Pk^{sple} / PK1 in human), Diego (Dgo; Diversin and Inversin in vertebrates), and Flamingo/starry night (fmi/stan; CELSR1-CELSR3 genes in human) (Mlodzik, 2002). Some of the proteins are transmembrane receptors, while others are cytoplasmic. As described in Drosophila, the PCP pathway genes are divided into three groups (Wong and Adler, 1993). The first group may play a role in tissue polarity and comprises Dsh, Fz, and Pk (Shulman et al., 1998). The second group, known as PCP effectors, is composed of *Inturned* (*Int*) and *Fuzzy* (fuz) (orthologues *Fuz* in mouse and *Xenopus*) (Gubb et al., 1999). Inturned and Fuzzy are tri-login domain proteins forming a Rab23 guanine nucleotide (GEF) complex (Gerondopoulos et al., 2019), and a Rab similar GTPase 1 (RSG1) complex (Gray et al., 2009) in ciliogenesis and during vertebrates embryonic development (Zeng et al., 2010). Null mutant mice for *Int* or *Fuz* exhibit multiple defects including failure of closure of the spinal cord, exencephaly, widened limb buds, severe polydactyly, and craniofacial malformations (Gray et al., 2009; Zeng et al., 2010). A third group of PCP genes identified in the Drosophila contain the family of *multiple wing hairs (mwh)*. *mwh* are downstream PCP genes that antagonize the actin cytoskeleton in *Drosophila* wings (Lu et al., 2015). Fuz, Intu, and mwh transduce polarity signals

directed by PCP type1 genes in *D. melanogaster* (Vinson et al., 1989). Therefore, combined effect of Int with Dvl can be localized at the apical cell surface in multi-ciliated epithelial cells (Park et al., 2008).

In the Wnt/PCP pathway, one of four Fz co-receptors NRH1, PTK, ROR2, and Ryk may activate Dvl (Komiya and Habas, 2008). Activated Dvl transduce the signal to three branches which will converge to induce actin polymerization and guide convergent extension during gastrulation via the DEP and PDZ domains of Dvl. Dvl recruits small GTPases of the RHO subfamily (Rho, Rac, and cdc42), the Rho-associated kinase (Arensdorf et al.), Profilin, and the JNK-type mitogen-activated protein kinase (MAPK) (Komiya and Habas, 2008; Yang and Mlodzik, 2015). Rho Activation requires Dvl interaction with Daam1 (Dishevelled associated activator of morphogenesis 1) to mediate ROCK (Yang and Mlodzik, 2015). Also, Rac and Profilin can produce the actin network without heterodimerization with Daam1.

1.1.3.3 Planar Cell Polarity

Mediated by the actin network, the PCP pathway establishes the polarity by orienting the cells according to their tissue localization. For instance, in *Drosophila*, the cells orient themselves in a medial-proximal orientation in the wing; in the thorax, an anterior-posterior orientation, and in the eyes, in an anterior-posterior and dorsal-ventral axis (Mlodzik, 2002). Before the establishment of the PCP pathway the PCP genes pk, stbm, fmi, and dgo are localized apically at the membrane in drosophila's R3 and R4 photoreceptors (Jenny et al., 2005). Upon recruitment, the PCP genes asymmetrically divide themselves into two groups to establish the polarity of the cells. Therefore, Fz, dvl, and dgo act as positive regulators while pk and vangl2 function as negative regulators of the PCP (Jenny et al., 2005).

1.1.3.4 PCP and Cilium/ primary cilium

The Wnt/PCP pathway regulates actin cytoskeleton assembly at the apical surface of ciliated cells, guides basal bodies migration, ciliogenesis, and ciliary secretion of vesicles called ectosomes (Reynolds et al., 2019). Disruption of actin cytoskeleton impaired ciliary formation (Park et al., 2008). The Wnt/PCP pathway controls the position of the basal bodies; therefore, it regulates the position and the formation of the cilium in a cell (Goetz and Anderson, 2010). The PCP pathway effector proteins *Inturned (Int)* and *Fuzzy (Fuz)* are associated with Rab23 and are essential for the docking of the ciliary vesicle to mother centriole prior to the elongation of the axoneme and the ciliary membrane (Gerondopoulos et al., 2019). Ciliary vesicle docking is also dependent of Dvl and Rho's actions to polarizing the basal bodies after establishing cellular planar polarity (Park et al., 2008). *Int* is an essential regulator of ciliary formation (Zeng et al., 2010). Besides controlling ciliogenesis, *Fuz* controls protein trafficking to enable ciliary elongation and membrane biogenesis (Zeng et al., 2010). The PCP components *Inversin/Diego* and *Vangl2* are found cellularly localized near the base of the primary cilia during embryonic development (Simons et al., 2005). In addition, Prickle1 may regulate primary and motile cilia's morphogenesis and function (Gibbs et al., 2016). In zebrafish, Cao et al. (2010) suggested a genetic interaction between Prickle1 and IFT-88 (a core component of the intraflagellar transport necessary for ciliary assembly), and two other IFT particles (IFT-57 and IFT-172). The ciliary pocket might guide the position of the cilium in the cell because of a stable and dynamic actin filament (Ghossoub et al., 2011; Molla-Herman et al., 2010). Thus, proper PCP establishment is important for a functional cilium that can transduce ciliary-mediated signalling pathways.

1.2 Primary cilia

1.2.1 Primary cilia structure

The cilia or primary cilia is a finger-like protrusion on eukaryotic cells during the G0 phase of the cell cycle (Figure 3). Cilia are composed of 9 pairs of microtubules that provide the skeleton of the cylinder that extends from the cell. A specialized plasma membrane surrounds the microtubules that interact with the extracellular environment. Ciliary length varies from 2 to 10 μm; it can reach up to 200 μm in specialized organs such as olfactory neurons (Nachury and Mick, 2019). On the cell surface, the primary cilium acts as a sensory organelle to perceive extracellular signals and execute signaling transduction (Qin et al., 2011). In respiratory, fallopian tube, and epididymis epithelia ciliary motility is essential to move extracellular fluid and facilitate mucus clearance (Fliegauf et al., 2007). In the kidneys and the brain, motile cilia act as mechanical sensors to generate flow induction stimulating clearance (Michaud and Yoder, 2006).

All cilia are not created equal. Neural crest cells have a single primary cilium with a basal body, however, in some specialized epithelia, cells can be multi-ciliated that lack the basal bodies (cited in (Jensen et al., 2004)). In addition to multiciliated cells, cells in organs that secrete mucous often have motile cilia. An additional central microtubules pair distinguishes motile cilia from primary cilia (Qin et al., 2011). The organization of microtubules in motile cilia is designated 9+2, and primary cilia is 9+0. Four types of cilia have been identified in human cells: the motile cilia in respiratory or ependymal epithelia (9+2), nodal cilia (9+0); and the solitary non-motile primary cilia in most cells (9+0), or hair cell kinocilia (9+2) (Fliegauf et al., 2007).

The primary cilium is composed of three main parts: an axoneme, a transition zone, and a basal body. The axoneme or the skeleton of the ciliary shaft is composed of nine microtubules

pairs extending from the basal body (Figure 3) (Reiter and Leroux, 2017). Ciliary microtubules are long hollow polymers assembled from heterodimers of α- and β-tubulin of approximately 25 nm in width, and ranging from less than 1 μm to 100 μm or more in length (Goodson and Jonasson, 2018). They are post-translationally modified (acetylation, palmitoylation, tyrosination/ detyrosination, glutamylation, and glycylation) to form stable structures and regulate ciliary motility (Goodson and Jonasson, 2018; Keeling et al., 2016). Microtubules are found in all eukaryotes where they participate in the organization of the cytoskeleton, they attract molecular motors and transport vesicles in the cells (Mohan and John, 2015). The microtubules participate in many cellular functions in concert with the actin filaments mediated by the microtubule-associated proteins (Mohan and John, 2015). The cilium controls the axoneme length through a balance between ciliary assembly and disassembly mediated by particles transport within the cilium and the cell (Keeling et al., 2016). Axoneme elongation coupled with ciliary membrane biogenesis (Wang and Dynlacht, 2018).

Assembly and disassembly of the primary cilia depends on how cell types respond to diverse cues during embryonic development and under specific physiological conditions (Wang and Dynlacht, 2018). The mitotic kinase Aurora A stimulates ciliary disassembly in two signaling waves: in G1 after mitogenic stimulation of non-dividing cells and before mitosis (Wang and Dynlacht, 2018). Thus, the cilium negatively regulates the cell cycle by coordinated disassembly to prepare the cell for mitosis (Keeling et al., 2016). After cytokinesis, the primary cilium assembles using the mother centriole as basal body (Figure 3).

While protruding in the extra-cellular environment, the cilia grow with a continuous plasma membrane to the cell surface. Although, the ciliary membrane is specialized, and its lipid composition differs from that of the cell by containing higher level of phosphatidylinositol-4

phosphate, cholesterols, and sphingolipids (Nachury and Mick, 2019; Reynolds et al., 2019). These ciliary membrane lipids from filipin-sterol complexes and may be more ordered than those of the plasma membrane (Reynolds et al., 2019; Rohatgi et al., 2007). The primary cilium is unable to synthesize proteins, therefore, controlled delivery of soluble proteins for the ciliary membrane and axoneme originates from an adjacent Golgi apparatus that supplies a ciliary vesicle for transport to the cilia (Goetz and Anderson, 2010; Rohatgi and Snell, 2010). The PCP genes (*Fuz, Int*), described earlier, contribute to, and maintain the equilibrium between ciliary formation, maintenance, and membrane secretion through transport of vesicles filled with ciliary components (Kumar et al., 2019). Transmission electron microscopy (TEM) revealed ciliary membrane secretions which can be non-membrane or membrane bound particles anchoring specific receptors allowing the cilium to sense the extracellular milieu (Jensen et al., 2003). Shedding of vesicles at the cilium tip or ciliary ectosomes could help the cilium eliminates excess material and maintain the length of this structure (Nachury and Mick, 2019; Satir, 2017).

The transition zone contains transitional fibers or alar sheets that emanate from the mature basal body microtubules triplets before ciliogenesis and attach to the plasma membrane ((Jensen et al., 2004; Rohatgi and Snell, 2010). The transition zone forms a necklace where the cilium and the cell surface meet, and it positions in a remnant structure of the ciliary vesicle called the ciliary pocket (Rohatgi and Snell, 2010). The transition zone selectively controls signal intensity and protein trafficking by forming a highly selective barrier that prevents free mixing of plasma membrane and ciliary proteins (Rohatgi and Snell, 2010).

Adjacent to the transition zone, the ciliary pocket (CP) resembles a docking site domain for IFT positive vesicles (Benmerah, 2013). The CP remains a vestige of the ciliary vesicle that attaches the cilium to the cellular body (Benmerah, 2014). This periciliary structure varies in shape

and length depending on the cell type (Ghossoub et al., 2011). Nonetheless, mutations in the actin network modify the ciliary pocket width causing a lack of communication between the ciliary membrane and the cell membrane (Molla-Herman et al., 2010). Clathrin-coated pits and actin filaments surrounding the proximal part of the cilium suggest that the CP that could function as mechanical stress transducer, or to position the cilia (Molla-Herman et al., 2010). Thus, the CP possibly controls cilium-associated vesicular trafficking through its functionally distinct membrane domain (Ghossoub et al., 2011; Molla-Herman et al., 2010). In trypanosomatids flagellum ciliogenesis model, the CP seems to monitor endocytosis and exocytosis, which are two processes used by the cilium to internalize cargoes or to remove excessive materials (Benmerah, 2013).

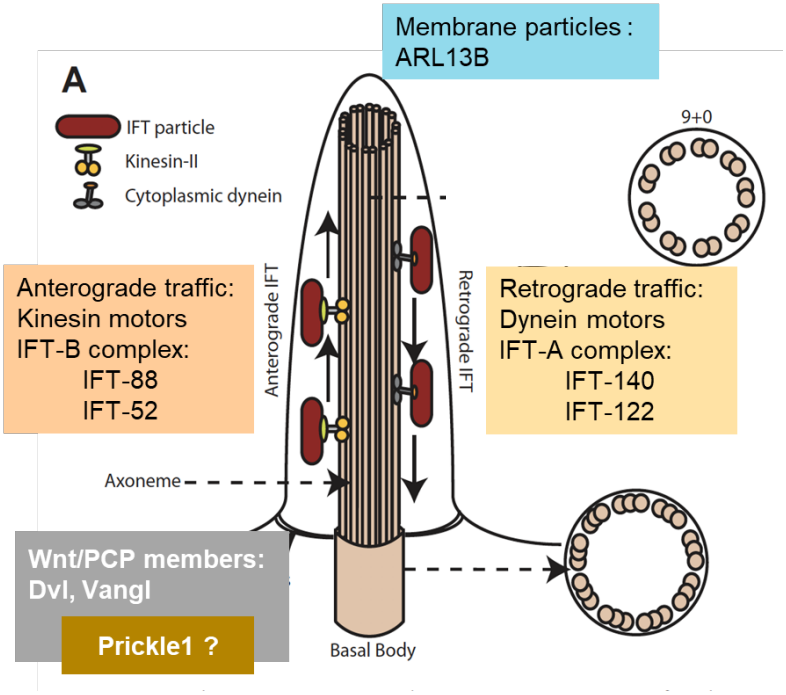

Figure 3: Primary cilia homeostasis is maintained by intraflagellar transport.

The primary cilium is devoid of organelles specialized in protein synthesis. Therefore, tubulin and other proteins necessary for the homeostasis of the cilium are transported from the cell to the tip via the anterograde intraflagellar transport via kinesin motors and IFT-B complex particles (e.g IFT-88 and IFT-52). Ciliary membrane particles such

as ARL13B interact with IFT-B particles during ciliary membrane biogenesis. Ciliary maintenance is organized through the retrograde transport that facilitates proteins return to the cell body via dynein motors and IFT-A complex particles (e.g. IFT-140 and IFT-122). Wnt/PCP members such as Dvl and Vangl orient the positioning of the basal bodies during ciliary assembly. Knowing the physical interactions between Dvl, Vangl, and Prickle1 during the establishment of the cell polarity, Prickle1 may participate in the regulation with ciliary assembly. Figure was adapted from Cardenas-Rodrigues and Badano, 2009 (Cardenas-Rodriguez and Badano, 2009).

1.2.2 Pathways of ciliogenesis

The primary cilium binds to the cell through the basal bodies to provide a platform enabling the projection of the axoneme extracellularly (Jensen et al., 2004). Basal bodies consist of modified mother and daughter centrioles docking to the plasma membrane or ciliary vesicle through their distal appendages depending on ciliation formation pathway (Kumar et al., 2019). Centrioles convert to basal bodies occurs when the cell finishes cytokinesis and proceeds to the G0 stage (Lattao et al., 2017). The basal bodies are cylindrical structured in 9 + 1 microtubules triplets' disposition. The ultrastructure of the distal (mature) basal body differs from the proximal (immature) basal body. A mature basal body lacks the cartwheel structure at the proximal end like for the immature, a dense core at the distal end, and contains satellites at the outer surface of the microtubule's triplets (Dawe et al., 2007; Jensen et al., 2004; Marshall, 2008). The apical side of the terminal plate attaches the distal basal body to the cell, a thick striated rootlet ends the basal side (Garcia et al., 2018; Marshall, 2008). Pericentriolar materials like Pericentrin surrounds the orthogonally oriented basal bodies (Garcia and Reiter, 2016; Lattao et al., 2017). The basal body proteome contains a variety of proteins such as Cep164, Talpid3, and Sclt1. Some of them are required for ciliogenesis to recruit IFT particles for the build-up and maintenance of the cilia (Garcia and Reiter, 2016).

Primary cilia or cilia grow either through intracellular or extracellular pathway depending on the cell type. The intracellular pathway is observed in cells like the fibroblasts and neuronal precursors whereas the extracellular route is most common in epithelial cells lining the kidney or the lungs (Keeling et al., 2016). In the intracellular pathway, the principal ciliogenesis route, the centrioles duplicate deep within the cell in a juxta-nuclear position and convert into basal bodies that will dock to a ciliary vesicle (CV) near a trans face Golgi apparatus (Keeling et al., 2016; Wang and Dynlacht, 2018). Helped by protein transport, the axoneme will elongate simultaneously with the ciliary membrane inside the mother basal body-capped ciliary vesicle until reaching and fusing with the plasma membrane of the cell (Keeling et al., 2016; Wang and Dynlacht, 2018). The cilium will remain invaginated in a structure called ciliary pocket or ciliary pit because the basal body is placed deep within the cell in this route (Molla-Herman et al., 2010). The extracellular pathway occurs mostly in multi-ciliated and epithelial cells as a cilium biogenesis alternative (Bernabé-Rubio et al., 2016). In this route, the mother basal body localizes apically to the plasma membrane and fuses with the cell without forming a ciliary pocket as the cilium elongates (Bernabé-Rubio et al., 2016; Keeling et al., 2016).

1.2.3 Function of the primary cilia

The vast array of functions of the primary cilia in vertebrate development were discovered through a genetic screen to identify required factors for mouse embryo survival and patterning (Goetz and Anderson, 2010). The screen identified proteins associated with ciliary functions or cilia-dependent signaling such as ARL3, ARL13, SUFU, and the centrin gene Cdc31. ARL13, SUFU and Cdc31 participate in the spindle pole body, influence gene expression, and are implicated in DNA repair such as for the centrin-associated protein pericentrin (PCNT) (McClure-

Begley and Klymkowsky, 2017). The primary cilia regulate the cell cycle by coordinated assembly and disassembly to utilizing the centrioles as a base for axonemal elongation, or freeing them for mitotic spindle formation (Michaud and Yoder, 2006).

Primary cilia control neural crest cells migration, craniofacial development and differentiation (Schock et al., 2017). Loss of Kif3A in mouse neural crest cells compromises development of the craniofacial complex as Kif3A mutants displayed severe congenital defects including bifid nasal septum, cleft lip/palate, micrognathia, aglossia and dental defects (Schock et al., 2017). The primary cilia regulate all stages of tooth morphogenesis (Hampl et al., 2017). Primary cilia length depend on their localization in the tooth signaling centers, like the enamel knot, where they control cellular differentiation and deposition of mineralized dental materials (Hampl et al., 2017). The primary cilia contribute to proper heart embryonic development and maturation in humans and mouse models (Myklebust et al., 1977). But in rats, the primary cilia develop only during embryonic development (Kaur et al., 2018). The mesoderm requires the cilia for anterior-posterior limbs' patterning and to transduce HH signaling (Haycraft and Serra, 2008). Mutations in many genes encoding ciliary components cause syndactyly, polysyndactyly, brachydactyly confirming the role of the primary cilia in transducing HH signaling (Haycraft and Serra, 2008).

Primary cilia direct skeletal development to maintain articular chondrocytes function in endochondral bone formation and development of the post-natal growth plate through IHH (Haycraft and Serra, 2008). They participate in bone collar development via mediation of both canonical and non-canonical Wnt signaling; and preserve the bone mechano-sensation's ability via intracellular calcium signaling (Haycraft and Serra, 2008). Primary cilia act as tumor suppressors because loss of cilia deregulates cilia-dependent signaling pathways enabling tumorigenesis

(Wang and Dynlacht, 2018). In contrast, the persistence of primary cilia promotes tumorigenesis by overactivation of HH or Wnt signaling (Wang and Dynlacht, 2018).

1.2.4 Signaling pathways dependent of the cilia

Although controversial, primary cilia regulate both canonical and non-canonical Wnt/ PCP signaling by behaving like a switch between them (Goetz and Anderson, 2010). In mouse or in zebrafish, Vangl2 gene and BBS proteins colocalize in the ciliary axoneme and the basal body suggesting a role of the cilia in PCP pathway establishment (Fliegauf et al., 2007). The Canonical HH is another pathway dependent on ciliary function during early embryonic development and during adult age. Cilia can sequester negative and positive regulators of the HH pathway such as SUFU, TULP3 and Kif7 in the ciliary tip (Qin et al., 2011). The intraflagellar transport particle IFT122 regulates the HH pathway by balancing the transport of activators and repressors in the cilia (Qin et al., 2011). In addition, initiation HH signaling cascade requires SMO translocation to the ciliary membrane (Briscoe, 2006; Briscoe and Therond, 2013; Wu et al., 2002).

Purmorphamine, which is a 2,6,9-trisubstituted purine compound, was discovered through cell-based high-throughput screening from a heterocycle combinatorial library. It differentiates multipotent mesenchymal progenitor cells into an osteoblast lineage. It will serve as a unique chemical tool to study the molecular mechanisms of osteogenesis of stem cells and bone development.

In some signaling pathways, associated receptors localize in the cilia. Cultured human fibroblasts showed two TGFβ receptors (TGFβRI and TGFβRII) along the axoneme and the tip of the cilia (Anvarian et al., 2019). The platelet-derived growth factor (PDGF) signaling pathway serves in cell proliferation, survival, and migration during embryonic development (Eggenschwiler

and Anderson, 2007; Fliegauf et al., 2007). In *in-vitro* experiments, the ciliary localization of the platelet-derived growth factor receptor α (PDGFRα) may facilitate binding to the PDGF ligand (Eggenschwiler and Anderson, 2007; Fliegauf et al., 2007). Recent discoveries pinpointed several G proteins- coupled receptors (GPCRs), and their downstream effectors into the cilia (Anvarian et al., 2019). Lastly, new data linked the cilia and the Hippo-signaling, a pathway that controls organ size, cell proliferation, and tumorigenesis (Basten and Giles, 2013; Keeling et al., 2016).

1.2.5 Hedgehog (HH) pathway

1.2.5.1 Functions of HH pathway

The primary cilia and the motile cilia are the primary centers for the canonical HH pathway in vertebrates in a tissue-specific manner (Figure 4). The HH ligand was first discovered in Drosophila. In mammals, three HH counterparts have been identified: Sonic Hedgehog (SHH), Indian hedgehog (IHH) and Desert Hedgehog (DHH) (Anvarian et al., 2019). HH is an important signalling pathway that directs multiple functions during embryonic development by providing instructions for tissue patterning, left-right asymmetry, limb development, neurogenesis, and contribution to post-developmental tissue homeostasis (Satir and Christensen, 2008). HH signaling remains important for the maturation of the brain and the maintenance of neuronal progenitors (Goetz and Anderson, 2010). Each HH counterpart has a specific role: IHH and SHH act regulates bone and cartilage development, while DHH activity is on the testis and the peripheral nerve where it is essential for germ cell development and sheath formation, respectively (Briscoe and Therond, 2013). The HH ligands are a paracrine tissue secreted morphogen composed of an N-terminal, a C-terminal that undergoes a rapid proteolytic cleavage before dual lipidation by cholesterol and palmitic acid (Briscoe and Therond, 2013). The presence of these lipidic groups restricts its

location to the plasma membrane. From the SHH-secreted cells, the ligands are transported out to the region of interest by multiple carriers (soluble multimers, lipoproteins, exosomes, and extracellular vesicles). Lipidated SHH secretion is regulated by Dispatched (DISP) and SCUBE2 (a secreted glycoprotein), whereas its stabilization and diffusion through the tissues are monitored by glypicans (Briscoe and Therond, 2013).

1.2.5.2 Ciliary-mediated canonical HH pathway

The canonical HH pathway is dependent on transcription factors (Glioma-associated oncogene (Gli)), receptors (Smoothened (SMO)) and co-receptors (Patched (Ptc)) proteins (Figure 3). Ptc1 is a 12-pass transmembrane receptor that binds HH ligands using the sterol-sensing domain (SSD) to form a receptor complex with the adhesion molecule CDO, or BOC (Briscoe, 2006; Briscoe and Therond, 2013). Smoothened, a seven-pass G-protein coupled receptor (GPCR) of the frizzled family, activates production of arachidonic acid from downstream response of phospholipase A2 (Arensdorf et al., 2017). The Gli transcription factor proteins transcribe full-length activator (GliA) proteins that can be proteolytically cleaved to smaller repressor protein (GliR) (Wang et al., 2010).

In the absence of HH ligand, Ptc restrain SMO function by physically inhibiting its activation (Briscoe, 2006). Upon binding of HH ligand to the SSD domain, Ptch1 relieves SMO repression and allows its transit to the cilia. By an unknown mechanism, in the absence of SHH ligand Ptch1 can also inhibit the signaling cascade by restricting SMO to the plasma membrane (Goetz and Anderson, 2010). In the primary cilia tip, the suppressor of fused (SUFU) binds to Gli proteins and prevents their activation and transit into GliA and GliR out of the cilia in *Drosophila* and mice (Goetz and Anderson, 2010; Hui and Angers, 2011). SUFU is a negative regulator of mammalian HH signalling, that prevents the transit of GliA and GliR out of the cilia (Goetz and

Anderson, 2010). Arachidonic acid binds intracellularly to SMO and promotes a conformational change that facilitates its migration to the ciliary membrane where it will dissociate Gli from SUFU and permit the transit of Gli proteins from the distal tip of the primary cilia (Arensdorf et al., 2017).

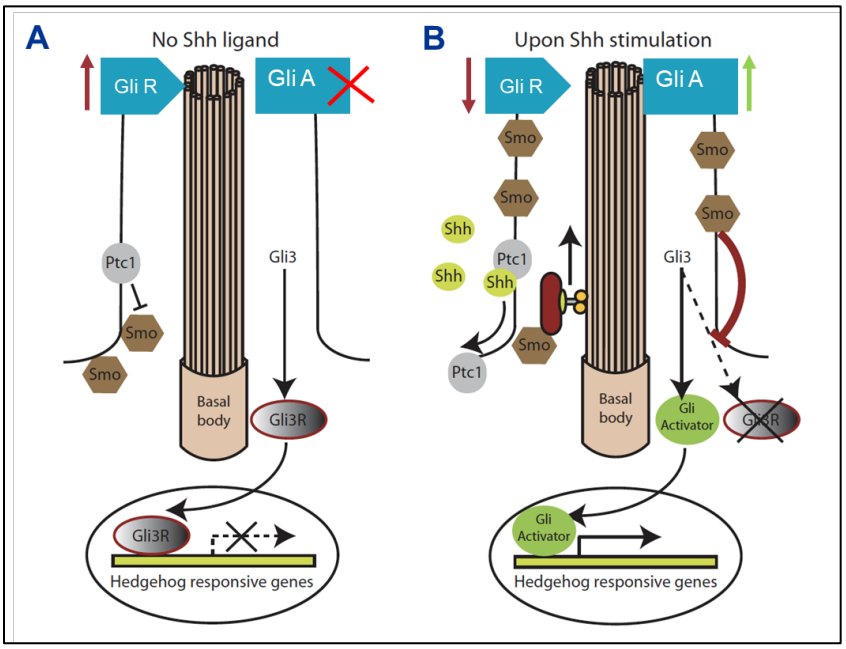

Figure 4: The Canonical Hedgehog Signaling Pathway.

In the absence of HH ligand, Gli 2 and Gli3 transcription factors are converted only in Gli repressor (GLiR) as Ptc1 inhibits Smo migration to the ciliary membrane. GliR represses transcription of HH responsive genes in the nucleus (A). In the presence of HH ligand, the ratio of Gli processing increased towards the activator form following Smo translocation to the ciliary membrane. This translocation can happen only when HH ligands bind to Ptc1that released the inhibitory effect of Smo. Gli activator (GliA) enable transcription of HH responsive genes in the nucleus (B). Figure adapted from Cardenas-Rodrigues & Baldano, 2009 (Cardenas-Rodriguez and Badano, 2009).

Three Gli transcription factors (Gli1, Gli2 and Gli3) had been identified in the mouse. Phosphorylation of full length Gli proteins predominantly Gli2, and in a lesser extent Gli1, will generate GLIA (Arensdorf et al., 2017). This activator form of Gli transcription factor will be

transported out of the cilia via the retrograde intraflagellar transport complex to the nucleus to induce transcription of HH-responsive genes (Satir and Christensen, 2008). On the contrary, in the absence of SHH ligand, Ptch1 suppresses SMO and restricts its position to the plasma membrane (Figure 4). Therefore, GLI transcription factors, mostly Gli3, are proteolytically processed to the N-terminal GliR domain (Wang et al., 2000). GliR, the repressor form, turns off transcription of HH-responsive genes in the nucleus (Satir and Christensen, 2007; Wang et al., 2000). Therefore, the levels of HH signaling can be estimated by the abundance of GliA / GliR in the tissue (Goetz and Anderson, 2010; Huangfu and Anderson, 2006). In addition, the sequestration of GliA or GliR in the cilia can also affect the level of HH signaling in the cell.

1.2.6 Molecular Motors

Molecular motors are proteins machinery that perform a variety of biological functions like moving cellular cargoes, facilitating cell locomotion, and participating in cell division (Schliwa and Woehlke, 2003). They enable a cell to grow and maintain a cilium or primary cilium by supplying the axoneme with tubulin, and other particles necessary for signaling transduction and the build-up of a specialized ciliary membrane (Bisgrove and Yost, 2006). Two molecular motors proteins: Dynein and Kinesin, move cargo using the microtubules as their traffic track from the cell to the cilium, within the cilium and from the cilia to cell (Bisgrove and Yost, 2006). Within the cilia, Kinesin motors support the anterograde traffic (to the cilia tip) with the intraflagellar complex B particles while Dynein motor organizes the retrograde (to the cell) transport with the complex A(Bisgrove and Yost, 2006; Davenport and Yoder, 2005; Satir, 2017) (Figure 2).

1.2.6.1 Kinesins motors

Kinesins molecular motors proteins comprise 15 sub-families that transport cargo toward the microtubule plus end by transforming chemical energy from ATP turnover in mechanical energy (Gilbert et al., 2018). All Kinesin proteins contain a conserved molecular motor domain; however, they are structurally unique and perform different functions in the cell based on their N-terminal or C-terminal structural organization in homodimers, heterotrimers, or tetramers (Gilbert et al., 2018; Mickolajczyk and Hancock, 2017). Kinesin 1, the Kinesin 2, the Kinesin 5, and the Kinesin 7 are among N-terminal Kinesin motors (Gilbert et al., 2018). In many models studied, Kinesin 2 functions in intraflagellar transport, DNA repair, organelles repositioning, and microtubules dynamic (Verhey et al., 2011). In mammals, Kinesin-2 subdivides in four essential genes KIF3A, KIF3B, KIF3C and KIF17 and the Kinesin associate gene3 (KAP3) (Keeling et al., 2016; Mickolajczyk and Hancock, 2017). In vertebrates, another kinesin motor (KIF7), associated with anterograde intraflagellar cargo, may tether the HH pathway (Keeling et al., 2016; Verhey et al., 2011).

1.2.6.2 Dynein motors

Dynein are dimeric motors proteins that direct cargo toward the microtubule minus end and accomplish different biological functions in the cells. In *Drosophila*, *Xenopus*, or other species, they identified two cytoplasmic dyneins: dynein-1 and dynein-2. Dynein-1 participates in mitosis, cell migration, and intracellular organization, while dynein-2, the ubiquitous form, coordinates intraflagellar transport (Prevo et al., 2017; Roberts, 2018). Dynein-2 possesses two isoforms (DYNC2H1 and DYNC2LI1) that function during ciliogenesis with the IFT-A complex to transport protein cargo back to the cell in the retrograde transport (Roberts, 2018). Structurally, Dynein-2 proteins contain two heavy chains, two light chains, a motor domain with two linkers or

intermediate portions, a coiled-coil configuration at the tip, and a C-terminal domain (Prevo et al., 2017; Roberts, 2018). Prior to ciliary assembly, Dynein-2 undergoes a conformational change to activate its motor domain in the cytoplasm enabling the IFT-cargo to be released in the cell body (Roberts, 2018). Dynein-2 also propels ciliary beating of motile cilia (Prevo et al., 2017; Satir and Christensen, 2008).

1.2.7 Intraflagellar transport

Cilium biogenesis occurs primarily through bidirectional protein traffic named intraflagellar transport (IFT). The cilium lacks protein synthesis organelles such as endoplasmic reticulum, so it must transport all essential proteins into and out of the cilia. The cilia have evolved two complementary transport mechanisms to accomplish the delivery and removal of protein complexes called IFT-A and IFT-B complexes (Haycraft and Serra, 2008). Kinesin-2 motors and the IFT-B complex execute the anterograde transport to supply the axoneme with tubulin, and other particles from the cell body. Proteins return to the cell via the Dynein-machinery and the IFT-A complex in the retrograde transport. (Haycraft and Serra, 2008). The intraflagellar transport controls ciliary assembly, maintenance, length and signaling (Prevo et al., 2017). Thus, ciliary assembly requires several components: functional Kinesin-2 motors, an intact IFT-B complex to move proteins loads towards the tip of the cilium, dynein motors and IFT-A to recycle ciliary components back to the cell, an additional protein complex (Bardet-Biedl Syndrome (BBSome), and members of ADP-Ribosylation factors families (Dupont et al., 2019; Prevo et al., 2017).

The IFT- B Complex contains sixteen IFT proteins divided into a core sub-unit, the IFT-B1 and a satellite complex, the IFT-B2 (Prevo et al., 2017). Of the 10 IFT-B1 proteins, IFT-88 and IFT-52 were shown to be essential for ciliogenesis (Prevo et al., 2017) (Figure 3). IFT-52 also

connects the core complex to six IFT-B2 peripheral particles (Prevo et al., 2017). Similarly, the IFT-A complex comprises six IFT particles regrouped into an IFT-A core including IFT-122, and 140 that guides proper ciliary assembly, with the three peripheral particles (Duran et al., 2017). As the IFT system is evolutionary conserved, it requires specific interactions between core proteins and peripheral subunits to channel ciliation such as IFT-88 and IFT-52 dimer that stabilizes the IFT-B complex (Duran et al., 2017; Keeling et al., 2016; Zhang et al., 2016). Those protein-protein interactions may enhance tubulin binding affinity to IFT particles depending of the subunits (Keeling et al., 2016). Though, the intraflagellar transport occurs in a dense environment where several motor proteins work jointly with the IFT particles to elongate and maintain a cilium (Prevo et al., 2017). IFT-88 or Polaris homolog (known also as hTg737) organizes particles trafficking to support ciliary building (Basten and Giles, 2013). Ciliary depletion of essential IFT-88 inhibits ciliogenesis on fly sensory cells (Keeling et al., 2016). Equally, IFT-A proteins stability requires a functional core to avoid disruption of the retrograde transport (Duran et al., 2017; Takahara et al., 2018). Mutations IFT-122 destabilize IFT-A core complex and block ciliogenesis (Duran et al., 2017; Satir, 2017; Takahara et al., 2018). Therefore, ciliogenesis requires both proper anterograde and retrograde transports (Figure 3). Other IFT-A mutations result into ciliary aberration into short, bulged, and non-functional cilia (Pedersen et al., 2008). Additional to their role in ciliogenesis, several IFT particles are multi-taskers and perform ciliary independent functions like IFT-88 that contribute in cytokinesis (McClure-Begley and Klymkowsky, 2017).

Besides the IFT particles, the basal bodies comprise several proteins (BBSome) such as Centrins and Pericentrins that participate actively into the IFT-machinery (Garcia and Reiter, 2016; Keeling et al., 2016). The BBSome forms a cilia-specific transport module scrutinizing and recruiting vesicles transport during ciliogenesis (Basten and Giles, 2013; Goetz and Anderson,

2010). Hence, Ciliogenesis necessitates Pericentrin as an anchor to localize IFT particles at the base of the cilium (Keeling et al., 2016; Tuma, 2004). BBSome mutations disrupt ciliogenesis by causing dissociation of IFT-A and IFT-B complexes in the cilium causing therefore a failure of ciliary assembly (Keeling et al., 2016; Tuma, 2004).

The ADP-Ribosylation Factors (Arf and Arl) is a large family of ciliary complementary proteins that support ciliogenesis by interacting with numerous GTPases like Rab8 (Basten and Giles, 2013; Larkins et al., 2011; McClure-Begley and Klymkowsky, 2017). Arl13b, in the ciliary membrane, is considered as the most upstream regulators of ciliogenesis as it involves in direct binding of tubulin and IFT-B particles, it is also necessary for proper SHH signaling transduction (Nachury and Mick, 2019). Exclusive ciliary positioning of Arl13b is required for length regulation via modulated vesicles ferrying from the Golgi apparatus (Basten and Giles, 2013; Cevik et al., 2010; Larkins et al., 2011). Although, Arl13b depletion in C. elegans did not block ciliogenesis (Larkins et al., 2011).

The transition zone at the base of the cilium, is a selective barrier made of soluble proteins forming a necklace to regulate ciliary composition (Garcia et al., 2018). Those proteins form a Y-linked fibers structure with the transmembrane domain-containing proteins (TMEM) to facilitate ciliary entry of IFT particles docking at the transition zone (Basten and Giles, 2013; Garcia et al., 2018; Wang and Dynlacht, 2018). IFT proteins enter the cilium via cytoplasmic particles. The ciliary gates also promote localization of ciliary membrane component, participate in Hedgehog and Wnt/PCP signaling pathways, and they are involved in diseases (Basten and Giles, 2013; Garcia et al., 2018; Kunova Bosakova et al., 2018).

1.3 Ciliopathies and Wnt/PCP pathway related diseases

1.3.1 Ciliopathies

Ciliopathies are a group of human malformations that are caused by problems with the primary cilia. Recent work on the biology and function of the primary cilium has uncovered more than 50 loci involved in ciliopathies (Basten and Giles, 2013). Ciliary defects can occur at different stages of ciliogenesis in motile or non-motile (sensory) cilia causing distinct ciliopathic phenotypes (Reiter and Leroux, 2017). Motile ciliopathies happen in multi-ciliated epithelia causing embryonic death or failure of embryonic turning (Cardenas-Rodriguez and Badano, 2009). Less severe ciliary motility phenotypes include a reduction of the ability to propel waste out of the respiratory tract resulting in disfunction (Cardenas-Rodriguez and Badano, 2009). On the other hand, sensory ciliopathies affect nearly all organs and ages, and result from defects in non-motile ciliary structures that contain sensors to detect the extracellular environment and their signaling functions (Cardenas-Rodriguez and Badano, 2009). Ciliary assembly and disassembly aberrations cause brain malformation, congenital heart defects and skeletal malformations (Wang and Dynlacht, 2018). In cancer, the abrogation of ciliary-mediated HH signaling deregulates the cell cycle (Wang and Dynlacht, 2018). Primary Cilia Dyskinesia (PCD) are a group of rare genetic disorders where only the motile cilia are impaired while the primary cilia are normal (Satir, 2017). PCD results in left-right asymmetry or situs inversus, bronchitis, sinusitis, and infertility (Cardenas-Rodriguez and Badano, 2009; Reiter and Leroux, 2017). The PCD disorders are classified into first-order or second order ciliopathies. First order ciliopathies refer to protein dysfunction within the cilia proper, whereas second order ciliopathies affect proteins situated outside of the cilia but function in ciliogenesis and function (Reiter and Leroux, 2017).

Disruption of ciliary assembly or morphogenesis occurred in humans and mice with mutations of intraflagellar particles of complex A and B such as IFT-88, IFT-52, IFT-122, and IFT-140 (Reiter and Leroux, 2017). Limb buds of *IFT-88*$^{-/-}$ mutant mice have defects in ciliary assembly. The IFT-88 defective cilia have impaired processing of Gli3 at the tip of the cilium which disrupts HH signal transduction (Cardenas-Rodriguez and Badano, 2009; Satir and Christensen, 2007, 2008). In addition to the limb defects, the *IFT-88*$^{-/-}$ mice developed severe craniofacial defects notably cleft lip and palate (Tian et al., 2017). Furthermore, IFT-88 mutation caused polycystic kidney ciliopathy in mouse (Schrick et al., 1995). Together, these observations suggest that IFT-88 is required for ciliogenesis, HH signaling, and embryonic development (Schrick et al., 1995). IFT-52 interacts with IFT-88 and facilitates binding of the IFT-B core and IFT-B peripheral (Dupont et al., 2019; Takei et al., 2018). IFT-52 mutations destabilize the anterograde transport complex and cause ciliopathies such as short rib polydactyly syndrome (Dupont et al., 2019).

IFT-122 regulates retrograde axonemal transport and is required for ciliary formation and maintenance. *IFT*$^{sopb/sopb}$ mutant mice form shortened, swollen cilia (Basten and Giles, 2013; Qin et al., 2011). In mouse models, IFT-122 is required for embryonic survival and it mediates SHH in the developing limbs (Cortellino et al., 2009). Additionally, IFT-122 negatively regulates SHH by transporting the HH activators and repressors from the tip of the cilium (Qin et al., 2011). *IFT-122*$^{-/-}$ knockout in mice impaired SHH during neuronal patterning (Cortellino et al., 2009). In human, IFT-122 mutations are associated with some cases of autosomal recessive cranio-ectodermal dysplasia or Sensenbrenner Syndrome characterized by craniofacial, skeletal, and ectodermal abnormalities (Walczak-Sztulpa et al., 2010).

IFT-140 in the IFT-A complex participates in the formation and the maintenance of eukaryotic cilia (Figure 3) (Zhang et al., 2019). IFT-140 mutations block ciliary trafficking at the tip of the cilium which generate a bulged cilium (Basten and Giles, 2013). IFT-140 mutations also reduce the number of ciliated human skin fibroblasts (Geoffroy et al., 2018). IFT-140 is required during bone development as mutations involve in skeletal ciliopathies such as Mainzer-Saldino Syndrome characterized by phalangeal cone-shaped epiphyses, chronic renal disease, and retinal dystrophy (Geoffroy et al., 2018; Zhang et al., 2019).

Arl13b is evolutionary conserved and required for normal cilium biogenesis, ultrastructure and function (Cantagrel et al., 2008; Cevik et al., 2010). *Arl13b*$^{-/-}$ mutant animals have defective cilia including missing, truncated, or an enlarged ciliary axoneme (Cevik et al., 2010). Absence of Arl13b impaired cells signaling and hinder their ability to respond to SHH cues (Larkins et al., 2011). Arl13b mutations are associated with autosomal-recessive Joubert Syndrome, a pleiotropic condition affecting the retinal, renal, digital, oral, hepatic, and cerebral organs (Cantagrel et al., 2008; Cevik et al., 2010).

1.3.2 Wnt/PCP signaling pathway related human diseases

Proper ciliary assembly requires directed protein trafficking and instructive signals from the Wnt/PCP pathways. Links with diseases were first uncovered from amphibian epidermis multi-ciliated cells (Butler and Wallingford, 2017). In many animals studied, incorrect PCP establishment results in neural tube defects, nephronophthisis (cystic kidneys) (Butler and Wallingford, 2017; Humphries and Mlodzik, 2018; Simons and Mlodzik, 2008). As the Wnt/PCP pathway involves in convergent extension during gastrulation and neurulation, mutations in CELSR1, VANGL1, NHP2 are associated with human diseases such as nephronophthisis,

craniorachischisis or spina bifida (Simons and Mlodzik, 2008). Surprisingly, CELSR1, VANGL1, NHP2 proteins are located into the basal body of the cilia. Those findings suggest that defective Wnt/PCP pathway affects the organization of the actin cytoskeleton, the correct positioning of the basal body and thus perturb ciliary formation, morphology, and function (Basten and Giles, 2013). NHP2 gene, translated into the ciliary Inversin (Inv) protein, interacts with Dvl to promote its stability in *Drosophila* (Simons and Mlodzik, 2008). Inv is a critical regulator of the Wnt/PCP signaling pathway and $Inv^{-/-}$ mice developed ciliopathic phenotypes such as *situs inversus* and polycystic kidney disease (Simons and Mlodzik, 2008). Mutation in Vangl1 also destabilizes physical interaction with Dvl and disrupts PCP (Simons and Mlodzik, 2008). Other PCP pathways genes like Prickle1 are also involved in human diseases.

1.3.3 PRICKLE1 mutations cause human familial myoclonus epilepsy

During embryonic development, Prickle1 is required for the asymmetric positioning of the Wnt/PCP pathway genes, it modulates convergent extension during gastrulation and neurulation. Prickle1 is essential for mouse survival as $Prickle1^{-/-}$ null mutant mice are early embryonic lethal because of gastrulation defects, while hypomorphic *Prickle1* alleles mutants survive until late gestation (Gibbs et al., 2016; Liu et al., 2013; Tao et al., 2009). *Prickle1* is expressed during all stages of mouse embryonic development in the hippocampus, cerebral cortex, thalamus, and the primitive cerebellum, which are regions implicated in epilepsy (Bassuk et al., 2008; Tissir and Goffinet, 2006). In mouse developing brain, *Prickle1* modulates axon and dendrites growth, glial processes formation as well as axonal anterograde transport for vesicle dynamics (Ehaideb et al., 2014)Bassuk et al., 2008). In many organisms studied including flies, zebrafish, and mice, *Prickle1* mutations are associated with neurological disorders, and implicated in the

pathophysiology of epilepsy (Ehaideb et al., 2014). In fly, the balance between Prickle^{sple} and Prickle^{pk} proteins control transport of neuronal vesicles and protect from seizures (Ehaideb et al., 2014). In humans, a missense mutation in the highly conserved PET domain disrupts protein binding between PRICKLE1 and REST causes progressive myoclonus epilepsy (Bassuk et al., 2008). Progressive myoclonus epilepsy is a group of multigenic heterogenous disorders characterized by rapid, irregular, and involuntary contractions, cognitive impairment, ataxia, and other neurologic deficits (Satishchandra and Sinha, 2010). *Prickle1* mutation is linked with both autosomal dominant and recessive progressive myoclonus epilepsy (Algahtani et al., 2019). An additional *de novo* missense *PRICKLE1* mutation (c.1444 G>A, p. D482N) is causative in the heterozygous form of the disorder (Todd and Bassuk, 2018).

1.3.4 Genome-Wide Association Studies (GWAS) and links to human orofacial clefts (OFC)

Neural crest cells (NCCs) migration is a critical event for craniofacial development. Prior to collective migration, NCCs must undergo an epithelial-to-mesenchymal transition (EMT) (Garmon et al., 2018). Like Fz and Dvl's role in NCCs migration, in zebrafish, *Prickle* orthologs *prickle1a* and *prickle1b* facilitate the EMT and the collective translocation to the craniofacial area (Ahsan et al., 2019). *Prickle1*-deficient zebrafish showed altered NCCs disposition and those cells remained blocked in the pre-migratory stage (Ahsan et al., 2019). In addition, mice mutants for *Prickle1* present several craniofacial abnormalities including completely penetrant median cleft lip and incompletely penetrant cleft palate (CP) (Wan et al., 2018; Yang et al., 2014). A GWAS performed in a Filipino population with high familial prevalence of CLP revealed two rare *PRICKLE1* missense mutations at c.1138C>T and c.2026C>T, and one Single Nucleotide Polymorphism (SNP, rs12658) (Bassuk et al., 2008; Yang et al., 2014). In addition, several SNPs,

nonsense, and missense mutations of Wnt/PCP pathway members (i.e. WNT5A, DVL1, FZD2, FZD6 and ROR2) have been attributed in both syndromic and non-syndromic cleft palate (Carlson et al., 2019; Menezes et al., 2010; Reynolds et al., 2019). Furthermore, Wnt/PCP members have been associated with Robinow Syndrome.

1.3.5 Human Robinow Syndrome (RS) phenotypes and genotypes

Robinow Syndrome was first described by Robinow et al. (1969) and features dwarfism, craniofacial dysmorphology, vertebral and gonadal phenotypes (Robinow et al., 1969). This dwarfism is characterized by dysregulation of PCP genes likely the WNT5A-ROR2-DVL route (White et al., 2016). The known genetic mutations include WNT5A, DVL1, DVL3, FZD2, FZD6 and ROR2, but most cases (~70%) of RS remained genetically unidentified (Mazzeu et al., 2007; Person et al., 2010; Reynolds et al., 2019; Roifman et al., 1993; White et al., 2015; White et al., 2016) (Figure 5). Because of the clinical similarities, it is likely that mutations in other PCP pathway genes are responsible for RS (Schwabe et al., 2004). Both autosomal dominant and recessive patterns of inheritance occurred in human RS, however recessive RS is more severe (10% more lethal) than the dominant one (Reynolds et al., 2019; Schwabe et al., 2004). 5 to 10% of affected patients die during infancy due to related congenital defects (Robinow and Beemer, 1990). As the molecular diagnosis in ~ 70% of the autosomal dominant forms remained unknown, other core genes of the Wnt/PCP pathway such as Prickle1 should be investigated for potential roles in Robinow Syndrome. In addition, there is a paucity of data regarding crosstalk with other signaling pathways such as Hedgehog pathway in the pathogenesis of Robinow Syndrome.

ROR2$^{-/-}$ mice present many skeletal, craniofacial, and genital defects that phenocopy human autosomal recessive RS (Takeuchi et al., 2000). The mutants displayed a craniofacial

outgrowth defect, hypertelorism, midface hypoplasia, and oral abnormalities (Schwabe et al., 2004). *ROR2*$^{-/-}$ mice have also somitogenesis defects resulting in vertebral and rib malformations, missing vertebral discs, and a shortened tail. In addition, the genital hypoplasia phenotype is consistent with findings in humans (Schwabe et al., 2004). The Wnt5a$^{-/-}$ develop shortened limbs, and cranial base and other anatomical defects that phenocopy the human autosomal dominant RS (Yamaguchi et al., 1999). A Prickle1 null and hypomorphic mouse model also phenocopies human RS (Liu et al., 2014; Liu et al., 2013). The hypomorphic *Prickle1*$^{c/c}$ develop several defects that are a hallmark of disrupted Wnt/PCP signaling, including neural tube defects, and RS-like skeletal, craniofacial and genital phenotypes (Liu et al., 2014; Reynolds et al., 2019). The *ROR2*$^{-/-}$ and *Wnt5a*$^{-/-}$ mice models showed similar palatal defects with *Prickle1*^{C251X} resulting from defects in HH signaling (Yang et al., 2014).

1.3.6 Clinical features of RS and RS standard treatment

Regardless of the patient specific genetic mutations, individuals with Robinow Syndrome present skeletal anomalies including short stature, mesomelic limbs shortening mostly the upper limbs, and brachydactyly. Affected males and females have hypoplastic genitalia (Mazzeu et al., 2007; Person et al., 2010). Their distinctive facial features resemble a fetal face comprising protruded forehead, widened and depressed nasal bridge, short nose, micrognathia, large mouth with dental anomalies (Robinow et al., 1969; Roifman et al., 1993). Nonetheless, no intellectual disability has been reported in 80% of the cases (Bunn et al., 2015; White et al., 2015). Approximately 75% of those clinical features are present in recessive cases of RS rendering the clinical diagnosis easier than the dominant form, which has variable presentation of the mesomelic shortening phenotype (Mazzeu et al., 2007). Also, rib fusions guide in the differential diagnosis of

the recessive variant while brachydactyly type B is pathognomonic of the dominant form (Mazzeu et al., 2007). A variant type of the autosomal dominant RS is characterized by widespread osteosclerosis (increased bone density) affecting the skull particularly the base, axial and appendicular skeleton (Bunn et al., 2015).

Current RS therapies are directed towards specific symptoms and require a multidisciplinary approach. The recommended surveillance comprises regular visits to evaluate the craniofacial, ears, cardiovascular, genito-urinary, and neurologic systems for early detection of any pathognomonic manifestations (Roifman et al., 1993). Some dysmorphic facial features may require surgical management in severe cases to improve functionality (Mossaad et al., 2018). Patients with osteosclerosis associated with Robinow Syndrome, that impinges on cranial nerve foramina often need to undergo neurosurgery to remove the problematic bony growths.

1.3.7 Gorlin Syndrome or Nevoid Basal Cell Carcinoma (NBCC)

Gorlin Syndrome or Nevoid Basal Cell Carcinoma is a rare form of autosomal dominant skin cancer, and craniofacial dysmorphology. Initial manifestation of the disease consists of development of multiple basal cell carcinomas (BCCs) at an early age (Bresler et al., 2016). Besides BCCs, other major diagnostic signs include odontogenic keratocysts of the jaw, pits of the palm and sole, progressive intracranial osteosclerosis (Booms et al., 2015). The craniofacial features of patients with diagnosed Gorlin syndrome include hypertelorism, wider mid-face (National Organization for Rare Disorders 2017, 2020). Affected individuals can develop additional pathognomonic features comprising macrocephaly with protruded forehead, and skeletal abnormalities (spine, ribs, and skull defects). Gorlin Syndrome predisposes the patients to both benign and malignant tumors such as fibromas or medulloblastomas (Booms et al., 2015;

Bresler et al., 2016). NBCC originates from increased HH signaling caused by a loss-of-function mutation in at least one PTCH1 allele (in ~ 80% of BCC), or by a gain-of-function mutation in SMO, or a *p53* tumor suppressor gene mutation (Athar et al., 2014; Bakshi et al., 2017; Lupi, 2007).

The understanding of the pivotal role of constitutive upregulation of HH signaling in the development of Gorlin Syndrome and other types of BCC enabled researchers to design molecular therapies targeting upstream or downstream HH signaling. NBCC therapy uses small molecule inhibitors to antagonize PTC1 or SMO, prevent their ciliary accumulation to inactivate the HH pathway (Bakshi et al., 2017). Most drug therapy in advanced, inoperable or metastatic BCCs are directed against SMO (Noubissi et al., 2018). In preclinical trials, Cyclopamine suppresses NBCC proliferation by binding to SMO and inhibiting downstream activation of the HH pathway, however multiple unpleasant side effects prevented human clinical application (Athar et al., 2014). Other therapeutic strategy developed Vismodegib, which is structurally similar to Cyclopamine, to inhibit SMO (Athar et al., 2014). Vismodegib is the first FDA approved HH pathway-targeted molecule for NBCC's treatment (Bresler et al., 2016). Although beneficial, Vismodegib long-term results in NBCC therapy are debatable due to high recurrence rates and the development of resistance in ~20% of the cases (Athar et al., 2014; Noubissi et al., 2018). Additional HH inhibitors are available in the cases where the tumors develop resistance to Vismodegib.

1.3.7.1 Relationship to HH pathway

Many signaling pathways coordinate proper embryonic development, tissue homeostasis, and stem cells maintenance (Noubissi et al., 2018). Those signaling pathways are in distinct gradient and spatial-temporally required (Bertrand et al., 2012). Developmental signaling cascades imbalance disrupt tissue homeostasis and generate a variety of diseases and tumors (Noubissi et

al., 2018). Overexpression of HH and Wnt are common in human cancers (Watt, 2004). In addition, those signaling pathways communicate or share molecular points in development and diseases (Bertrand et al., 2012; Wallingford and Mitchell, 2011; Wilson and Stoeckli, 2012). Therefore, cross-talk between HH and Wnt have been seen in NBCCs where GLI1 overactivation drive the initiation of the tumors, or the HH pathway can antagonize Wnt signaling in colon cancer (Bertrand et al., 2012; Noubissi et al., 2018). The shared phenotypes between Gorlin and Robinow Syndrome, and what we know about HH and Wnt signaling suggest that Wnt/PCP signaling may drive cellular polarity and the growth of endochondral elements, while the disruption of HH signaling contributes to the osteosclerotic elements.

1.4 Central Hypothesis

The *Prickle1*$^{Bj/Bj}$ mice mutants present several skeletal and congenital heart defects, and craniofacial malformations (Gibbs et al., 2016; Wan et al., 2018). The *Prickle1*$^{Bj/Bj}$ mutants develop a Robinow-like phenotype, which correlates to many characteristics of skeletal ciliopathies and defective SHH signaling. We observed that *Prickle1*$^{Bj/Bj}$ mutants have increased HH signaling in the medial nasal prominences at E10.5, and the presphenoid synchondrosis at E16.5 (Wan et al., unpublished). In addition, by STED microscopy, we observed swollen cilia in the *Prickle1*$^{Bj/Bj}$ cranial base mesenchyme at E12.5. These data support the hypothesis that the *Prickle1*^{Bj} missense mutation leads to a primary defect in intraflagellar transport that causes swollen cilia which subsequently increases HH signaling due to defective translocation of SMO and/or GliA/R to or from the cilia. Therefore, we further hypothesize that increased HH signaling is the major contributor the Robinow-like phenotypes in the *Prickle1*$^{Bj/Bj}$ mutants. We propose the *Prickle1*$^{Bj/Bj}$

as a model to study Robinow Syndrome, the crosstalk between the HH pathway and the Wnt/PCP signaling and to determine if targeted therapies can modify Robinow Syndrome phenotypes. To test this hypothesis, we will approach it with three different experimental paradigms. We will determine if both the axoneme and the ciliary membrane are normal in *Prickle1*$^{Bj/Bj}$ mutants using double immunofluorescence staining to intraflagellar transport proteins and ciliary membranes. We will determine if dampening HH signaling with Vismodegib can improve the *Prickle1*$^{Bj/Bj}$ craniofacial phenotypes. Further, we will directly test if HH signaling is increased in Human Robinow Syndrome fibroblast cells and if it can be reduced with Vismodegib.

2.0 Materials and Methods

2.1 *Prickle1^{Bj}* mice, IACUC, breeding schema, genotyping

The *Prickle1^{Bj}* mouse lines are maintained as a heterozygote line, outbred to wildtype C57/Bl6^{j} individuals purchased from Jackson Laboratories. The founder male was received from the Lo lab at University of Pittsburgh (Gibbs et al., 2016). The animal work described in this thesis is approved by the University of Pittsburgh Institutional Animal Care and Use Committee. To obtain *Prickle1$^{Bj/Bj}$* mutants we interbred *Prickle1$^{Bj/+}$* females and males. We recovered the expected Mendelian ratios of *Prickle1$^{+/+}$, Prickle1$^{Bj/+}$* and *Prickle1$^{Bj/Bj}$* embryos. For embryo collection, or treatment we performed timed mating, where presence of the plug was designated at Embryonic Day 0.5 (E 0.5). On the appropriate day of pregnancy (e.g. E 10.5 or E 14.5) we euthanized the pregnant dam by CO_2 asphyxiation and confirmed the embryonic development stage of the harvested embryos and fetuses based on their anatomical morphologies.

To genotype the embryos and mating adults, we collected a small sample of tissue and digested it using proteinase K. We removed proteins and lipids using supersaturated NaCl and cleared the supernatant with centrifugation. We precipitated DNA using isopropanol and washed with 70% ETOH. We air-dried the extracted DNA for 5 minutes before dissolving in 100 µl or 500 µl 0.1X TE. We determined DNA concentration with the NanoPhotometer and I adjusted the final concentration to 10 ng/µl. The genotyping PCR was performed using 5.5 µl TaqMan PCR Genotyping master mix, 0.5 µl Prickle1 TAQMAN assay (AH7041R), and 4.5 µl of 10 ng/µl DNA. The genotyping PCR reaction was run on the StepOne Q-PCR system. The Prickle1 TAQMAN assay has the wildtype allele with a VIC reporter, and the *Prickle1^{Bj}* allele with the FAM reporter.

The genotype is assigned by the relative abundance of amplicons with either the VIC/FAM signals after amplification.

2.2 Vismodegib oral gavage.

We inhibited HH signaling with Vismodegib (GDC-0049) from E10.5 to E13.5, a time range corresponding to primary and secondary palate formation (Table 1; Figure 5). We administered Vismodegib, via oral gavage. Vismodegib stock concentration is made in DMSO at 85 mg/ml; 200mM. For gavage the drug was sequentially diluted to the working concentration by adding the diluents in this order: 2% DMSO, 30% PEG300, 5% Tween 80 and distilled water. For the control group, we used the equivalent volume we replaced the Vismodegib with an equivalent amount of DMSO. We gavaged pregnant *Prickle1*$^{Bj/+}$ females with no more than 250 ul of fluid by passing a flexible plastic feeding needle through the mouse mouth to its stomach. Following oral administration, each mouse was observed for signs of distress and resumption of normal behavior. We treated three experimental groups for Vismodegib treatment. Each pregnant mouse received a dose concentration of Vismodegib at either 15mg/kg, or 30 mg/kg, or 60 mg/kg. All the pregnant mice were weighed daily before the oral feeding, to allow for the adjustment of the volume of drug for changes in body weight of the mouse.

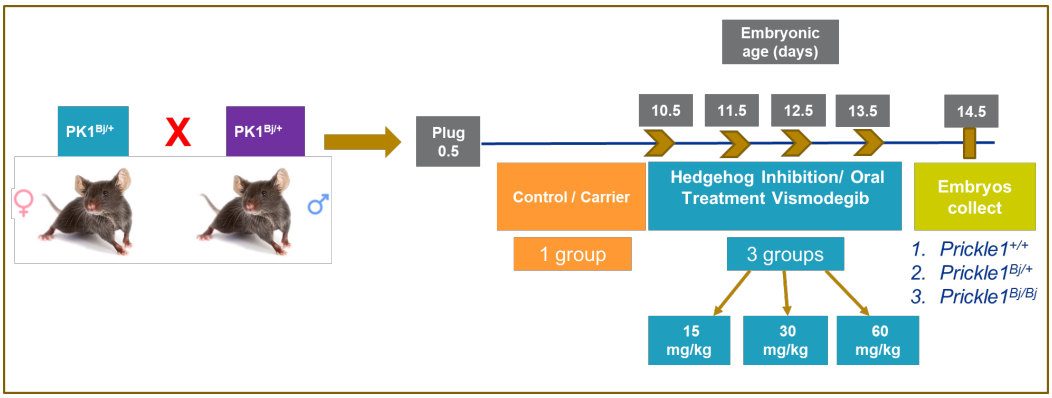

Figure 5: Experimental design of HH dampening.

We crossed adult *Prickle1*$^{Bj/+}$ females and males, and used time-pregnant females for dampening HH signaling. We treated three experimental groups with either Vismodegib (GDC-0449) 15 mg/kg, 30 mg/kg, or 60 mg/kg from pregnancy day E 10.5 to E 13.5. For the control group, the pregnant dams received the carrier (2% DMSO, 30% PEG300, and 5% Tween-80). We collected the embryos on E14.5 and analyzed all genotypes.

Table 1: Animal experiment litters, fetuses genotypes

Parameters	Control (DMSO)	15mg/kg	30mg/kg	60mg/kg
Females (n)	2	1	5	3
False plug	3	0	1	1
Fetuses collected	0	8 WT: 2 Het: 5 MT: 1	25 WT: 5 Het:18 MT: 2	11 WT: 3 Het: 2 MT: 4
Litter size	-	Litter1: 8	Litter 1: 7 Litter 2: 8 Litter 3: 6 Litter 4: 4	Litter 1: 9 Litter 2:

2.3 Histology and paraffin sectioning

Following harvest and dissection, E10.5 and E14.5 *Prickle1* ^{Beetlejuice} embryos/fetuses were washed in PBS buffer, and fixed overnight at 4° C in PFA. On day two, they were post-fixed in 70% ETOH and stored at -20° C for at least 24 hours before histological tissue processing. We performed both manual and automated tissue processing techniques before embedding the samples in paraffin blocs that we sectioned in 0.8 μm thickness. The sections were placed on TESPA ((3-aminopropyl) triethoxysiloxane)- treated slides. We stored the sections on slides at 4° C.

2.3.1 Double Immunofluorescence of medial nasal prominences

We used double immunofluorescence labelling to assay the ciliary particles and HH components. We studied ciliary morphology by using antibodies against

Table 2: Primary Anibodies used in this thesis

Component	Cilia compartment	Supplier/catalog #	Raised in/used for:
ARL13b	Ciliary Membrane	17711-1-AP, Proteintech	Rabbit/IF
acetylated α-tubulin	Ciliary Axoneme	T7451, Sigma-Aldrich	Mouse/IF
IFT-88	Anterograde transport	13967-1-AP, Proteintech	Rabbit/IF
IFT-52	Anterograde transport	17534-1-AP, Proteintech	Rabbit/IF
IFT-122	Retrograde transport	19304-1-AP, Proteintech	Rabbit/IF
IFT-140	Retrograde transport	17460-1-AP, Proteintech	Rabbit/IF
SMO	HH receptor	ab 113438, Abcam	Rabbit/IF
Gli2	HH responsive transcription factor	ab223651, Abcam	Goat/IF
γ-tubulin	Basal body		Rabbit/IF
Prickle1 F5	?	Sc-393034, Santa Cruz	Mouse/IF
Gli3	HH responsive transcription factor	AF3690, R &D	Rb/WB
IF, immunoflourescence; WB, western blotting			

On day 1, after dewaxing and rehydration, the slides were washed twice with PBS and pretreated with 0.3% hydrogen peroxide in PBS for 10 minutes. We performed antigen retrieval

with proteinase K (1µg/ml) in proteinase K buffer (0.1 M Tris pH 8.0, 5 mM EDTA pH 8.0,) for 10 minutes. The slides were blocked for 30 minutes at room temperature in 10% goat serum, PBS, and 0.1% Triton X-100 blocking buffer. We incubated the samples overnight at 4°C with primary antibodies diluted in the blocking buffer solution at a concentration of 1:100. On day 2, we washed the slides three times with PBS for three minutes to remove the primary antibodies solution. Then, we incubated the slides with the secondary antibodies (1:200) at room temperature for one hour and twenty minutes. After washing the secondary antibodies off, we applied DAPI for 5 minutes and mounted the slides using glass coverslips with Prolong gold (Invitrogen, P10144). In some experiments, we utilized mounting medium containing DAPI and Prolong Gold anti-fade (Invitrogen, P36935).

2.3.2 Hematoxylin and Eosin staining

To study the histological structure, we stained the sections with hematoxylin to stain the cytoplasm and counterstained nuclei with eosin following standard H & E protocols.

2.3.3 Alcian Blue and Picro-Sirius Red staining

We visualized the nasal cartilage, the vomeronasal organ, and the state of mineralization of Vismodegib-treated fetuses at E14.5 via Alcian Blue and PicroSirius Red. Alcian blue will stain glycosaminoglycans in cartilage and Sirius Red binds to collagens in bone. The sections were dewaxed, rehydrated, and treated for 10 minutes in 0.5% acetic acid. We stained with Alcian Blue (1%) for 10 minutes in 3% acetic acid (pH 2.5). We removed excess Alcian Blue stain by washing twice with 0.5% acetic acid for 3 minutes. Then, we stained with 0.5% Sirius Red in saturated

Picric Acid for one hour in the fumehood. We rinsed Picro-Sirius Red stain with acetic acid, dehydrated the sections with 100% ethanol and xylene, and mounted using Thermo Scientific Mounting Medium 4111.

2.3.4 Whole-mount alizarin red and alcian blue staining

We dissected the forelimbs and hindlimbs of Vismodegib-treated embryos at 30 mg/kg and performed skeletal preparation with alizarin red to stain mineralized tissue and alcian blue, for glycosaminoglycans and glycoproteins in cartilage. We followed the staining method published from (Gibbs et al., 2016; Wan et al., 2018).

2.4 Transmission Electron Microscopy

We studied ciliary morphology of E10.5 embryos using transmission electron microscopy. Following dissection, we fixed the embryos in Karnovsky's fixative solution (1% paraformaldehyde, 1.25% glutaraldehyde in PBS) for at least one hour. We washed the samples three times with PBS for 15 minutes, each. Following this we continued for chemical staining with 1% osmium tetroxide and potassium ferrocyanide for 1 hour. We rinsed the samples with PBS before dehydration, for 15 minutes each, in increasing gradient of ethanol. The samples remained overnight in 70% ETOH at 4˚C. On day 2, we continued the dehydration process until 100% ethanol. After the samples were in 100% ethanol, they were rinsed twice in propylene oxide solution for 10 minutes each. We carried out the infiltration preparation process overnight on fumehood in solution of 1:1 Epon and Propylene Oxide. On day 3, we finished samples infiltration

with Epon for four hours, and replaced new Epon solution every hour at room temperature. We embedded the samples in Epon at 37° C for 24 hours and cured at 60° C for 48 hours. The samples were sectioned with diamond knife and cut at a thickness of 70 nm.

2.5 Cell culture experiments

In collaboration with Dr. Louis Rapkin, we obtained a skin punch biopsy from a Robinow Syndrome patient following informed consent. In a sterile biosafety cabinet, we dissected the specimen into small pieces that we placed on tubes containing 2.5% trypsin for overnight digestion. We neutralized trypsin digestion with fresh medium; and we removed tissue debris before plating four petri dishes with the cells in DMEM + 20% FBS, Glut, and ABAM. We incubated those plates in a humidified incubator at 37°C and 5% CO_2 in air. We exchanged the cultured medium every 2–3 days. When the cells reached confluency, we trypsinized and plated them for sets of experiments. For a subset of experiments, we plated the cells on a 22 X 22 coverslip in a 6-well dish.

We performed immunofluorescence assessment of cilia morphology with antibodies to: acetylated α-tubulin, γ-tubulin, ARL13b, SMO, GLI2, Prickle1 (Table 2). We followed this immunofluorescence staining protocol: We performed antigen retrieval with proteinase k treatment (1μg/ml) at room temperature for 15 minutes. We blocked in PBS + 10% FBS buffer, and we incubated the slides with the following primary antibodies at 1:100 unless otherwise except: Smo at 1:200). We used secondary antibody in concentration of 1:200. We mounted the slides with glass coverslips with prolong gold containing DAPI for confocal imaging.

In the second set of experiments, we tested the effects of Vismodegib (HH inhibitor), and Purmorphamine (HH agonist) on RS cultured human fibroblasts. We plated the cells on coverslips in six well dishes before serum starvation in DMEM and glut for 48 hours. We applied DMSO for the control group, and different concentrations of Vismodegib or Purmorphamine plus a combination in the treatment group: 1) 1 μM Vismodegib, 2) 10 μM Vismodegib, 3) 100 μM Vismodegib, 4) 50 μM Purmorphamine, and 5) 100 μM Vismodegib + 50 μM Purmorphamine. After 24 hours of treatment, we fixed the cells in 2% PFA followed by immunostaining.

2.6 Western Blot

RS-fibroblasts cells were harvested in RIPA buffer and lysed through freezing at -80 and thawing and mechanically through pipette tip maceration. *Prickle1*$^{+/+}$ and *Prickle1*$^{Bj/Bj}$ embryos were collected at E10.5 and were stored at -80 until mechanical lysis in RIPA buffer. Prior to freezing we dissected the embryos into the face (including the medial, lateral and maxillary prominences) and limbs (fore and hindlimbs) for protein lysis. Protein was quantified by BCA (Biorad) and 10 mg/ well was run in a 4-12% Bis-Tris gel with MOPS buffer. The gel was transferred to PVDF membrane for 1.5 hours at 4°C. The membranes were dried, rehydrated, and blocked in 5% milk in TBST. The primary antibodies were used at 1:1000, the secondary 1:5000 (Gt antirabbit HRP), and GAPDH-Rhodamine (1:3000). We imaged the blots on the ChemiDoc MP using both chemiluminescence and fluorescence.

2.7 Imaging and images analysis:

We imaged the fluorescent slides on Olympus Confocal microscope 1000 using the 60X objectives with 2 times optical magnification. The images were captured as Z stacks with 0.2 μm steps with at least 25 slices/section. The littermates were captured with the same laser power, and exposure settings. We analyzed the images on Image J, and NIS Elements analysis software to generate maximum intensity projection of Z-stacks to analyzed ciliary morphology and measure ciliary axonemal length.

We captured the H&E and Picro-Sirius Red stained sections on Zeiss Axioskop A1 light microscope with an MrC450 Axiocam.

We performed Transmission Electron Microscopy on a JEM 1400Plus TEM at the Center for Biologic Imaging of the University of Pittsburgh with the expert help of Dr. Hajime Yamazaki and Dr. Mara L.G. Sullivan.

2.8 Statistical analysis

The maximum intensity projection of Z-stacks from Nikon Elements were opened in ImageJ. In ImageJ we counted the number of cells (via DAPI staining), the total number of cilia (based on acetylated α-tubulin staining), and the double positive cilia that included the protein of interest (ARL13B, IFT88, IFT140 & SMO) and acetylated α-tubulin. We then calculated the proportion of double positive cilia by taking the number of double positive cilia divided by the number of cilia in the image. The mean and standard deviation are presented in the graphs. Since

the presence of cilia is a categorical data, we used the Chi-squared test to determine statistical significance and calculate p-values.

We evaluated ciliary length of the hRS fibroblasts based on acetylated α-tubulin staining. Each cilium was measured with the curved length measurement tool of the Nikon Analysis Software as many cilia were bent. We excluded from our measurement highly tortuous cilia. At least 5 cilia were measured for each treatment. We studied the variance between the samples via one-way ANOVA and Tukey HSD test to determine statistically significant differences between groups.

3.0 *Prickle1*^{Bj} protein affects intraflagellar transport and the localization of HH-signaling components in the medial nasal prominences.

3.1 Introduction:

The primary cilia are membrane-bound organelles that protrude in the extracellular environment. They are composed of a central shaft made of nine pairs of microtubules called the axoneme, a transition zone that formed a necklace that control ciliary composition and function, two basal bodies that attach the cilia to the cell body, and a specialized membrane that transduce mechanical and chemical signaling (Goetz and Anderson, 2010). During embryonic development, the primary cilia participate in diverse biologic functions that include regulation of the cell cycle, cell proliferation and survival, patterning, and organogenesis (Haycraft and Serra, 2008). They are required for the development of several organs such as the brain and the heart.

The cilia elongate into the extracellular environment using intraflagellar transport (IFT) to build the axoneme with cargo filled with proteins necessary for axonemal growth, ciliary membrane build-up, and maintenance. IFT transports cargo into and out of the cilia the cell aided by two molecular motor proteins (Kinesin and Dynein), and the IFT-A and IFT-B complexes. Intracellular ciliary assembly initiates after basal body docks to a ciliary vesicle and IFT complexes are the main ciliary particles that function to transport cargo into the cilia. Cilia can also be formed via direct binding to the plasma membrane and grow extracellularly.

The primary cilia direct many signaling cascades during embryonic development. The most studied is the HH pathway that coordinates left-right symmetry, patterning, and digits formation. Besides the numerous functions of HH ligands in organogenesis, SHH is spatiotemporally required

for palatogenesis. Proper HH signal transduction is intimately linked with ciliary structure (meaning having cilia in normal length and shape) because the cilia act as a reservoir for HH inhibitors and activators whose function depend on their ciliary or extraciliary location.

3.2 Results:

3.2.1 Prickle1 protein localization:

We tested the expression and the localization of Prickle1 in a pair of littermates by dual immunolabelling of ARL13B. Prickle1 was visualized in the nucleus of both mutant and wild-type embryos in the medial nasal prominences at E 10.5 (Figure 6: Intracellular localization of Prickle1 in MNP of E10.5 *Prickle1*$^{+/+}$ and *Prickle1*$^{Bj/Bj}$.). In the *Prickle1*$^{Bj/Bj}$ cilia, Prickle1 signal is adjacent to the ARL13B signal, in comparison to the wildtype where the two signals colocalized (Figure 7). This result suggests that Prickle1 may physically interact with members of the ciliary membrane.

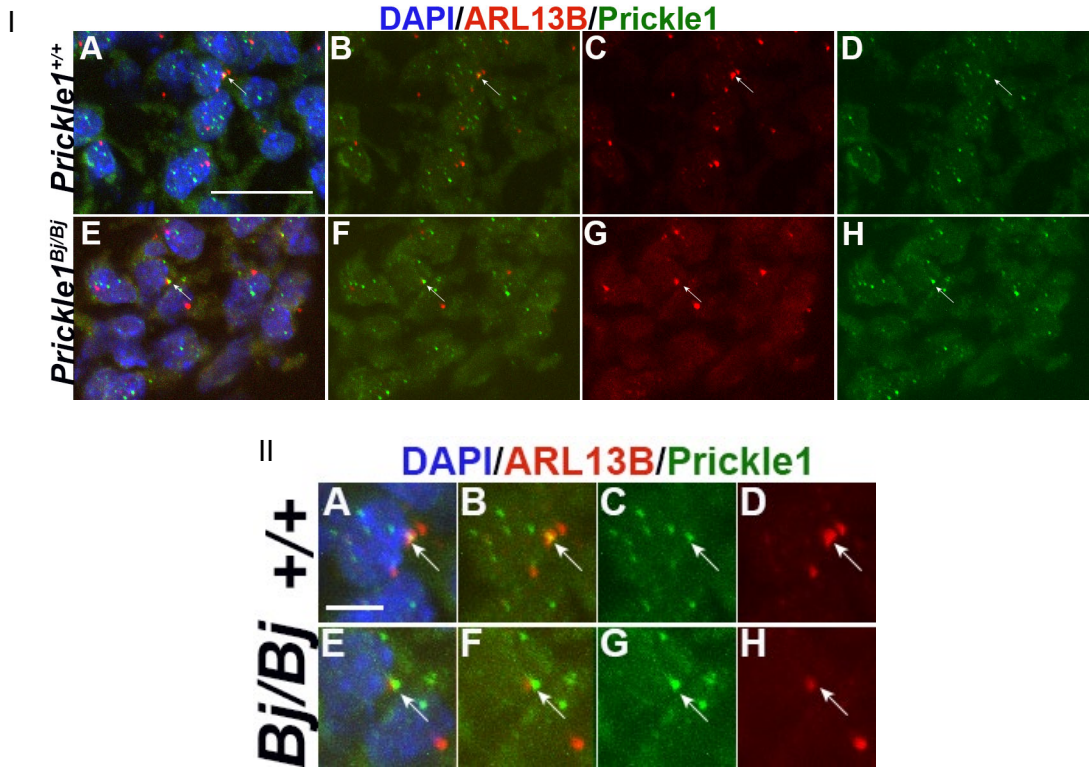

Figure 6: Intracellular localization of Prickle1 in MNP of E10.5 *Prickle1*$^{+/+}$ and *Prickle1*$^{Bj/Bj}$.

(I) Maximum intensity projection images of Z-stacks representing single channel and combination performed on dual immunofluorescence labelling of Prickle1 and ARL13B in *Prickle1*$^{+/+}$(A-D) and *Prickle1*$^{Bj/Bj}$ (E-H) medial nasal prominences. Prickle1 protein is localized in bright puncta in the nucleus in both genotypes (A, E). (A-D) Prickle1 and ARL13B colocalize in the *Prickle1*$^{+/+}$ cells (arrows). (E-H) Prickle1^{Bj} is detected adjacent to the ARL13B signal, and not colocalized in the ciliary axoneme (arrow). White arrows pointing at cilia. (II) images of a single cilia from I. Scale bar in IA= 40 µm applies to IB-IH; in IIA=10 µm and applies to IIB-IIH .

3.2.2 Increased HH signaling in the *Prickle1*$^{Bj/Bj}$ faces.

We tested the level of HH signaling in the upper face (including the medial nasal, lateral nasal, and maxillary prominences) and limbs of E10.5 *Beetlejuice* mutants by western blotting with antibodies that detect the C-terminus of Gli2 and Gli3 (Figure 7). The antibodies enable us to

detect the Gli Activator (GliA) and Gli Repressor (GliR) to calculate the ratio GliA to GliR to quantify the level of HH signaling. Gli2 and Gli3 are translated into a GliA form at ~190 kDa, and then proteolytically processed into a major species of the GliR at ~83 kDa. In some tissues, an additional GliR band is detected between ~60-75 kDa (Wang et al., 2000).

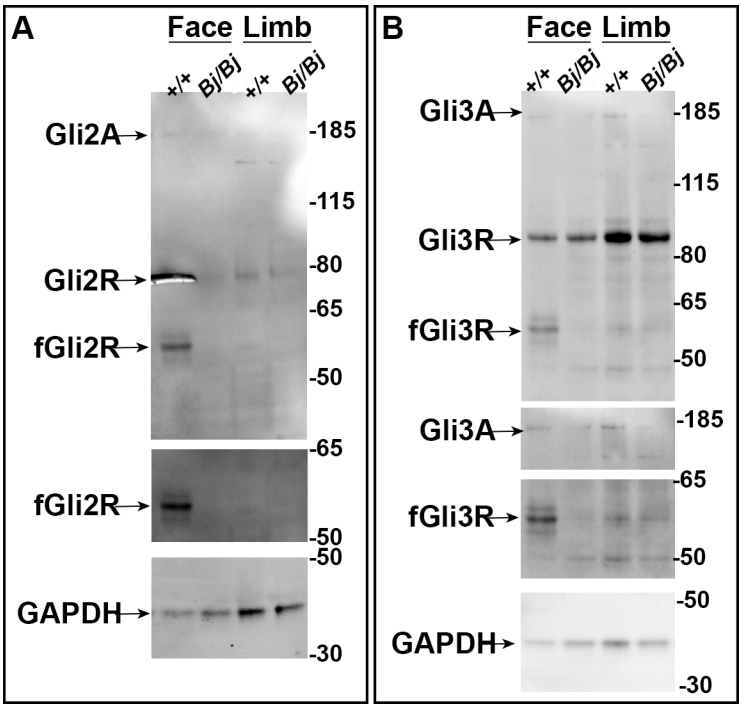

Figure 7: Defective GliR processing in the *Prickle1*$^{Bj/Bj}$.

Prickle1$^{Bj/Bj}$ mutants are experiencing increased HH signalling due to decreased abundance of GliR proteins. Facial and limb protein extracts subjected to western blotting with antibodies to Gli2 and Gli3. (A) Gli2R proteolytical processing is abnormal in the *Prickle1*$^{Bj/Bj}$ face and limbs. Wildtype face protein extracts contain 3 species of Gli2: Gli2A, Gli2R and fGli2R. Unfortuneately, the membrane is torn at the Gli2R species. The *Prickle1*$^{Bj/Bj}$ face does not have the lower molecular weight form fGli2R. The *Prickle1*$^{Bj/Bj}$ limbs have decreased Gli2R. Longer exposures below confirm these findings. (B) Gli3R proteolytical processing is reduced in the *Prickle1*$^{Bj/Bj}$ faces. Similar to Gli2, Gli3 has 3 forms: GliA, GliR, and fGli3R in *Prickle1*$^{Bj/Bj}$ faces and limbs, while the fGli3R band is almost undetectable from both genotype limb extracts. The fGli3R species is almost undetectable in the *Prickle1*$^{Bj/Bj}$ face.

In the *Prickle1*$^{+/+}$ face protein extracts, we detected full length Gli2A, and Gli3A at approximately 190 kDa, Gli2R, and Gli3R at ~83kDa. Surprisingly, we also detected one additional cleavage product of Gli2R and Gli3R at ~60kDa, that we named fGliR. The fGliR band was weakly detected in the *Prickle1*$^{+/+}$ limbs (Figure 7). In the face extracts, we detected more Gli3A than in the *Prickle1*$^{+/+}$ face compared to the *Prickle1*$^{Bj/Bj}$ mutants (Figure 7, longer

exposure). In the face of the *Prickle1*$^{Bj/Bj}$ mutants, we only detected the Gli3R form, while the fGli3R is undetectable. The fGli3R, and fGli2R were present with similar low abundance in the *Prickle1*$^{+/+}$ and *Prickle1*$^{Bj/Bj}$ limbs. The Gli3R ~83kDa was reduced in the *Prickle1*$^{Bj/Bj}$ limbs. From these data, we conclude that there is a net gain of HH signaling in *Prickle1*$^{Bj/Bj}$ mutants, resulting from the loss of the fGli2R, and fGli3R in the face, and the decreased abundance of Gli2R ~83kDa and Gli3R ~83kDA isoform. Based on this finding, we hypothesize that the Prickle1 missense mutation impairs the homeostasis of HH signaling, by affecting the processing of GliR.

3.2.3 *Prickle1*$^{Bj/Bj}$ have ciliary morphology and length defects but can use both ciliogenesis pathways

3.2.3.1 STED Microscopy

Previous work in our laboratory explored the ciliary morphology in the E11.5 cranial base using Super-resolution Stimulated Emission Depletion (STED) microscopy. STED microscopy was used to visualize the cilia axoneme labeled with acetylated α-tubulin. Super-resolution STED microscopy bypasses the diffraction limit of conventional confocal microscopy. These images were taken on Leica Stimulated Emission Depletion (STED) 3X microscope with 3 depletion lines with a 100x objective lens and 10x optical zoom. In the *Prickle1*$^{+/+}$control littermates, ciliary axonemes were visualized in a rod shape with small curvatures or bending (Figure 2, panel G, I). But the *Prickle1*$^{Bj/Bj}$ axonemes exhibited, swollen morphology. The bulges were located at the tip or along the axonemes (Figure 2, panel H, J.). In addition, those swollen cilia of the *Prickle1*$^{Bj/Bj}$ mutants appeared shorter compared to the axonemal length of the *Prickle1*$^{+/+}$control littermates (n=5 cilia/genotype).

3.2.3.2 Ciliary membrane and morphology

We re-examined the ciliary morphology and axonemal length of *Prickle1*$^{Bj/Bj}$ mutants by studying the primary cilia of medial nasal prominences and neuroepithelial cells of embryos harvested at E10.5. We studied the expression of ciliary membrane marker ARL13B via dual immunolabelling with acetylated α-tubulin (Figure 8). Immunofluorescent ciliary staining demonstrated the location of ARL13B and acetylated α-tubulin in both *Prickle1*$^{Bj/Bj}$ mutants and *Prickle1*$^{+/+}$control littermates in a similar pattern. Acetylated α-tubulin was present in the axoneme, and ARL13B extended along the ciliary axoneme and the ciliary membrane. Both proteins colocalized in the middle of the ciliary axoneme where we detected a yellow signal. However, there are significantly fewer *Prickle1*$^{Bj/Bj}$ cilia exhibiting colocalization of ARL13B and acetylated α-tubulin staining, it is far more common to ARL13B-positive puncta adjacent to the acetylated α-tubulin. However, the mutant had less double positive cilia for both markers (Figure 8). A defective intraflagellar protein transport may explain the uncoupled mechanism of membrane biogenesis and ciliary elongation in the *Prickle1*^{Beetlejuice} mutant: ARL13B can be stuck in the membrane because it does not surround the cilia, and ciliary axonemal elongation can be impaired as acetylated α-tubulin can be trapped in the cells.

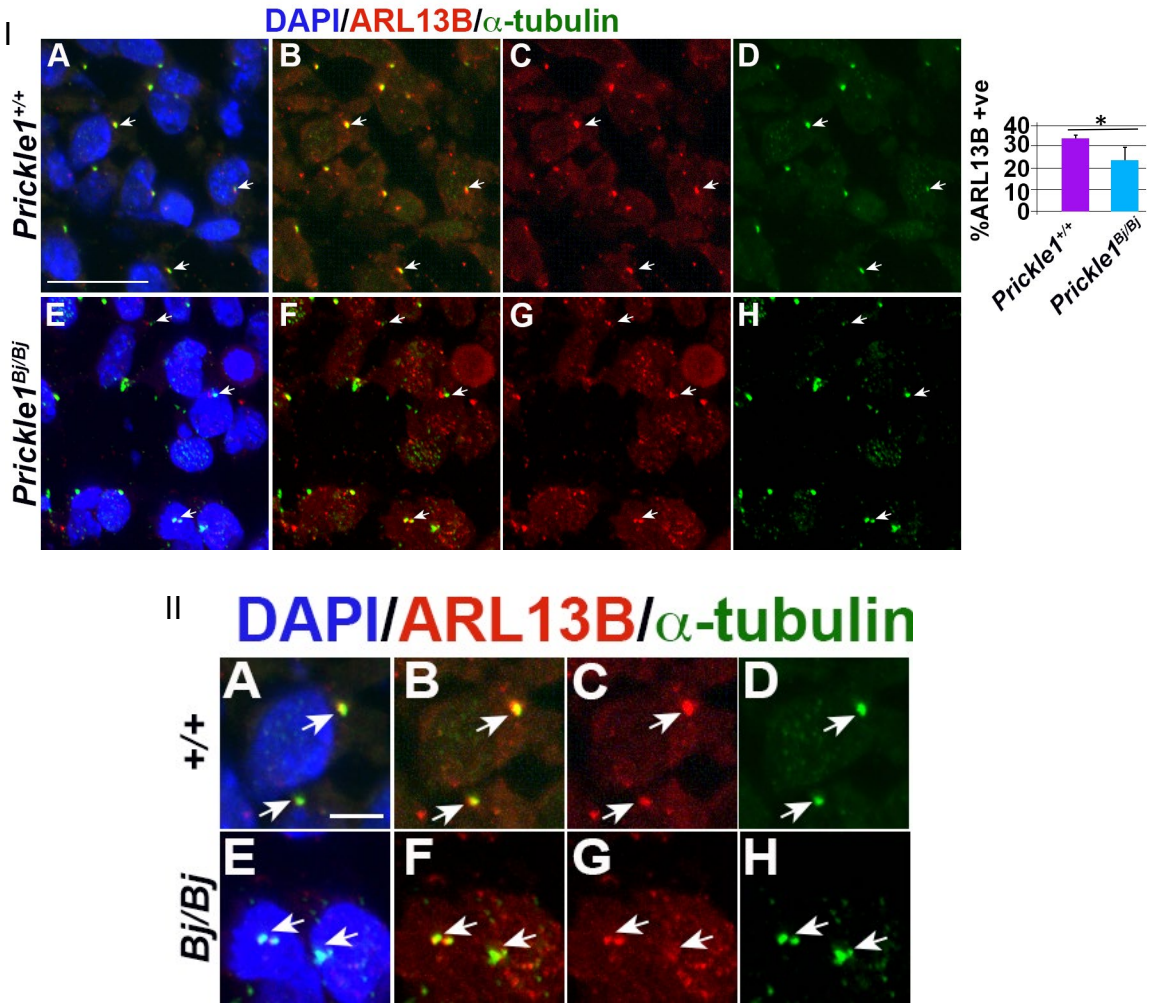

Figure 8: Decreased colocalization and proportion of of ARL13B and acetylated α-tubulin double positive cilia suggests impaired ciliary membrane synthesis in *Prickle1*$^{Bj/Bj}$ in the MNP at E 10.5.

Via double immunofluorescence labelling for antibodies against ARL13B and acetylated α-tubulin, we localized ARL13B in the cilia and other cellular compartments (IA-H; IIA-H). For some cilia in *Prickle1*$^{Bj/Bj}$ (E,F), the pattern of colocalization was similar to staining in control littermates (A-B). But, fewer cilia were positive for both antibodies, and ARL13B was more frequently adjacent to the acetylated α-tubulin (F). The percentage of cells with cilia that colocalized ARL13B and acetylated α-tubulin at E 10.5 (3 Prickle1$^{+/+}$ embryos, 275 cells; 3 *Prickle1*$^{Bj/Bj}$ embryos, 246 cells). Chi-square test, p-value= 0.014300885. (II) Inset view of two cilia showing ARL13B and acetylated α-tubulin from (I). Error bars= standard deviation. Scale bar in I = 40 µm and applies to all; II = 10 µm applies to all.

Both ARL13B and acetylated α-tubulin are used to measure the length of cilia (Caspary et al., 2007; Larkins et al., 2011). As expected, the *Prickle1*$^{+/+}$ control littermate exhibited homogeneous cilia in length and shape (Figure 8). Importantly, the *Prickle1*$^{Bj/Bj}$ cilia displayed a ranged of shape and length (Figure 8). Some appeared shorter, bulged, irregularly long, dysmorphic, twisted or folded in manner that render length measurement difficult in immunofluorescent sections. Thus, the trafficking of ciliary components is be impaired in the *Prickle1*$^{Bj/Bj}$ medial nasal prominence.

3.2.3.3 *Prickle1*$^{Bj/Bj}$ are capable to forming cilia in both intracellular and extracellular ciliogenesis

To determine if the ultrastructure of the cilia was affected in the *Prickle1*$^{Bj/Bj}$ mutants, we performed Transmission electron microscopy (TEM). We observed that the ciliary membrane was present. We found that the *Prickle1*$^{Bj/Bj}$ mutants maintain the ability to use both the intracellular and the extracellular ciliogenesis pathways (Figure 9). In the neuroepithelial cells, TEM showed growing cilia in their ciliary vesicles deep inside the cell body confirming the ability to use the intracellular route (Figure 9). It also revealed elongated cilia docking near the plasma membrane that characterizes the extracellular pathway. Based on these results, we can conclude that the ciliogenesis pathways are not affected in the *Prickle1*$^{Bj/Bj}$ mutants.

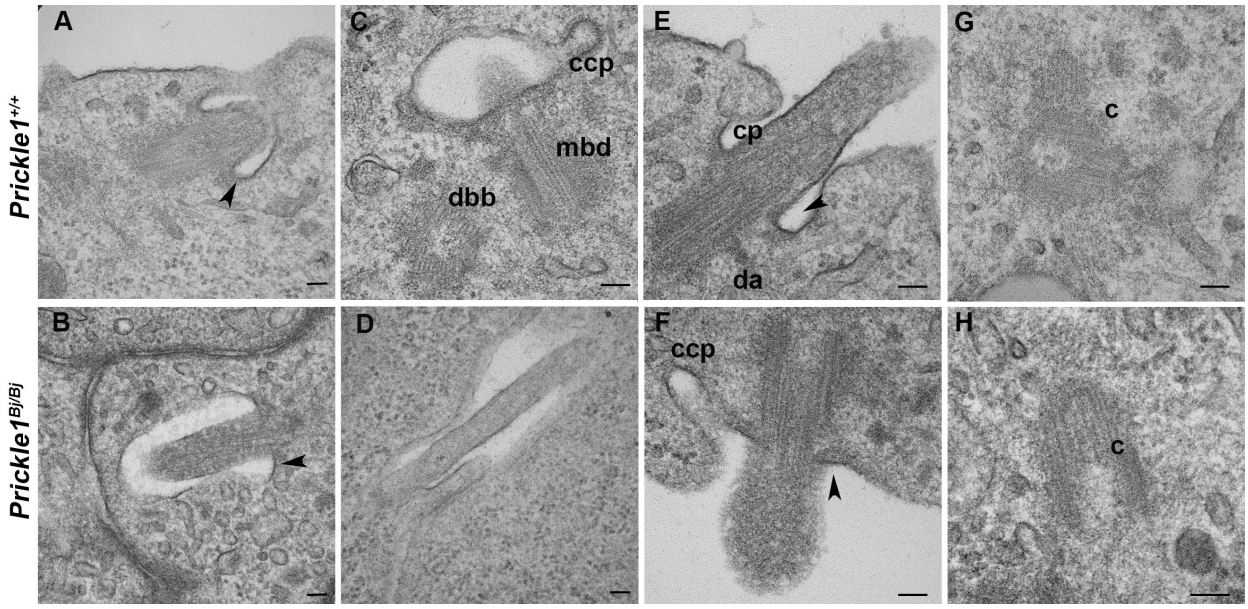

Figure 9: The *Prickle1*$^{Bj/Bj}$ has a widened ciliary pocket and length defects at E 10.5.

Transmission electron microscopy (TEM) revealed no sigificant defect in the ultrastructure of the cilia and centrioles of neuro-epithelial cells in *Prickle1*$^{Bj/Bj}$ mutants embryos compared to those of *Prickle1*$^{+/+}$ control littermates besides the widening of the ciliary pocket marked with black arrowheads (A- H). Cilia elongating inside a ciliary vesicle in the intracellular pathway of ciliogenesis (A, B). Abnormally elongated cilia in the mutant embryo (D). Presence of clathrin-coated pits (ccp) at the base of the ciliary vesicle of both wild-type and control littermates (C, F). Swollen cilia formed via the extracellular pathway with the basal bodies positioned close to the plasma membrane in the mutant embryo (F). No difference observed in the centrioles (c) of both embryos (G, H). c, centrosome; ccp, clathrin coated pit; cp, ciliary pocket; dbb= daughter basal body, da= distal appendage; mbd, mother basal body. e. Scale bar= 100 nm and applies to all.

3.2.3.4 Ciliary morphology and length

Using TEM, we imaged in the neuroepithelial cells, some bulged and long cilia in *Prickle1*$^{Bj/Bj}$ mutants (Figure 9). We observed the presence of clathrin-coated pits in the ciliary vesicles of elongating cilia, and in the ciliary pocket in both groups. No difference was observed in the ultrastructure of the basal bodies and the centrioles of *Prickle1*$^{Bj/Bj}$ mutants. However, the ciliary pocket was flattened in some ciliated cells in the mutants. The *Prickle1*$^{Bj/Bj}$ ciliary pocket is

wider and not as deep (Figure 9B-F). The defects in the ciliary pocket suggest that the transition between the ciliary and plasma membrane is disrupted and may cause proteins transport dysregulation in the cilia.

3.2.4 *Prickle1*$^{Bj/Bj}$ mutants have defective anterograde and retrograde intraflagellar transport

3.2.4.1 Anterograde Intraflagellar transport

Using TEM and immunofluorescence staining, we demonstrated that *Prickle1*^{Bj} mutation did not inhibit ciliogenesis in the neuroepithelial cells and in the medial nasal prominences. In E10.5 embryos, we determined the intraflagellar transport by looking at two components of the anterograde transport by using antibodies against IFT-88 and IFT-52. In *Prickle1*$^{+/+}$, IFT-88 is localized in the entire axonemal length, or delineated to the tip, or in dots along the axoneme, while little IFT-88 signal is detected in the cytoplasm (Figure 10). However, in *Prickle1*$^{Bj/Bj}$ mutants, IFT-88 is mainly present in dots at the ciliary tip and rarely present along the axoneme of *Prickle1*$^{Bj/Bj}$ mutants. In addition, IFT-88 is highly enriched in the cytoplasm, almost to the exclusion of the axoneme in *Prickle1*$^{Bj/Bj}$ animals as compared to control embryos. Nearly twice as many ciliated *Prickle1*$^{+/+}$ MNP cells [N (embryos) = 4; n (cells) = 286] had IFT-88-postive cilia compared to *Prickle1*$^{Bj/Bj}$ cells [N (embryos) = 4; n (cells) = 294] (p-value= 6.48677E-06) (Figure 10, I). This result suggests that anterograde transport is deficient in the *Prickle1*$^{Bj/Bj}$.

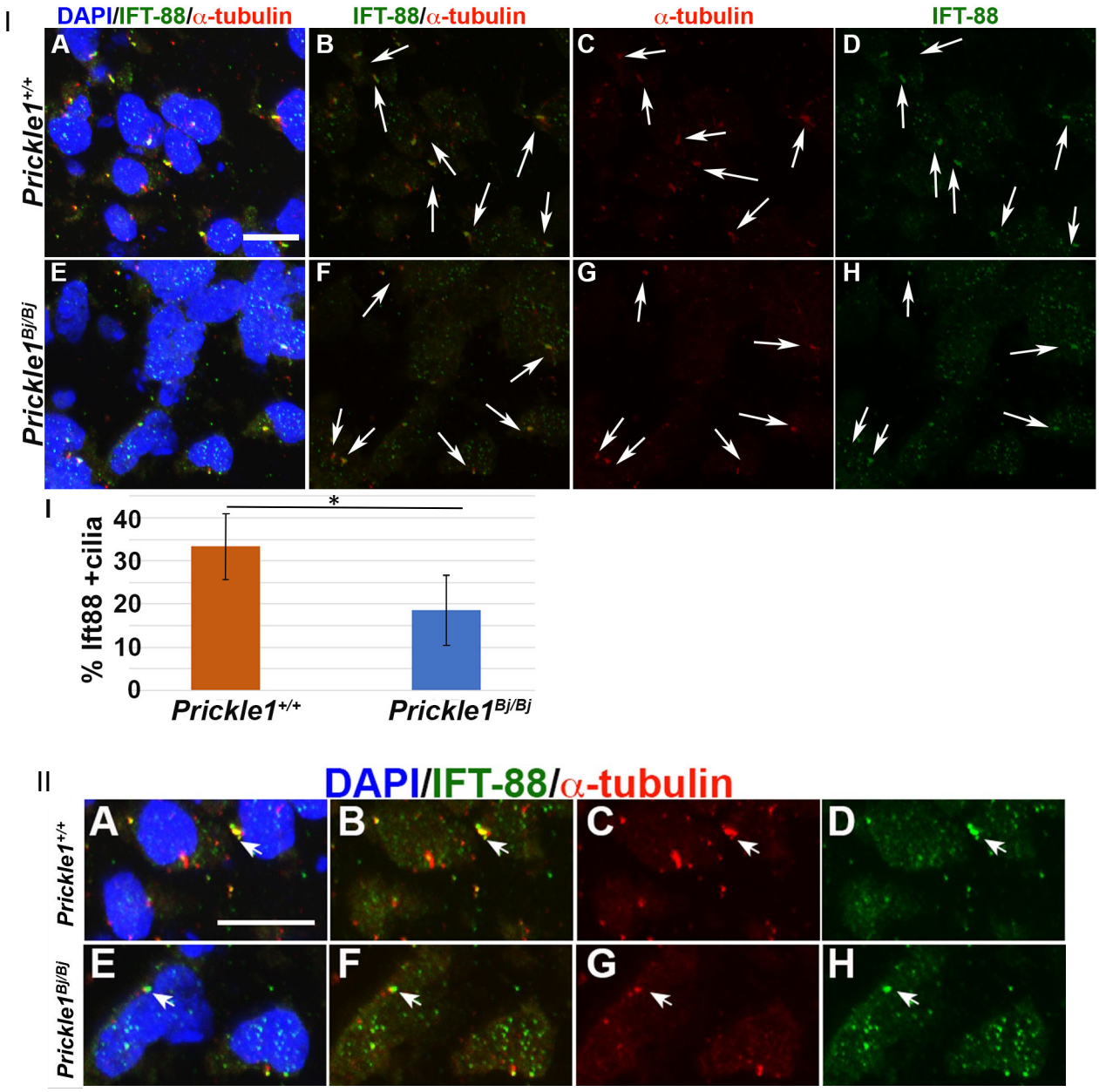

Figure 10: : Less IFT-88 abundance in the ciliary axonemes of the *Prickle1*$^{Bj/Bj}$ MNP at E10.5.

Dual immunoflourescence staining of IFT-88 and acetylated α-tubulin. (I) In *Prickle1*$^{+/+}$ cilia, IFT-88 is found at the tip, along the axoneme and at the base (IA-D,). While the *Prickle1*$^{Bj/Bj}$ cells IFT-88 remained mostly in the cytoplasm rather in the ciliary axonemes in the mutants compared to its expression in control littermates (D, H). (I I) Percentage of cells observed with colocalized IFT-88 and acetylated α-tubulin in *Prickle1*$^{+/+}$ and *Prickle1*$^{Bj/Bj}$ MNPs. Chi-square test, p-value = 6.48677E-06. High magnification images depicting single channels and combinations of dual immunolabelling for IFT-88 and acetylated α-tubulin in *Prickle1*$^{+/+}$ and *Prickle1*$^{Bj/Bj}$ (A-H). IFT-88 is found

along the entire axoneme in most cilia and colocalized with acetylated α-tubulin in *Prickle1*$^{+/+}$ (A-D). We observed decreased staining in the cilia and an enrichment in the cytoplasm in the *Prickle1*$^{Bj/Bj}$ (E-H). (I). Scale bar in I A= 10 µm, applies to B-H, IIA = 10 µm, applies to to B-H.

We further tested the function of anterograde transport by the localization of IFT52 protein, a component of the IFT-B2 complex (Figure 3). In *Prickle*$^{+/+}$ IFT52 was localized in the cytoplasm and in a lesser extent, in the ciliary axoneme (Figure 11). IFT-52 showed decreased abundance in the cytoplasm of the *Prickle1*$^{Bj/Bj}$ and few positive signals were found colocalized with acetylated α-tubulin in the ciliary axoneme. Our double immunofluorescence staining for acetylated α-tubulin varies from other figures presented because of difference in antigen retrieval as the IFT52 antibody worked with citrate buffer but not with Proteinase K.

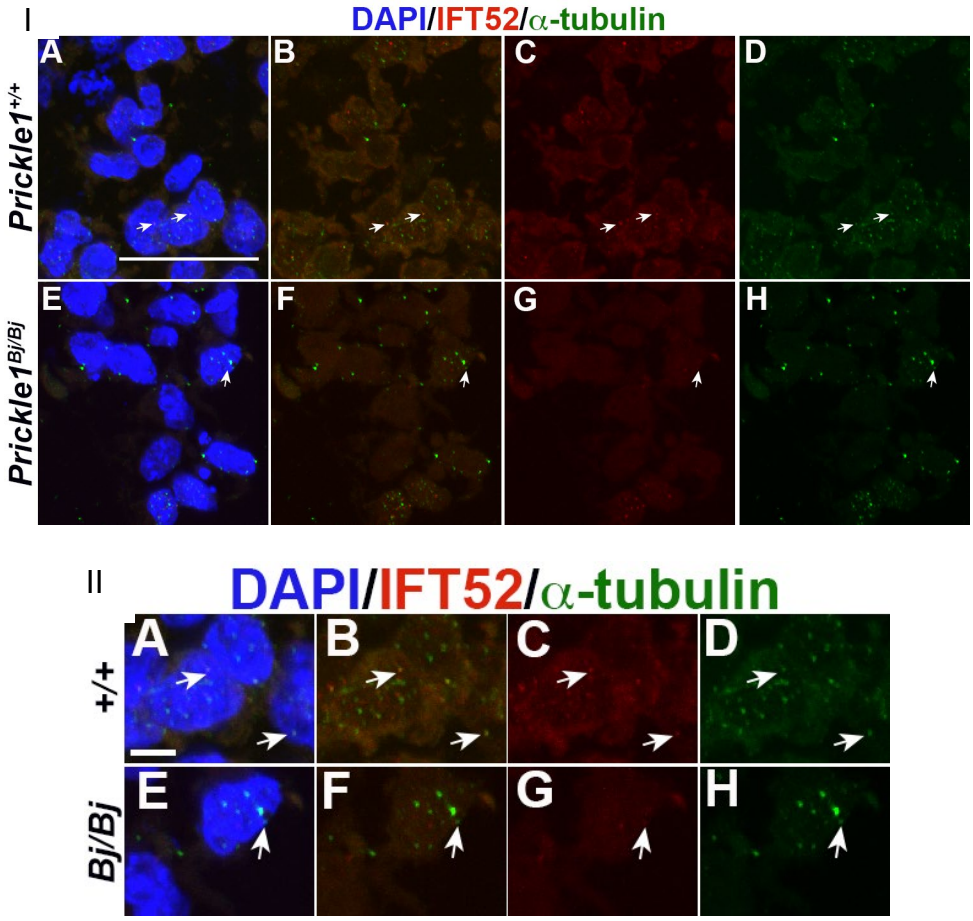

Figure 11: Decreased intracellular abundance of IFT-52 in the *Prickle1*$^{Bj/Bj}$.

Double fluorescence staining of MNP at E 10.5 showed decreased positive signals in the *Prickle1*$^{Bj/Bj}$ compared to the *Prickle1*$^{+/+}$ (C, G). White arrows pointing at IFT-52 in the cells of *Prickle1*$^{+/+}$ wild-type littermate (A-D), and in the *Prickle1*$^{Bj/Bj}$ mutant (E-H). (IIB) High magnification images depicting single channels and combinations of dual immunolabelling for IFT-52 and acetylated α-tubulin in *Prickle1*$^{+/+}$ and *Prickle1*$^{Bj/Bj}$ (A-H). IFT-52 abundance in the cells decreased in the *Prickle1*$^{Bj/Bj}$ (E-H) compared to *Prickle1*$^{+/+}$ (A-D).

Antigen retrieval with citrate buffer. Scale bar in IA= 40 μm, applies to B-H; in IIA =10 μm and applies to B-H.

3.2.4.2 Retrograde Intraflagellar Transport

We tested the efficacy of the retrograde transport by performing immunofluorescence staining with antibodies against two IFT-A particles: IFT-122 and IFT-140. Similar to the anterograde IFT particles, we showed a decreased expression of IFT-140 in the MNP of *Prickle1*$^{Bj/Bj}$ embryos (Figure 12). Only 3% of the *Prickle1*$^{Bj/Bj}$ ciliated cells had IFT-140 in the ciliary axoneme of the MNP compared to 11% in *Prickle1*$^{+/+}$ embryos (Chi-square test, p-value= 0.002549428) (Figure 13). In the control littermates, IFT-140 was localized at the ciliary tip and the basal portion of the axoneme. IFT-140 localization was similar in *Prickle1*$^{Bj/Bj}$ cilia.

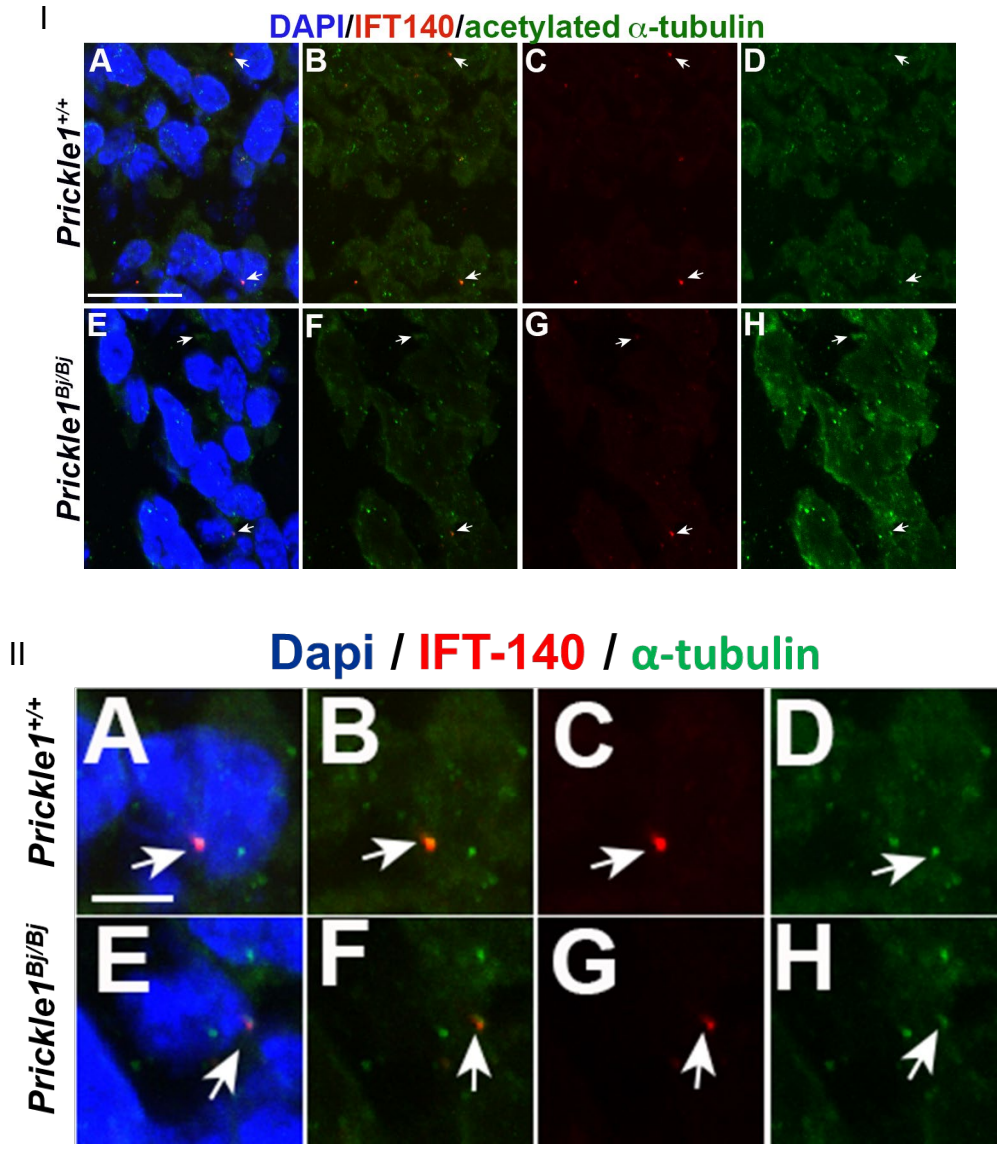

Figure 12: Intracellular localization of IFT-140.

IFT-140 was mainly localized in the ciliary tip and the base of the axoneme in *Prickle1*$^{+/+}$ control littermates similarly with *Prickle1*$^{Bj/Bj}$ mutants (I A-H). However, the mutants exhibited less double positive cilia for IFT-140 and acetylated α-tubulin (F, B). White arrows in pannels C and G showing IFT-140 positive signals in cilia; in D and H single , the ciliary axoneme. (II) High magnification images depicting single channels and combinations of dual immunolabelling for IFT-140 and acetylated α-tubulin in *Prickle1*$^{+/+}$ and *Prickle1*$^{Bj/Bj}$ (A-H). IFT-140 and acetylated α-tubulin colocalized in the cilia of *Prickle1*$^{+/+}$. In the *Prickle1*$^{Bj/Bj}$ cilia, they were adjacent to each other (E, F). White arrows on cilia. Scale bar in I A, and II A =10 μm, and applies to B-H.

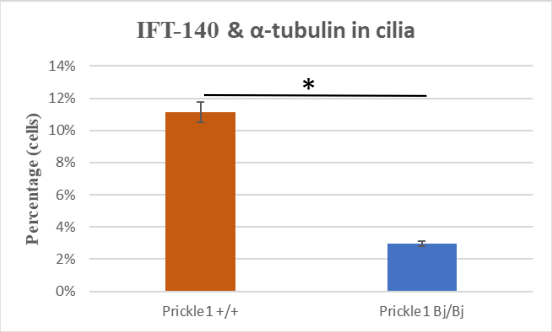

Figure 13: Proportion of cells that colocalize IFT-140 and acetylated α-tubulin in the ciliary axoneme.

We calculated the percentage average of cells that colocalized IFT-140 and acetylated α-tubulin in the cilia for 4 embryos at E 10.5 (2 *Prickle1*$^{+/+}$ n=209 cells; 2 *Prickle1*$^{Bj/Bj}$ embryos n= 206 cells). Chi-square test, p-value= 0.002549428. Error bars= standard deviation.

IFT-122 abundance was increased in the ciliary axoneme of *Prickle1*$^{Bj/Bj}$ embryos compared to *Prickle1*$^{+/+}$ embryos (Figure 14). We observed IFT-122 protein in the *Prickle1*$^{Bj/Bj}$ in one side along the axoneme of *Prickle1*$^{Bj/Bj}$ embryos, but it was found mostly at the ciliary tip of *Prickle1*$^{+/+}$ embryos. Decreased IFT-140 in the cell body and increased staining within the axoneme in the *Prickle1*$^{Bj/Bj}$ mutants, support the conclusion that the mechanism that facilitates the trafficking of retrograde IFT components is blocked. The inability of the IFT particles to return to the cell may be responsible for the dysmorphic ciliary shape causing it to swell or elongate. These results suggest that transport of retrograde IFT particles require Prickle1 function.

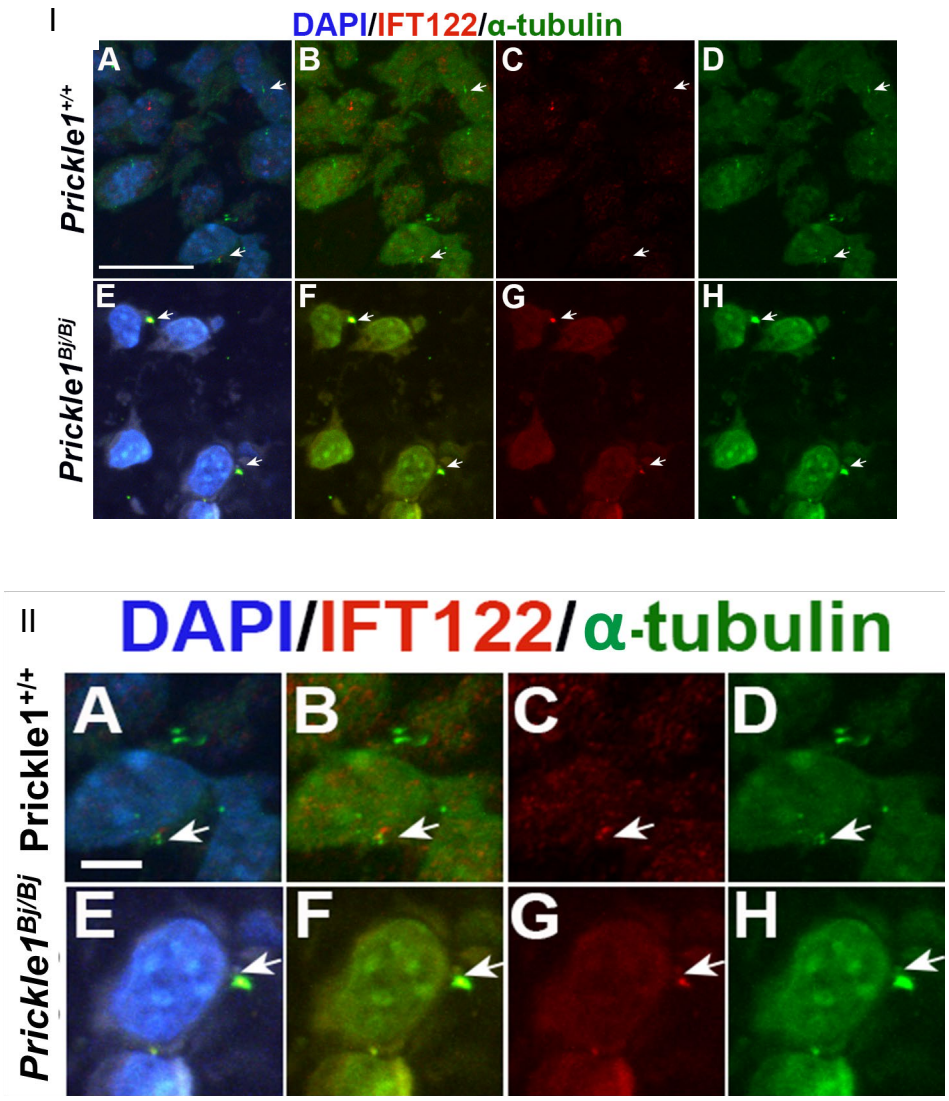

Figure 14: Retention of IFT122 in the *Prickle1*$^{Bj/Bj}$ cilia suggesting defective retrograde transport.

IFT-122 is enriched in localized in the cilia and the cells in the *Prickle1*$^{+/+}$ (I A-C). In the *Prickle1*$^{Bj/Bj}$ IFT-122 is exclusively localized in the cilia in bright puncta in one side of the axoneme (I E-G). From yellow signals, we showed colocalization with acetylated α-tubulin (I E-F). White arrows on normal cilia in *Prickle1*$^{+/+}$ (I D), and a bulged cilia in *Prickle1*$^{Bj/Bj}$. (II A-H) High magnification images depicting single channels and combinations of dual immunolabelling for IFT-122 and acetylated α-tubulin in *Prickle1*$^{+/+}$ and *Prickle1*$^{Bj/Bj}$ (A-H). IFT-122 and acetylated α-tubulin are visualized in the ciliary tip and base as distinct puncta in *Prickle1*$^{+/+}$. In the *Prickle1*$^{Bj/Bj}$ cilia (E, H), IFT-122 was enriched in one side of the cilia forming a bulge. Scale bar IA = 40 µm, applies to B-H; IIA =10 µm

3.2.5 Intracellular location of SMO and Gli2 proteins

We studied the effects of *Prickle1* missense mutation on SHH signaling by mapping the intracellular location of two proteins: Smo (the receptor) and Gli2 (transcriptional activator). We detected Smo staining in the cytoplasmic region of the cells of both control and mutant embryos. We also visualized Smo along the ciliary axoneme and closely adjacent to the base of the axoneme in the *Prickle1*$^{+/+}$ (Figure 15). However, more *Prickle1*$^{Bj/Bj}$ cilia contained Smo inside the axoneme and the ciliary tip and colocalized with acetylated α-tubulin, Chi-square test, p-value= 1.08832E-05 (Figure 16). This result suggests an increased translocation of Smo in the cilia of *Prickle1*$^{Bj/Bj}$ mutants.

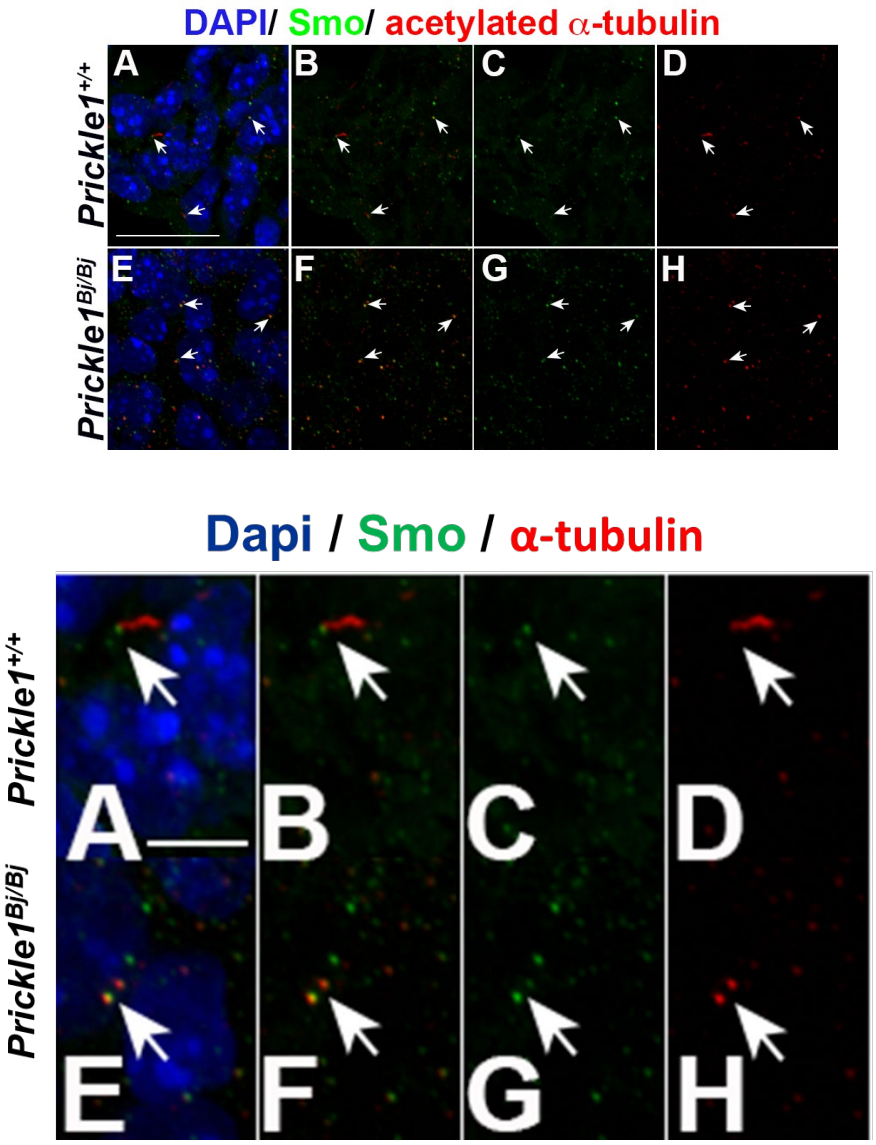

Figure 15: Intracellular localization of SMO.

SMO is mapped in the cilia and close to the base of the axoneme in the *Prickle1*$^{+/+}$ (I A-D). More cilia in the *Prickle1*$^{Bj/Bj}$ colocalized SMO and acetylated α-tubulin (E-H). This increased abundance of SMO in the cilia is suggestive of high level of HH signaling in the MNP at E 10.5. (II A-H) High magnification images depicting single channels and combinations of dual immunolabelling for Smo and acetylated α-tubulin in *Prickle1*$^{+/+}$ and *Prickle1*$^{Bj/Bj}$ (A-H). Smo is visualized in one point in the cilia labelled with acetylated α-tubulin in the *Prickle1*$^{+/+}$ (A-D). In the *Prickle1*$^{Bj/Bj}$ cilia (E, F), Smo is enriched along the cilia. Scale bar in I A = 40 µm, and applies to I B-H; Scale bar in IIA = 10 µm, applies to IIB-H.

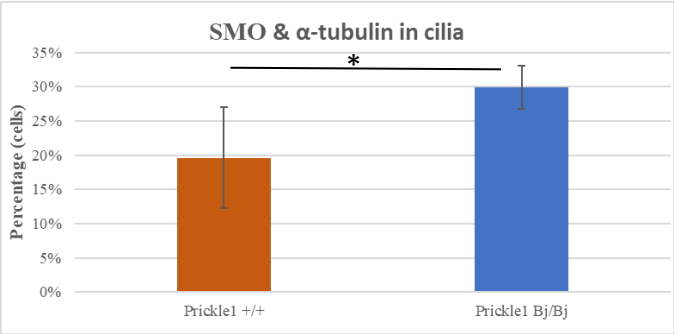

Figure 16: Proportion of cells that colocalize Smoothened and acetylated α-tubulin in the ciliary axoneme.

We calculated the percentage average of cells that colocalized Smo and acetylated α-tubulin in the cilia for 6 embryos at E 10.5 (3 *Prickle1*$^{+/+}$ embryos n=178 cells; 3 *Prickle1*$^{Bj/Bj}$ embryos, n=186 cells). Chi-square test, p-value= 1.08832E-05. Error bars= standard deviation.

In *Prickle1*$^{+/+}$, Gli2 is localized in the nucleus and in a few cilia of the control embryos. Similarily to Smo localization, we observed a greater number of Gli2- positive cilia in *Prickle1*$^{Bj/Bj}$ mutant MNP compared to *Prickle1*$^{+/+}$ (Figure 17). Gli2 was observed at the ciliary tip, along the axoneme in the nuclei and other cellular compartments of in both embryos. Intriguingly, we observed significantly increased Gli2 and SMO staining in the cytoplasm and cell body of the *Prickle1*$^{Bj/Bj}$ compared to wildtype littermates.

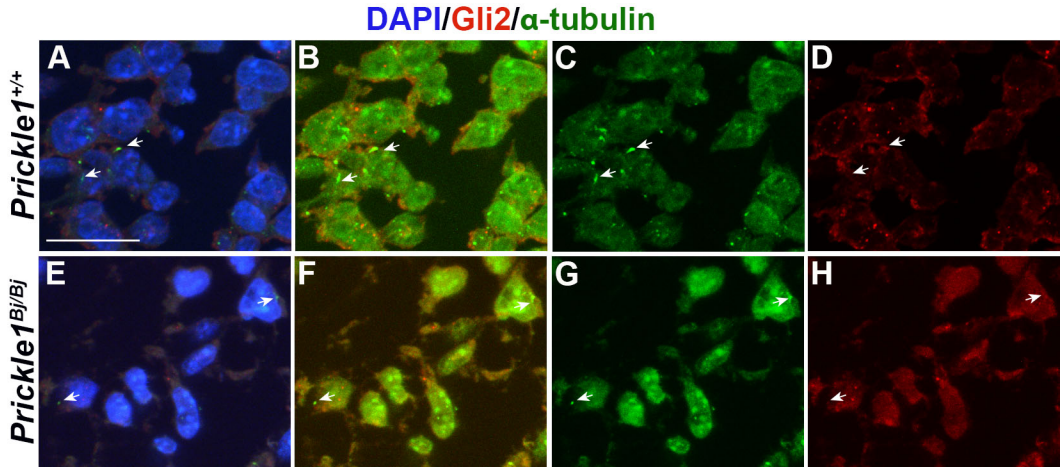

Figure 17: Gli2 is localized in the cilia and the nucleus in *Prickle1*$^{Bj/Bj}$.

Gli2 is colocalized with acetylated α-tubulin localized in the cilia, and visualized in the nucleus in the *Prickle1*$^{+/+}$ (A, B, D). In the *Prickle1*$^{Bj/Bj}$, it is detected in similar locations with more double positive ciliary axonemes (E, F, H). White arrows on cilia in *Prickle1*$^{+/+}$ (c), and in *Prickle1*$^{Bj/Bj}$ (G). Scale bar in A =10 μm, applies to A-H.

3.3 Discussion:

3.3.1 The role of primary cilia in diseases

Recent studies had confirmed the role of the cilia and the primary cilia during embryonic development (Reiter and Leroux, 2017). The primary cilia have numerous functions in interpreting mechanical stress and transducing chemical cues particularly the HH pathway. In many human disorders, they have shown defects in the structure and the function of the primary cilia causing different classes of diseases or syndromes called ciliopathies (Reiter and Leroux, 2017). Mutations in genes encoding for proteins located inside the ciliary organelle cause first-order ciliopathies. On the other hand, mutations in genes whose functions relate to the cilia are called second order ciliopathies (Reiter and Leroux, 2017). Another classification categorizes the ciliopathies based

on involvement of which type of cilia: non-motile or primary cilia only, motile cilia only, or both motile and non-motile cilia (Reiter and Leroux, 2017). Other authors based their classification on phenotypes by looking at clinical findings to link some syndromes with the pleiotropic proteins that can cause ciliary defects and/or dysfunction (Baker and Beales, 2009). It has been shown that proper ciliary assembly and maintenance are necessary for a functional cilium that can transduce mechanochemical signals from the intracellular and extracellular environments of a cells (Eggenschwiler and Anderson, 2007; Goetz and Anderson, 2010; Keeling et al., 2016; Larkins et al., 2011; Lattao et al., 2017; Marshall, 2008).

3.3.2 Role of Prickle1 mutation in ciliogenesis and proteins trafficking

Our mouse model presents a missense mutation at C161F at the LIM1 domain *Prickle1* with known impaired WNT signaling (Gibbs et al., 2016; Wan et al., 2018). Through whole-mount in-situ hybridization, Wan et al. (unpublished) have found increased HH signaling in the cranial base and the medial nasal prominences of the $Prickle1^{Bj/Bj}$ mutants. Also, using STED microscopy to capture the volume of cilia, the $Prickle1^{Bj/Bj}$ cilia are swollen. Based on these findings, we had hypothesized that the $Prickle1^{Beetlejuice}$ phenotype may be a ciliopathy and performed further assays to study the ciliary structure via TEM.

We did not observe a lot of difference in the ultrastructure of the $Prickle1^{Bj/Bj}$ mutants besides a widening and absence of the ciliary pocket. The cilia that we visualized growing from the intracellular pathway presented a flat and wide ciliary pocket instead of the well-defined bilateral invagination observed in the control animals. Many described the shape of the ciliary pocket in mammals as a narrow tube connecting a proximal bulging with wider diameter or a champagne cork like shape depending on cell types (Benmerah, 2013; Ghossoub et al., 2011). In

the flagellum of Trypanosoma, the flagellar pocket— with morphological and functional similarities with the ciliary pocket in mammals — is a membrane domain for endocytosis and exocytosis (Ghossoub et al., 2011; Molla-Herman et al., 2010; Perdomo et al., 2016). The presence of clathrin-coated pits (CCPs) at the ciliary pocket of the *Prickle1*$^{Bj/Bj}$ mutants shown that the missense mutation did not inhibit the ability to internalize cargoes necessary for the build-up of the ciliary axoneme and membrane. Actin filaments are present at the ciliary pocket and they have been shown to guide and stabilize microtubules at the cell cortex (Benmerah, 2013; Dupont et al., 2019). In addition, the PCP genes Inversin and Diego control the assembly of actin filaments at the apical site of the cilia (Park et al., 2008). Through dynamic polymerization, they regulate the activity of adhesion molecules by generating tensile forces that facilitate cell-ECM and cell-cell communications, and morphogenesis processes (Maruthamuthu et al., 2010). Therefore, the enlarged ciliary pocket observed pinpoints a disorganization in the actin cytoskeleton referring to a defect in cell polarity, and a lack of communication between the ciliary membrane and the plasma membrane of the cell. We did not perform assays to look at the actin cytoskeleton at the medial nasal prominences. But this result is supported by previous works on the *Prickle1*$^{Bj/Bj}$ mouse model where they visualized no specific polarized organization of the actin cytoskeleton through phalloidin staining on frozen sections (Gibbs et al., 2016). Whereas, in wild-type control littermates, actin filaments were oriented in the direction of cell migration (Gibbs et al., 2016). In other work from our lab, we have observed randomized polarity of chondrocytes in the *Prickle1*$^{Bj/Bj}$ limb and cranial base (Wan et al., unpublished). The velocity of the ciliary membrane assembly might be also impaired in the mutant as the percentage of colocalization ARL13B and acetylated α-tubulin cilia is decreased in the mutants even though both proteins were co-expressed.

We identified intraflagellar transport defects in the *Prickle1*$^{Bj/Bj}$ mutants. The mutant embryos possessed heterogenous ciliary axoneme that became bulged instead of elongating in a nice rod-like appearance that sometimes exhibit a bent portion. Some ciliary axonemes were abnormally elongated and displayed many bending angles and tortuosity; some grew some enlarged portion at the ciliary tip or along the axoneme creating a knot aspect. We excluded in our measurement analysis those highly irregular cilia after creating the maximum intensity projection image to reconstruct the ciliary axoneme. We looked at the expression of IFT-88 (IFT-B core particle) and IFT-52 (connects IFT-B core to the periphery) because of their essential roles in ciliary assembly and maintenance. Mouse mutants for both IFT-52 and IFT-88 displayed similar embryonic defects in patterning and HH signaling (Liu et al., 2005) In other published works, IFT-88 was localized in spot the base and the tip and fainted along the ciliary axoneme (Takei et al., 2018). We have detected enriched staining for IFT-88 in the cilia of our control in similar pattern and decreased abundance in our mutant animals. The role of IFT-88 was highlighted in Chlamydomonas IFT-88 mutants that failed to assemble the flagella, ciliogenesis was also disrupted in knockout mouse model (Gregory J. Pazour, 2000; Pazour et al., 2000). In previous published work, loss of IFT-88 proteins in the facial mesenchyme led to severe craniofacial defects to confirm the role of IFT-88 particle in palatal development and SHH signaling. This finding may explain the correlation between the decreased expression of IFT-88 in the MNP of *Prickle1*$^{Bj/Bj}$ mutants and the development of cleft lip and palate. In addition, IFT-88 had demonstrated strong interactions with IFT-52 with which it forms dimers that interact with IFT-70 to regulate ciliary assembly (Takei et al., 2018). In Chlamydomonas, IFT-52 was observed throughout the cell cycle around the basal bodies of the cilia in a horseshoe-shaped pattern and in a lesser amount in the axoneme (Deane et al., 2001). Consistent with that, the majority of IFT-52 that we visualized in

the *Prickle1*$^{+/+}$ MNP cells were in the cytoplasm and we detected few signals colocalized with acetylated α-tubulin. The decreased expression of the IFT-52 suggests the defective intraflagellar protein traffic in the *Prickle1*$^{Bj/Bj}$ mutants. Although, we need to investigate more the location of this anterograde transport protein in the cilia as we did not perform dual immunostaining for a basal body marker like pericentrin.

Similarly, for the retrograde transport, we analyzed the localization of IFT-140 in the IFT-A core, and IFT-122 that connects the IFT-A core to the IFT-A subcomplex. Studies in unicellular organisms like Chlamydomonas and Trypanosoma have mapped the locations of IFT trains that cycle between the cell and the flagellum. They have found IFT proteins concentrated at the base of the flagellum (Wingfield et al., 2017). When reaching the distal tip of the flagellum, IFT anterograde trains are split in shorter trains to return to the cell body (Buisson et al., 2013). In the *Prickle1*$^{Bj/Bj}$ mutants, we have seen decreased staining for IFT-140 in the cilia and the cytoplasm, we have also spotted IFT-122 clustered inside the ciliary axoneme. Consistent with our observations on the retrograde transport, null Chlamydomonas mutants *fla14* for the dynein light chain LC8 developed short, non-motile flagella that presented bulges on the side or the tip (Pazour et al., 1998). Aberrant retrograde transport can also be seen in mutation of the centrosomal marker Cep290 generated elongated cilia in Joubert Syndrome (Srivastava et al., 2017). Previous work on zebrafish PCP had proposed a role of Prickle1 in ciliary length regulation as they have seen shortened cilia and defective vesicle in Prickle1and Wnt11 double mutants (Oteiza et al., 2010). Other published works in zebrafish have found genetic interaction between Prickle1 and ift57, ift88 and ift172 (Cao et al., 2010). Those dysmorphic and abnormally elongated cilia that we confirmed via TEM and immunofluorescence staining suggest an alteration of the transition zone or the intraflagellar transport (Keeling et al., 2016).

3.3.3 Functional cilia are required for proper localization of SHH components

As *Prickle1*^{Bj} missense mutation may have destabilized the mechanism by which the cell controls ciliary length and regulates ciliary maintenance in the transition zone (diffusion barrier), the decreased colocalization of ARL13B is suggestive of defective HH signaling (Larkins et al., 2011). It has been shown that loss of ARL13B disrupted ciliary morphology, intraflagellar transport and SHH transduction (Gigante et al., 2020). In our assay, we tested at the intracellular location of Smo and Gli2 to study the SHH pathway in response to Prickle1 mutation, as well as the ratio of GliA:Gli3 for both Gli2 and Gli3. Translocation of Smo in the ciliary axoneme is dependent to the HH pathway activation (Corbit et al., 2005). They have also demonstrated exclusion of Smo in the ciliary axoneme in response to HH inhibition or Smo mutation. However, Smo shifting into the cilia can occur in absence of the Ptc1 or dynein retrograde motor (Goetz and Anderson, 2010; Rohatgi et al., 2007). A lateral transport of Smo translocation to the ciliary membrane had been proposed in response to SHH stimulation in which Smo enters more the cilia from the cell surface than the Smo pool in the plasma membrane (Milenkovic et al., 2009). In our experiments, we mapped more Smo enrichment in the ciliary axoneme of the *Prickle1*$^{Bj/Bj}$ mutants than in the control littermates. In addition, the IFT-A complex regulates SHH signaling, ciliary structure and recruitment of some IFT components such as Arl13b and Smo (Liem et al., 2012). We have seen defective retrograde transport in the Beetlejuice mutants that can lead to Smo accumulation in the cilia and continuous activation of downstream SHH events. Therefore, disrupted ciliary morphology of the cilia of the mutants MNP mesenchymal cells is consistent with increased HH signaling in the *Prickle1*$^{Bj/Bj}$ mutants. It supports the hypothesis that the mechanism for Smo activation is trapped in the cilia, due to the loss of retrograde transport leading to prolonged increased HH signaling.

Translocation of Smo in the cilia is a pivotal event in the mediation of Sonic Hedgehog signaling that trigger activation of Gli transcription factors (Rohatgi et al., 2007). The intracellular location of Gli2 in wild-type cells has been mapped in the nucleus and at the ciliary tip with normal retrograde transport and HH signaling (Chen et al., 2009; Liem et al., 2012). But complete absence of the ciliary retrograde complex seemed to increase Gli2 location at the tip of the cilia and a decrease activation of HH signaling (Liem et al., 2012). Although the retrograde transport seems to be defective in our mutant animals, we have observed Gli2 in other localization in the ciliary axoneme besides the tip, and in the nucleus. This result suggests that Gli2 translocation events occurred in the *Prickle1*$^{Bj/Bj}$ mutants, as well as trafficking events that permit Gli to translocated to the nucleus.

Consistent with the immunoflourescence observations, the western blot result for the level of GliA and GliR for both Gli2 and Gli3 suggest a net loss of the GliR repressor form. In the same manner the retrograde intraflagellar transport is required for the activation of the HH pathway, the anterograde transport, particularly IFT-88, is also essential for efficient processing of Gli3 (Haycraft et al., 2005; Liu et al., 2005). They have also shown that full-length Gli3 failed to inhibit HH pathway induced by activation of Gli1. Other published literature has shown the stability of full-length Gli3 depends on the Suppressor of fused (Sufu, an inhibitory effector) and Speckle-type POZ protein (Spop), but not the truncated repressor form that is necessary to suppress transcriptional target of the HH mediated signaling cascade (Wang et al., 2010). As IFT-88 expression decreased in the ciliary axonemes while the cytoplasmic pool was enriched in the *Prickle1*$^{Bj/Bj}$ mutants, we can suggest an IFT-88 transport deficit that led to insufficient Gli3R processing in our mutants that caused an increase HH activation. This mechanism should be elucidated in future investigation. It could also support the hypothesis, that the machinery needed

to facilitate the processing of the ~83kDa Gli3R/Gli2Rto the ~60kDa fGli2R/Gli3R is trapped in the cilia, preventing the ~83kDa Gli3R/Gli2R to be proteolytically processed.

4.0 Dampening of HH signaling with Vismodegib may rescue the *Prickle1*$^{Bj/Bj}$ mutant phenotype

4.1 Introduction

Summary of palatal development

In humans, craniofacial development happens at about 28 days of gestation in a timely and precise manner where cell proliferation and migration organize the formation of the different prominences. From reciprocal interaction between the ectoderm and the mesoderm, the frontonasal, the medial nasal, the lateral nasal and the maxillary prominences grow, meet and fuse to form the upper face. During this process, the frontonasal and the medial nasal processes coordinate the development of the primary palate that put a temporary and partial closure between the nasal and the oral cavities at the anterior midline. This portion will later develop into the premaxilla and the four upper incisors, the nasal septum, and the philtrum of the upper lip. Then, the primary palate will grow vertically to meet the maxillary and lateral nasal prominences to form the secondary palate. The maxillary prominences extend bilaterally to the tongue in a structure called palatal shelves. Helped by the extension of the head, the palatal shelves should elevate to overcome the physical barrier of the tongue, converge and merge to the midline to separate the nose and the mouth. Any disruption at this time, will contribute to the abnormal development of cleft. (Nanci, 2008; Sadler, 2012)

Mouse palatogenesis happens in similar events. At E 10.5, all the prominences are formed in the mouse embryo (Kaufman, 1992). At E 11.5, the medial nasal and the lateral nasal prominences are fused, and the palatal shelves initiate their extension. Between E 12 and E 13.5,

the palatal shelves grow downward the tongue meanwhile the vertical outgrowth of the primary palate. At E 14, the palatal shelves elevate and converge in the midline. By E 14.5 and E 15, signs of fusion can be observed in the epithelial seam. Palatogenesis ends in mouse at E 15.5 with the merging of the midline epithelial seam. (Bush and Jiang, 2012; Kurosaka, 2015; Lan and Jiang, 2009).

4.1.1 Summary of *Prickle1*^{Beetlejuice} phenotype

The *Prickle1*^{Bj} mouse line was initially developed to study human congenital heart defects due to cardiac outflow track misalignment and ventricular septum defect (Gibbs et al., 2016). The congenital cardiac defects in *Prickle1*$^{Bj/Bj}$ causes neonatal lethality (Gibbs et al., 2016; Wan et al., 2018). All the *Prickle1*$^{Bj/Bj}$ mutants developed a midfacial cleft along with other craniofacial abnormalities, whereas only 50% develop cleft palate (Wan et al., 2018). *Prickle1*$^{Bj/Bj}$ neonates are microcephalic with protruded forehead, short snout, and mandible (Gibbs et al., 2016; Wan et al., 2018). The skeletal defects in the limbs, and tails causes a short stature phenotype. Some features of the *Prickle1*$^{Bj/Bj}$ mutants correspond to some characteristics of skeletal ciliopathies (Handa et al., 2020). In addition, the dysmorphic fetal face and the skeletal dwarfism correlate the *Prickle1*$^{Bj/Bj}$ phenotype to Robinow Syndrome (Mazzeu et al., 2007). Autosomal dominant and recessive Robinow Syndrome are linked with mutations in the Wnt/PCP pathway including ROR2, Wnt5a, WNT11, DVL1, and DVL3 (Mazzeu et al., 2007; Person et al., 2010). Although, the molecular perturbations underlying many cases of RS in human remained uncovered (White et al., 2015; White et al., 2016). Therefore, the heterogeneity of RS suggests possible mutations in other core components of the PCP pathway such as *Prickle1*.

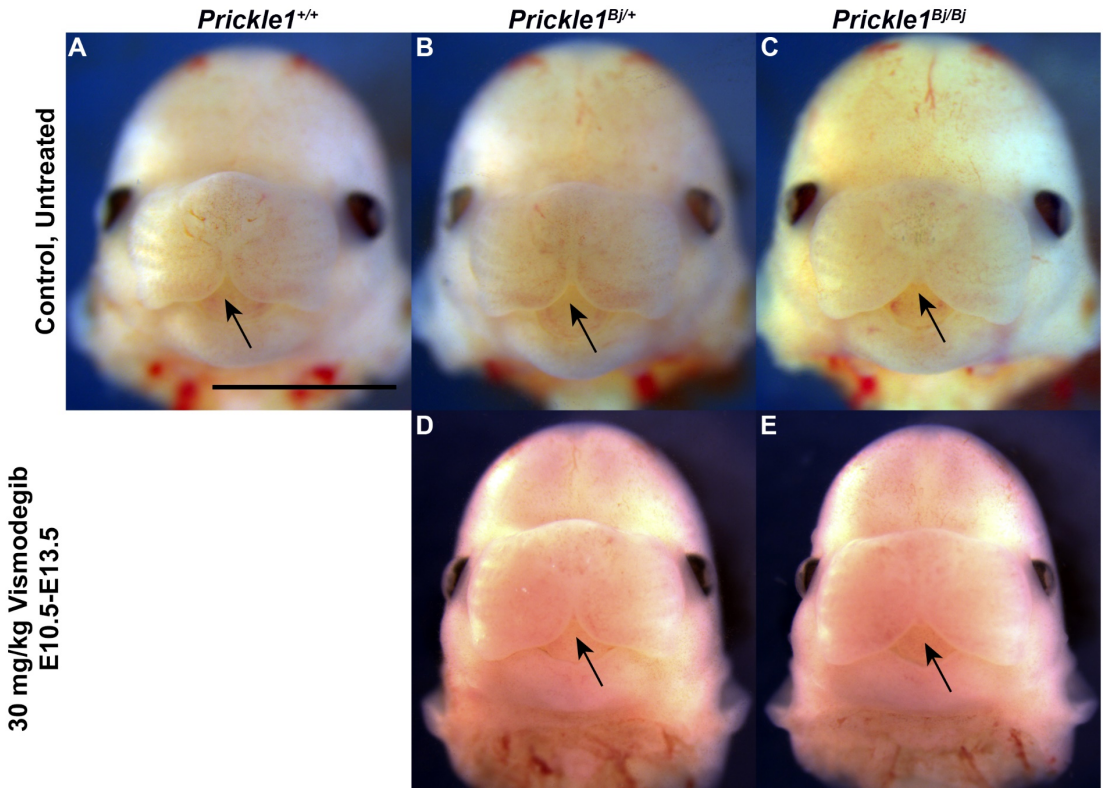

Figure 18: Median cleft lip is still develops in the E 14.5 Vismodegib-treated *Prickle1*$^{Bj/Bj}$.

(A-C) Historical, untreated E14.5 littermates showing the phenotypic spectrum of midfacial clefts (black arrows) from *Prickle1*$^{+/+}$ to *Prickle1*$^{Bj/+}$ to *Prickle1*$^{Bj/Bj}$. (D, E) 30 mg/kg Vismodegib treatment from E10.5 to E13.5 did not rescue the median cleft lip by E 14.5. Scale bar=3 mm.

Vismodegib and mechanism of action

Vismodegib (GDC-0449) or 2-chloro-N-(4-chloro-3-(pyridin-2-yl) phenyl)-4-(methylsulfonyl) benzamide is an FDA-approved oral capsule (available in 150 mg) with antineoplastic activity. It was originally developed by Genentech to antagonize continuous SMO activation due to Ptch1 mutation that is the most common molecular alteration found in BCCs (Athar et al., 2014). By binding to SMO and/or PTC1, Vismodegib selectively inhibits activation of HH downstream target genes. In pancreatic cancer cell lines, Vismodegib induced apoptosis by downregulating the ratio between genes that promote cell survival instead of cell death (Singh et

al., 2011). With a molecular weight of 421.3 g/mol, Vismodegib mostly circulates in the plasma where it binds to albumin and alpha-1-acid glycoprotein (Inc, 2012). Vismodegib absolute oral bioavailability after a single administration dose is 31.8% (Aditya and Rattan, 2013; Inc, 2012). In clinical trials, the duration of Vismodegib treatment ranged from a period of 0.7 to 18.7 months, with a median of 10.2 months (Aditya and Rattan, 2013). Pharmacokinetics studies showed that Vismodegib presented a slow elimination after absorption, and is processed primarily by the hepatic route via oxidation, glucuronidation, and common pyridine cleavage (Frampton and Basset-Séguin, 2018) and the metabolites are found in the feces (82%), and in a lesser extent (4.4%) in the urine (Graham et al., 2012; Inc, 2012; LoRusso et al., 2011).

Vismodegib is generally well-tolerated based on clinical trials observations (LoRusso et al., 2011; Von Hoff et al., 2009). Though, drug toxicity can occur and is carefully monitored. For antineoplastic activity, it can be prescribed in 28-days cycles paired with interruption of 4 to 8 weeks according to the disease progression state (Sekulic et al., 2015; Sekulic et al., 2012). Nonetheless, patients on Vismodegib treatment experienced commonly a range of mild or moderate side effects: muscle spasm, hair loss, loss of taste, decreased appetite, weight loss, nausea, vomiting, and constipation (Proctor et al., 2014). Vismodegib causes embryonic lethality and is teratogenic. Offspring of treated pregnant animals were born with several congenital anomalies such as severe midline defects and other irreversible malformations (Yang et al., 2015; Zhang et al., 2017). Therefore, both males and females' patients treated with Vismodegib are recommended to use two highly efficient birth control methods (Sekulic et al., 2012).

4.2 Results:

4.2.1 Morphologies of Vismodegib treated litters

After crossing heterozygotes *Beetlejuice* females and males, we treated the pregnant dams with Vismodegib at doses of 15 mg/kg, 30 mg/kg, and 60 mg/kg from pregnancy day E10.5 to E13.5 to decrease HH signaling in the developing fetuses. The overall external morphologies of all treated fetuses regarding their genotypes with the three drug concentrations varied with increased Vismodegib concentration compared to historical, untreated *Prickle1* Beetlejuice litters (Figure 18); (Figure 19). Vismodegib-treated *Prickle1*$^{Bj/Bj}$ fetuses at all doses still developed the microcephalic characteristics with protruded forehead, shorter snout, and mandible (Figure 19). The midfacial cleft was still present in the *Prickle1*$^{Bj/Bj}$ mutants (Figure 18).

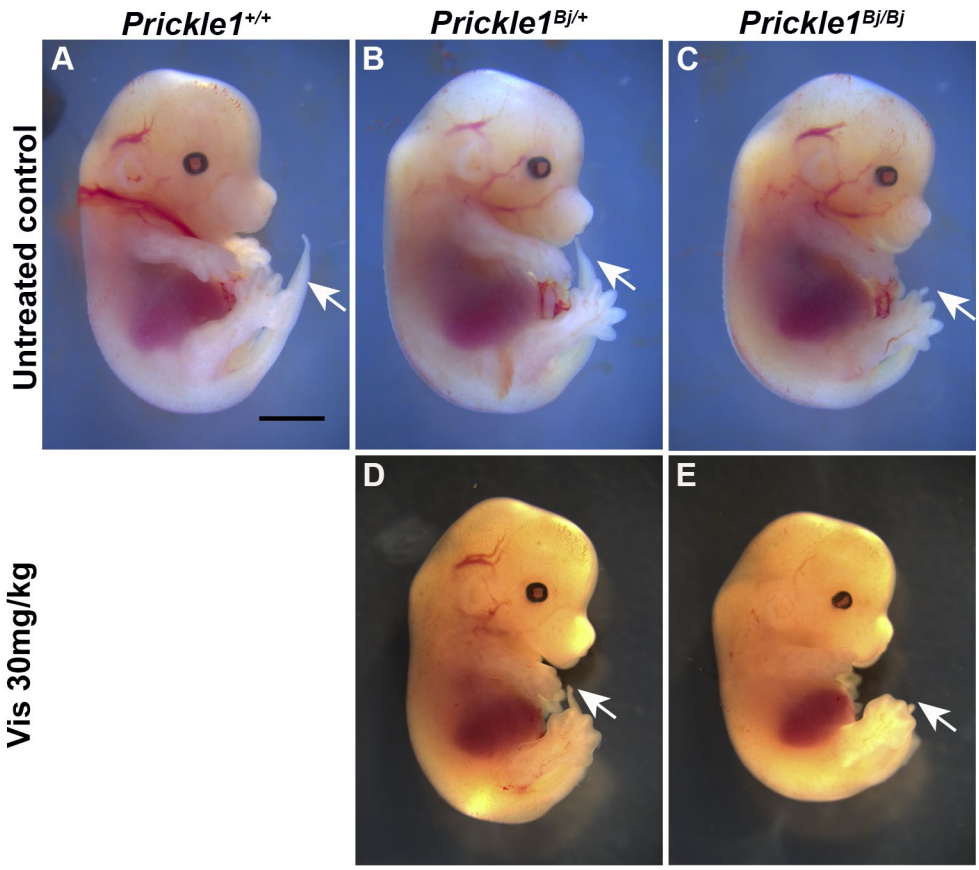

Figure 19: Morphology of vismodegib (30mg/kg) treated litters.

The overall morphology of Vismodegib-treated fetuses from E 10.5 to E.13.5 and harvested at E 14.5 (D-G) varied accordingly to HH inhibition compared to untreated fetuses at E 14.5 (A-C). In untreated mutant fetuses, the snout, the limbs, the tail are shorter compare to wildtype littermate (A, C). The presence of. a mild edema in the back of untreated *Prickle1*$^{Bj/Bj}$ (C). Following vismodegib treatment, the tail, snout, and hindlimbs are shorter in all genotypes (D, E). Scale bar in A= 1 mm, applies to all.

No improvement in stature was observed in the long axis of the body of Vismodegib-treated *Prickle1*$^{Bj/Bj}$: the tail, the forelimbs and the hindlimbs were shorter in comparison to *Prickle1*$^{Bj/+}$ and *Prickle1*$^{+/+}$ Vismodegib-treated fetuses. In one litter, treatment at 60 mg/kg caused embryonic lethality as only two fetuses were collected at E 14.5; while the average number of embryos harvested from non-treated *Prickle1*$^{Bj/+}$ pregnant dams is usually between 8 to 11 pups. No

noticeable defects in the number or shape were observed in the digits of all harvested fetuses. We did not observe edema in the body or limbs of the treated fetuses. However, some untreated mutant fetuses developed sometimes edema in their bodies (Figure 18).

4.2.2 Vismodegib treatment from E10.5 to E13.5 disrupted palatogenesis.

We studied the histology of the treated litters through H&E, and Alcian Blue and Sirius Red. The fetuses developed almost all the craniofacial structures that should be present at E14.5 except the secondary palate. From the primary palate, the nasal septum, the vomeronasal organ, and the upper lip developed. But the MNPs did not fuse completely as we observed a median cleft lip in almost all treated fetuses (Figure 20). All the treated animals lacked the secondary palate (Figure 20). The palatal shelves were formed from the maxillary prominences and started their elevation to close the nasal and the oral cavities. But they did not meet nor started the fusion at the midline even though vertical growth occurred for the primary palate.

The *Prickle1*$^{Bj/Bj}$ treated fetuses developed a misshapen and small tongue while we did not detect any difference in the other treated fetuses (Figure 20). We noted the presence of the oral epithelium and tooth germs in the Vismodegib-treated litters. In the *Prickle1*$^{Bj/Bj}$, tooth germs were in the cap stage, but they were in the bell stage in the treated *Prickle1*$^{Bj/+}$ and *Prickle1*$^{+/+}$ (Figure 20).

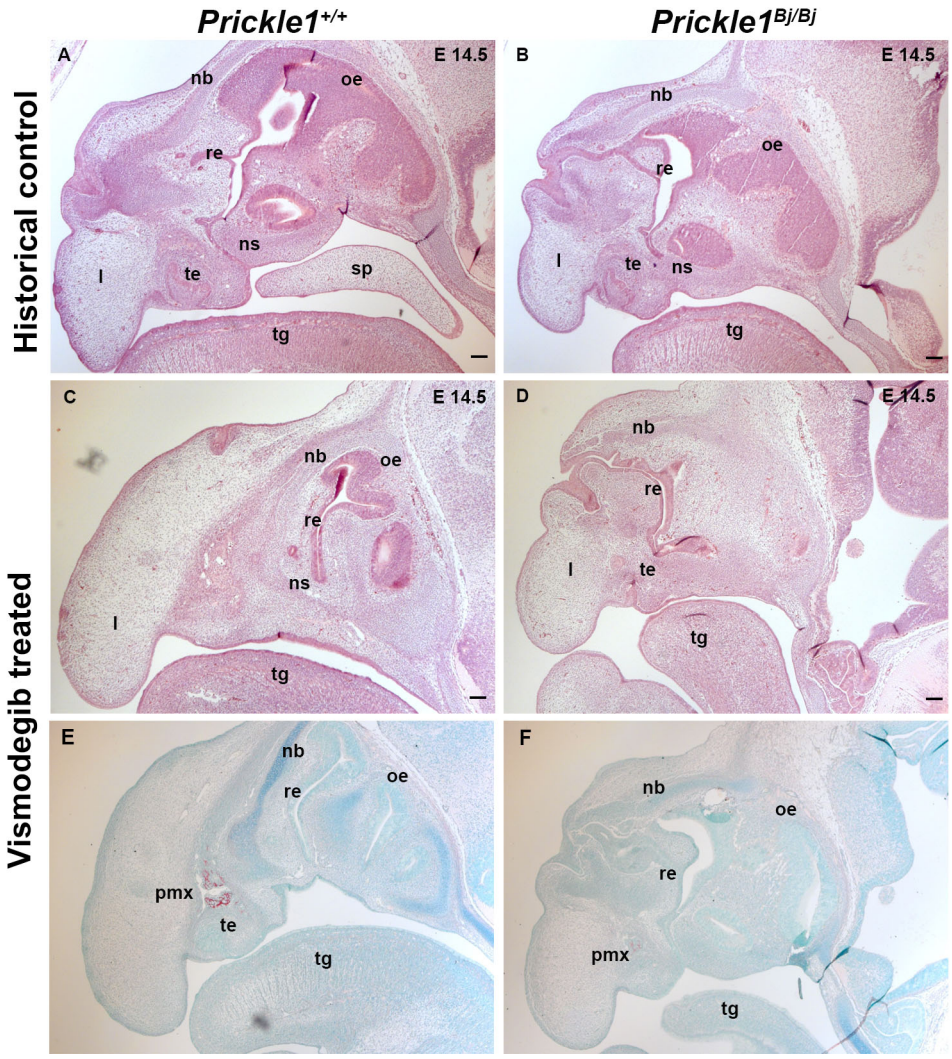

Figure 20: Histology Vismodegib treated and untreated Prickle1 litters at E 14.5 (sagital view).

At E 14.5, in untreated *Prickle1*$^{+/+}$, the secondary palate is formed (A), whereas it is lacked in same stage untreated *Prickle1*$^{Bj/Bj}$ mutant that developed cleft of the secondary palate (B), H& E staining. Absence of the secondary palate in Vismodegib-treated fetuses at 30mg/kg from E 10.5 to 13.5 (C-F). In treated *Prickle1*$^{Bj/Bj}$ mutant, the tongue is misshapen, tooth development arrested in cap stage (D,F). In the pre-maxilla (pmx) of both litters, we observed delayed mineralization in the *Prickle1*$^{Bj/Bj}$ mutant from Alcian Blue and Picro-sirius staining (E,F). Scale bar= 1mm.

Histological examination of the nasal septum in the *Prickle1*$^{+/+}$ Vismodegib-treated fetuses revealed that the round chondrocytes were arranged in regions of circular clusters while in the *Prickle1*$^{Bj/Bj}$, they were obliquely oriented with a rectangular shape (Figure 22). Alcian Blue

staining was stronger in the *Prickle1*$^{+/+}$ Vismodegib-treated than in the *Prickle1*$^{Bj/Bj}$. We observed mineralization in the cranial base, calvaria, frontal bone, maxilla, and the mandible of both genotypes (Figure 20).

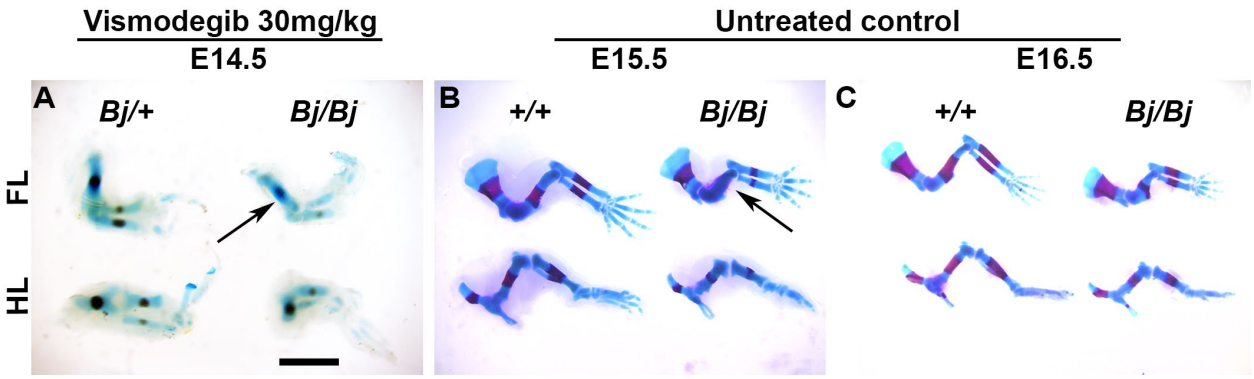

Figure 21: Vismodegib treated *Prickle1*$^{Bj/Bj}$ fetuses has initated by E14.5.

Alcian blue and Alizarin red staining to determine the status of bone and cartilage in the limbs. (A) The Vismodegib treated *Prickle1*$^{Bj/Bj}$ humerus has initated mineralization by E14.5. (B-C) In untreated Prickle1 litters, humerus mineralization occurs by E16.5 in *Prickle1*$^{Bj/Bj}$ mutant (B-C). Scale bar = 1mm.

We stained the limbs of the treated litters with alizarin red and alcian blue and found that the *Prickle1*$^{Bj/Bj}$ treated with 30 mg/kg of Vismodegib accelerated the mineralization of the forelimbs. In historical controls, we have not observed mineralization in the *Prickle1*$^{Bj/Bj}$ forelimb until E16.5 (Figure 21). These results suggest that Vismodegib treatment in mouse from E10.5 to E13.5 may have tissue specific effect in delaying or promoting chondrocytes maturation due to increased SHH signaling. Exploring this targeted therapy might be beneficial for the osteosclerotic form of Robinow Syndrome.

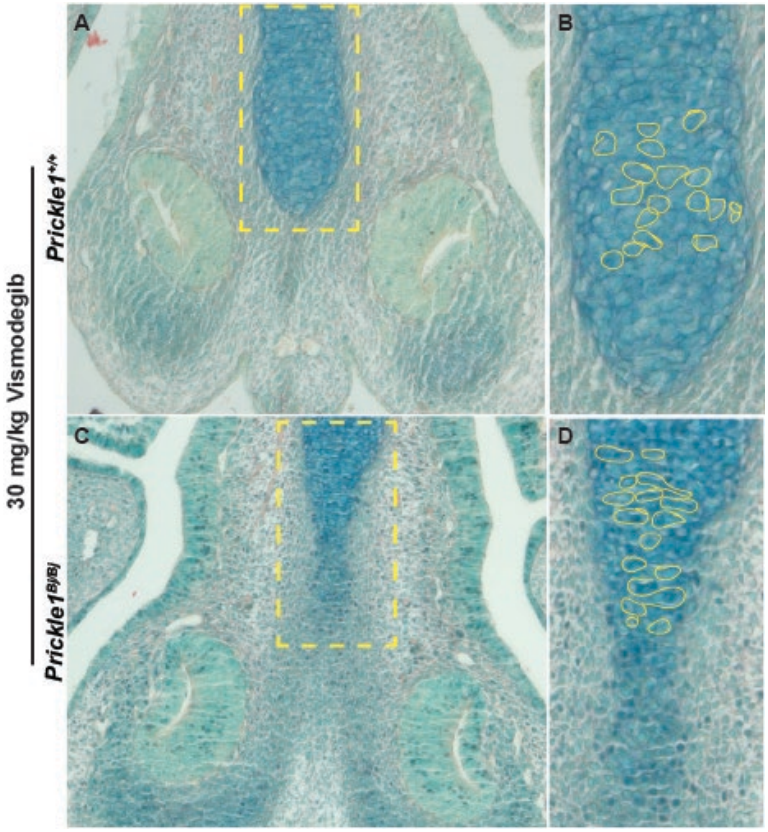

Figure 22: Nasal septum chondrocyte shape is changed with Vismodegib treatment (30 mg/kg).

Chondrocytes are round in the nasal septum cartilage of *Prickle1*$^{+/+}$ (A), higher magnification (B). The nasal septum chondrocytes are flattened in *Prickle* $^{Bj/Bj}$ suggesting a delayed in maturation of the nasal septum cartilage (C), higher magnification (D).

4.2.3 Intracellular localization of Gli2 proteins in *Prickle1*$^{Bj/Bj}$ Vismodegib-treated fetuses.

We characterized the expression of Gli2 in the upper lip mesenchyme by dual immunolabelling with acetylated α-tubulin. Vismodegib treatment rescued in some extent the ciliary morphology phenotype of the *Prickle1*$^{Bj/Bj}$ mutants (Figure 23). However, some bulge can be visualized at the ciliary tip of some axonemes in the mutant mesenchyme. In the Vismodegib-treated *Prickle1*$^{Bj/Bj}$ mutants, we observed that Gli2 protein localization was returned to normal, as judged by the similarity to Gli2 localization in untreated *Prickle1*$^{+/+}$. This finding also supports

the intraflagellar transport defect observed in ciliated mesenchymal cells of untreated *Prickle1*$^{Bj/Bj}$ mutants. While this data lacks a true control group that has been gavaged with the Vismodegib vehicle, we observed that Vismodegib treatment disrupted cilia morphology in the treated *Prickle1*$^{+/+}$. In the Vismodegib-treated *Prickle1*$^{+/+}$, I observed a shortened ciliary axoneme, and an exclusion of Gli2 from the cilia and its presence in the cytoplasm (Figure 23). In historical untreated *Prickle1*$^{Bj/+}$, we observed a similar ciliary phenotype like in the *Prickle1*$^{Bj/Bj}$: they developed bulged, long and twisted cilia with some in the normal length range (Figure 24). Interestingly, following Vismodegib treatment, all the ciliary axoneme grew normally in heterozygote fetuses.

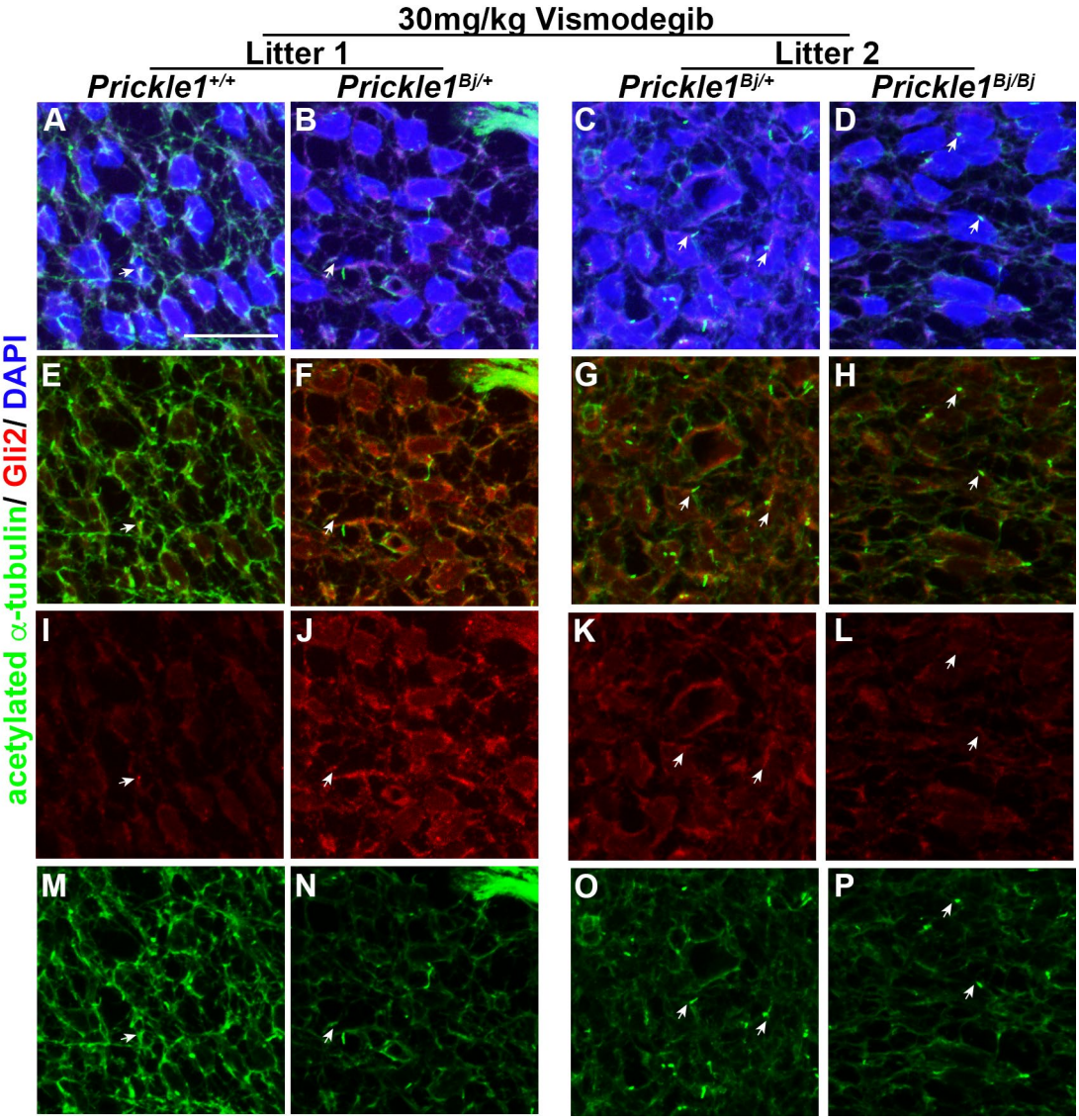

Figure 23: Intracellular localization of Gli2 in two litters treated at with 30 mg/kg Vismodegib.

We performed double immunofluorescence staining for antibodies against Gli2 and acetylated α-tubulin to study the ciliary phenotype and the intracellular localization of Gli2 following HH inhibition in the upper lip at E 14.5 (A-P). In the treated *Prickle1*$^{+/+}$ (A, E, I, M) , the cilia, the cilia became shorter compared to their length in untreated litters (M). Few ciliated cells were positive for both antibodies (A, E) and Gli2 staining of the cells structures showed a decreased brightness (I) . In two Vismodegib-treated the *Prickle1*$^{Bj/+}$, Gli2 was visualized in the cilia and enriched to the nucleus even in the presence of the inhibitor (B,C, F, G, J, K). The morphology of the cilia were no longer bulged nor heterogenous (N,O) compared to untreated cilia in heterozygous animals. In the *Prickle1*$^{Bj/Bj}$, we

detected more double positive cilia for both antibodies (D, H, L). The ciliary phenotype was also rescued in some cilia (P). White arrows on cilia and intracellular localization of Gli2. Scale bar= 40 µm.

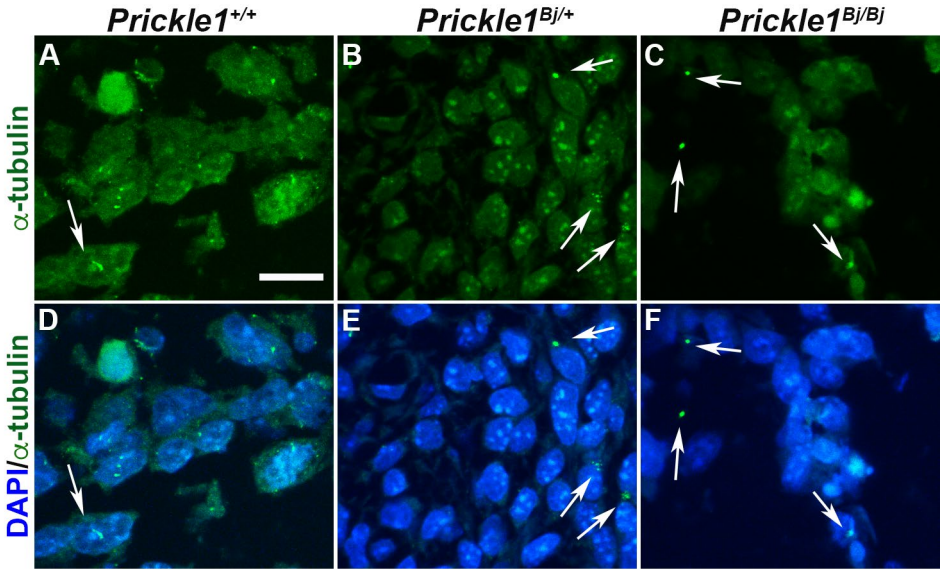

Figure 24: Ciliary morphology in Prickle1 litter at E 10.5.

White arrows pointing at normal cilia in *Prickle1*$^{+/+}$ (A,D). Bulged and dysmorphic cilia are observed in both heterozygote and mutant embryos (B, E, C,F). Scale bar= 40 µm.

4.3 Discussion

4.3.1 Wnt/PCP and HH signaling in the pathogenesis of cleft lip and palate

Cleft lip and cleft palate had been extensively studied as they are the most common congenital disorders in humans. The Wnt/PCP pathway had been evaluated in cases of syndromic and non-syndromic cleft lip/palate in different populations and they have found implications of many WNT ligands, receptors, and core genes (Menezes et al., 2010; Reynolds et al., 2019). Two rare missense *Prickle1* mutations related to incompletely penetrant cleft palate in a Filipino population were modeled in mouse (Liu et al., 2014; Yang et al., 2014). In other mouse model,

ectopic HH signaling caused cleft palate and defective bone formation (Hammond et al., 2018). Increased SHH in the palatal shelves of the mouse K14-SHH mimicked the craniofacial defects present in NBCCs (Cobourne et al., 2001). Also, high-level of SHH signaling resulted in hypertelorism due to the medio-lateral widening of the frontonasal prominences (Abramyan, 2019). In addition, disruption of HH contributed in the formation of cleft lip (Kurosaka, 2015; Kurosaka et al., 2014). In our mouse model, the missense Prickle1 mutation generated cleft lip in all the mutant embryos whereas their frequency of cleft palate varied (Gibbs et al., 2016; Wan et al., 2018). The elevated HH signaling found in the cranial base and the medial nasal prominences at E 10.5 and the midfacial widening phenotype of the *Prickle1*$^{Bj/Bj}$ mouse turned t as a good model to study palatogenesis and the crosstalk between WNT and HH signaling.

The importance of appropriate HH signaling had been demonstrated during craniofacial development in mice. High level of HH signaling caused arrest of tooth development, impaired cell proliferation and cleft palate (Cobourne et al., 2001). Conversely, loss of SHH signaling inhibited growth of the primordia and generated cleft lip/palate and hypertelorism (Hu and Helms, 1999). Therefore, SHH signaling is a key regulator of embryonic and craniofacial (Abramyan, 2019; Dworkin et al., 2016; Lan and Jiang, 2009; Li et al., 2017).

4.3.2 Rescuing HH signaling

We attempted to rescue to *Prickle1*$^{Bj/Bj}$ phenotype through timely inhibition of HH signaling during embryonic development from E 10.5 to E 13.5 via daily Vismodegib gavage of pregnant mice. We observed more severe craniofacial phenotypes in the treated embryos. Almost all treated fetuses developed a midfacial cleft lip. The secondary palate development was also delayed or absent in those embryos. The tongue of the mutant animal was misshapen and smaller compared

to other wild-type and heterozygotes treated fetuses. High concentration of Vismodegib at 60 mg/kg induced neural tube defect particularly a lack of closure of the neural tube and spina bifida. In the nasal septum of the mutants, we shown a delayed in chondrocytes maturation although the frontal bone, the mandible and the cranial base started their mineralization. Some of the ciliary phenotype of the *Prickle1*^{Beetlejuice} mouse mutant were also rescued. From published literature, HH inhibition with another SMO antagonist cyclopamine at single dose of 40 or 80 mg/kg from pregnancy day E 8.25 to E 9.5 in timed-pregnant C57Bl/6J mice generated a cleft lip and palate in the harvested fetuses (Lipinski et al., 2010). In addition, acute administration of Vismodegib at 40mg/kg impacted mouse craniofacial development according to the developmental stage: early exposure at E 7.5 caused craniofacial dysmorphy, whereas exposure between E 9.0 to E 10.0 cleft caused cleft of the secondary palate (Heyne et al., 2015). Surprisingly, the fetuses treated between E 7.0 to E 8.5 were normal (Heyne et al., 2015). Our experimental design differed from those above-mentioned works. They used Vismodegib in one high dose as a single or acute administration. Conversely, we tried to rescue the Beetlejuice phenotype with three different doses of Vismodegib of 15 mg/kg, 30 mg/kg, and 60 mg/kg. Consistent with their observations, high dose of Vismodegib indeed induced malformations in the treated fetuses while at low dose of 15 mg/kg we did not observed significant many differences. Dampening of HH signaling remains a challenge because of off-targets effects as demonstrated with two HH , inhibitors Sunitinib and Alisertib that promoted ciliary disassembly in normal and renal carcinoma cells (Kiseleva et al., 2019).

We plan to test another schematic to inhibit or restore HH signaling in the *Prickle1*^{Beetlejuice} mouse: A single dose regimen of Vismodegib in respect to normal HH kinetics during embryonic development; or Purmorphamine as single or acute administration to study if the agonist alone

would make the medial facial cleft wider; and the simultaneous addition of Vismodegib and Purmophamine to evaluate treatment efficiency. Also, we will need to assess any off-target effects of this proposed therapy for a better clinical application.

5.0 HH signaling in Robinow Syndrome.

5.1 Introduction:

5.1.1 Robinow Syndrome

Robinow Syndrome is a rare genetic disorder affecting more than 100 individuals in the world; some cases are related to history of familial consanguinity (Bacino, 1993). RS differential diagnosis based on forms of inheritance, is conflicted because of clinical reports' findings divergence (Bunn et al., 2014). The autosomal recessive form has been reported to be more severe than the autosomal dominant RS (Bunn et al., 2014; Person et al., 2010). Mutations in *DVL1, DVL3,* and *WNT5A* are associated with autosomal dominant RS, whereas mutations in *ROR2* are associated with autosomal recessive RS (Katoh and Katoh, 2017). An osteosclerotic form of RS is associated with *DVL1* mutations causing localized or widespread osteosclerosis in the face, the base of the skull, the spine and the long bones (Bunn et al., 2015; Bunn et al., 2014). The molecular mechanism underlying the etiology of RS suggests that the mutations in the PCP genes dysregulated both canonical and non-canonical WNT signaling (Bunn et al., 2014).

Following diagnostic of RS, clinical management assesses the presence of cleft lip/palate; evaluates the thorax to detect ribs and spinal defects through radiographs; and examines the cardiac, renal, and urogenital organs. RS is devoid of a standard treatment because of its heterogeneity. Current RS treatments address the clinical manifestations and weigh the need of surgeries to correct non-functional craniofacial, skeletal, and penile deformities. At present, pharmaceutical research is testing molecular therapies targeting activation or inhibition of WNT

signaling in phase I/II and in preclinical trials in many diseases: WNT signaling agonist are used in cancer and osteoporosis; and WNT antagonists, in cardiac and kidney fibrosis (Katoh and Katoh, 2017). There is no current available molecular treatment for RS. Therefore, there is a need to address a therapy that can improve health conditions of affected individuals particularly in the osteosclerotic RS that is considered as a progressive form (Shprintzen et al., 1982).

Besides those known mutations, the heterogeneity of skeletal phenotypes of Robinow Syndrome suggests other molecular interactions or overlaps with signaling pathways such as HH (Shprintzen et al., 1982; White et al., 2018). RS has been described as a potential ciliopathy due to the similarity of RS phenotypes to those of known ciliopathies (Baker and Beales, 2009). Knowing the importance of the primary cilia in the activation of the HH pathway, we hypothesized that HH signaling is defective in RS. Therefore, we are investigating a novel therapeutic approach targeting HH signaling in Robinow Syndrome.

We have primary fibroblasts from a patient with the osteosclerotic form of RS. The patient has a heterozygous mutation in DVL1 (c.1532delA; p. Gln511Argfs*138). The mutation is a frame shift mutation that results in a truncated protein with a nonsense N-terminal (White et al., 2015).

5.1.2 Purmorphamine

Purmorphamine or 2-(1-Naphthoxy)-6-(4-morpholinoanilino)-9-cyclohexylpurine is a member of the purine class with a molecular weight of 520.6 g/mol. Purmorphamine acts as a small molecule to induce osteogenesis activity that promotes the differentiation of multipotent progenitor cells into osteoblasts (Wu et al., 2002). It was also shown to upregulating the same sets of genes mediated by the HH pathway (Wu et al., 2002). Independently to Ptch1, Purmophamine binds directly to SMO by mimicking the natural agonist to initiate the HH signaling cascade (Sinha

and Chen, 2006). Purmorphamine had been also demonstrated to regulate SMO, and to stabilize the conformational change of this structurally similar G-protein receptor (Sinha and Chen, 2006). This step plays a pivotal role in initializing HH-mediated transcriptional activity (Sinha and Chen, 2006). Besides, in the presence of SMO antagonist such as Vismodegib, Purmorphamine acts as a competitive inhibitor to restore HH signaling (Sinha and Chen, 2006).

5.2 Results:

5.2.1 Prickle1 localization in human RS fibroblasts.

We tested the localization of Prickle1 in the RS-fibroblasts and observed it in the nuclei. In addition, Pk1 expression was also detected in the cytoplasm and colocalized with acetylated α-tubulin in the ciliary axoneme of the cultured fibroblasts (Figure 25). This result suggests that Prickle1 protein functions during cargo transport in the cilia.

5.2.2 Ciliary phenotype before HH stimulation

We performed double immunofluorescence staining to analyze the morphology of the cilia in the RS-fibroblasts serum starved for 24 hours. We found positive signals for the ciliary membrane marker ARL13B and for the axonemal marker acetylated α-tubulin (Figure 25). We observed length irregularities in the ciliary axoneme of this heterozygote RS fibroblasts varying from 1.71 μm to 7.67 μm (3.89 ± 1.46 μm, N =179) meaning some cells grew short cilia whereas other fibroblasts developed elongated ciliary axonemes. Some ciliary axoneme developed rod

shape-like structure but we had also detected increased ciliary tortuosity in ~16% of the cells. Few cilia were bulbous at the ciliary tip or along the axoneme (Figure 25).

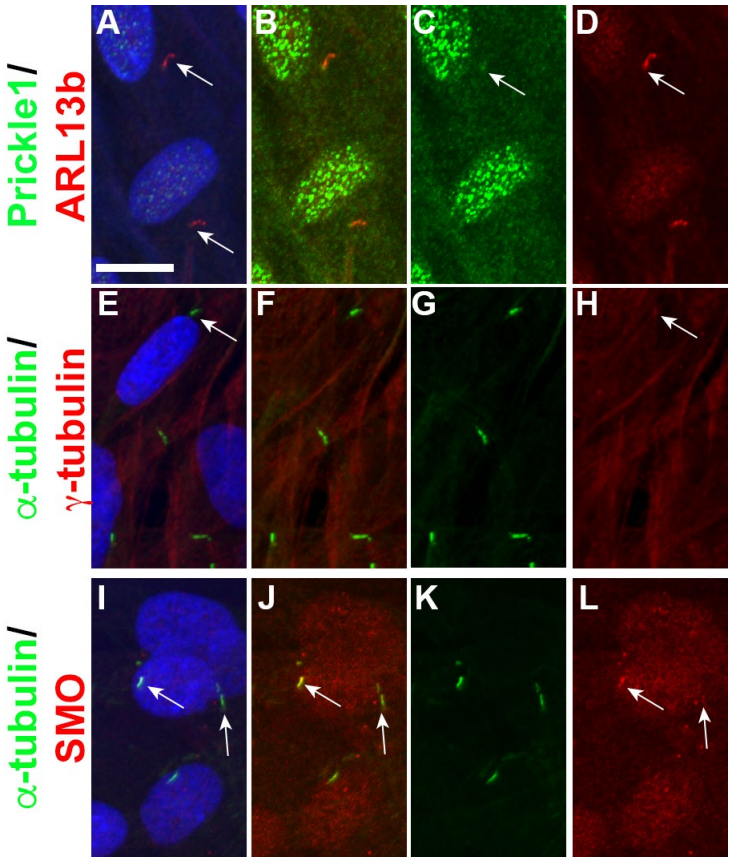

Figure 25: Ciliary phenotype in Robinow Syndrome cultured fibroblasts.

We cultured and serum starved isolated RS fibroblasts from a skin punch biopsy and performed dual immunolabelling (A-L). Some of the cilia were normal in rod shape-like, others were long, twisted or bumpy (E-H). We observed Prickle1 colocalized with the ciliary membrane marker ARL13B (A-D). SMO was in the cilia and the cell body (I-J). Scale bar= 20 µm.

5.2.3 Intracellular localization of SMO

We began to determine the level of HH signaling in the RS-fibroblasts, by double immunofluorescence staining to SMO and acetylated α-tubulin (Figure 25). In serum starved RS-fibroblasts, we observed widespread expression of SMO in the cytoplasm. In N=14/ 44 cells we detected SMO with acetylated α-tubulin in the axoneme. In the other cells, SMO was only localized into the cytoplasm (Figure 25). Translocation of SMO into the ciliary axonemes suggests that the DVL1 mutation does not affect ciliary translocation of SMO.

5.2.4 Response to HH signaling changes in RS-fibroblasts

We treated the cultured fibroblasts with different concentrations of Vismodegib, Purmorphamine, and a combination of both to restore the level of HH signaling (Figure 28). The control group received the drug solvent DMSO. We analyzed the ciliary phenotype and the location of SMO after 24 hours of treatments by double immunostaining with acetylated α-tubulin. In the group treated with DMSO, the ciliary length was similar to the untreated fibroblasts (2.59 ± 0.69 μm; N=12). SMO was localized in fainted signal in the ciliary axoneme but mostly it was mostly in the cytoplasm. In the group treated with 50 μM of Purmorphamine, the cilia were shorter (1.52 ± 0.13 μm; N=6) and appeared swollen like big dots near the cells. Purmorphamine treatment increased SMO staining in the cytoplasm and at the ciliary tip. Different doses of Vismodegib produced distinct ciliary phenotypes. At lower dose of Vis 1 μM, ciliary length was slightly shorter than the DMSO treated group but were more homogeneous (2.48 ± 0.27 μm; N=8). However, most cilia were enlarged at the axoneme base and tip giving the axoneme the aspect of “8”. SMO

colocalized with acetylated α-tubulin in those bulbous portions and was also enhanced at the ciliary axoneme. At concentration of 10 μM Vismodegib, the ciliary length varied (2.54 ± 1.28 μm; N=9) and the ciliary axonemes elongated without swelling, and SMO was mostly detected in the cytoplasm. At higher dose of Vismodegib 100 μM, caused the formation of shorter and swollen axoneme (2.4 ± 0.71 μm; N=9), with SMO enriched in the swollen portion of the axonemes and the cytoplasm of the cells. The combination of Purmorphamine 50 μM and Vismodegib μM cilia produced longer cilia (2.94 ± 0.39 μm; N=28). Although, SMO was enriched at the base of the axoneme producing a swollen portion in some cilia. The level of SMO decreased in the cytoplasm compared to the DMSO treated group. (Figure 26). Via one one-way ANOVA and Tukey HSD test, we found statistically significant results between length difference of the cilia in the DMSO control group and Purmophamine 50 μM treatment group; and between Purmorphamine 50 μM treatment and Purmorphamine μM+ Vismodegib 100 μM (p-value= 0.008511).

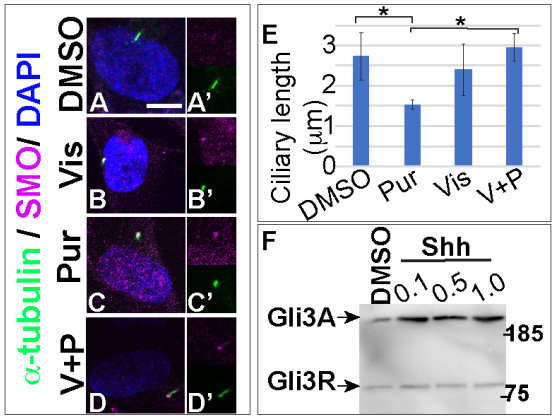

Figure 26: Translocation of SMO in response to HH stimulation.

SMO is visualized in the cilia in the DMSO control group (A, A'). SMO remained and increased in the cilia and the cytoplasm following HH inhibition with Vismodegib (B, B'). In the presence of the agonist Purmorphamine, the level of staining significantly increased in both the ciliary axoneme and the cytoplasm (C, C'). Simultaneous addition of bo th the agonist and the antagonist decreased the cytoplasmic pool of SMO, but it stayed at the base of

the axoneme (D,D'). Length of primary cilia in control and treatment groups; one-way ANOVA, p-value= 0.008511 (E). We detected the level of Gli3A versus Gli3R in response to SHH stimulation. The expression of full-length Gli3A is not dose dependent whereas the level of Gli3R do not remained the same suggesting a problem in Gli3R processing.

5.2.5 Western Blot testing for level of Gli3

In RS cultured fibroblasts, we analyzed the level of Gli3A and Gli3R in response to SHH treatment at doses of 0.1 µg/ml, 0.5 µg/ml, and 1 µg/ml. In PBS-treated control RS-fibroblasts, the level of full-length form of Gli3A at ~190 kDa was slightly lower than the repressor form at ~ 83 kDa (Figure 26). We did not detect the two forms of Gli3R in the RS-fibroblasts. These findings hint to increased HH signaling in Robinow Syndrome because of defective degradation of activated Gli proteins. Following SHH treatment, the level of Gli3A increased compared to the control group, while the Gli3R levels remained similar to the control group. As response to HH stimulation should be dose dependent, we suggest a problem in protein trafficking and Gli3R processing that led into constant activation of HH signaling.

5.3 Discussion:

5.3.1 Ciliary transport defects in autosomal recessive osteosclerotic form of Robinow Syndrome

5.3.1.1 RS may be a ciliopathy

We studied ciliogenesis after serum-starving for 24 hours the cultured untreated RS-fibroblasts. We did not observe a homogenous pool of cilia from the untreated cultured RS-fibroblasts. Some fibroblasts exhibited a smooth axoneme with limited bending whereas others were bumpy in different areas creating knots aspect. Some cilia were long cilia and twisted. We excluded from analysis some twisted cilia as some regions of the axoneme were not exposed to the Nikon Software analysis measurement tool. Based on our observation, we can conclude that cilia are abnormal in this autosomal dominant case of RS and propose to class of Robinow Syndrome as a ciliopathy.

The morphological defects present in the cultured fibroblasts can be used to demonstrate aberrant cilia in RS. This finding can be supported with published literature about the stability of primary cilia from cultured fibroblasts and those present in a body (Archer and Wheatley, 1971; Sorokin, 1962; Wheatley, 1972). Baker and Beales (2009) are the first to propose Robinow Syndrome in the list of syndromes with possible ciliary pathology. We can see a lack of ciliary investigation in Robinow Syndrome as most works have been focused on describing the phenotypes of affected individuals and finding the genetic cause that would enable them to explain the heterogeneity of clinical manifestations (Bunn et al., 2015; Bunn et al., 2014; Gignac et al., 2019; Robinow and Beemer, 1990; Robinow et al., 1969; White et al., 2015; White et al., 2016). Ciliary investigation had been also excluded in three proposed Robinow Syndrome mice models

(Liu et al., 2014; Schwabe et al., 2004; Yamaguchi et al., 1999). The *Prickle1*$^{Bj/Bj}$ is the first proposed RS mouse model that also has reported defects with cilia (Gibbs et al., 2016).

5.3.1.2 Intraflagellar transport defects

Because of time constraints due to the COVID-19 shutdown during the last 6 months of my work, we did not analyze components of the anterograde and the retrograde traffic in the hRS cultured fibroblasts. SMO translocation to the primary cilia can also be helpful to describe the anterograde transport from the cytoplasm, the lateral transport that is independent from the ciliary gate, and the retrograde transport that prevent SMO accumulation in the ciliary axoneme (Liem et al., 2012; Milenkovic et al., 2009). In untreated fibroblasts and in DMSO-treated control fibroblasts, we had observed faint SMO signals in the ciliary axonemes. The presence of SMO in the cilia before SHH inhibition or stimulation can indicate that anterograde and SMO lateral transport occur in hRS human fibroblasts and the pathway was activated (Corbit et al., 2005). As expected, SHH stimulation increase the level of smoothened in both the cilia and the cytoplasm. Consistent with a review about ciliary phenotypes in increased HH signaling, the cilia were bulged and short in the group treated with 50 μM of Purmorphamine (Goetz and Anderson, 2010). Surprisingly, the ciliary phenotype following HH inhibition was dose dependent causing the ciliary axonemes to shrink in response to higher dose. In contrast, to the exclusion of SMO in the cilia after administration of a HH agonist (Corbit et al., 2005), we detected brighter signals in the axonemes. In senescent fibroblasts, HH depletion with cyclopamine at dose of 20 μM diminished cell proliferation but increased ciliary length (Breslin et al., 2014). In our experiments, we did not observe length augmentation but a reduction. Interestingly, when we combined Purmophamine

and Vismodegib, the cilia grew longer, SMO remained inside the cilia and cause it to swell while the cytoplasmic pool decreased.

In the literature, Purmorphamine had been used to rescue an elongated ciliary phenotype of cultured fibroblasts of a patient with Joubert Syndrome that is a ciliopathy associated with cystic kidney disease (Srivastava et al., 2017). HH targeted inhibition therapy had been mostly used in BCCs (Athar et al., 2014; Bakshi et al., 2017; Booms et al., 2015; Bresler et al., 2016). We modeled the addition of the agonist simultaneously with the antagonist because it has been demonstrated to restore the HH pathway when Purmophamine was added with cyclopamine in culture Shh-LIGHT2 cells (Sinha and Chen, 2006). Based on our observations, we can propose a retrograde transport defect in this type of Robinow Syndrome causing SMO accumulation in the axoneme that created an imbalance in SHH gradient by overactivation of GliA.

5.3.2 Hedgehog Signaling defects

The result of the western blot pinpointed a defect in Gli3 processing in this osteosclerotic form of RS. The full-length of Gli3A was detected almost at the same intensity. Those cultured hRS fibroblasts' HH response was insensitive to dose stimulation. Gli3 kinetics after 5 minutes in cells culture had shown dose dependent increase and accumulation at ciliary tip (Wen et al., 2010). HH signaling also promotes degradation of full-length Gli3 by phosphorylation and ubiquitin proteasome degradation (Tempé et al., 2006; Wen et al., 2010). Moreover, Gli3 processing requires IFT (Haycraft et al., 2005; Tempé et al., 2006; Wen et al., 2010). Therefore, we can propose an impaired intraflagellar transport that led to a defect in Gli3 processing in Robinow Syndrome.

5.3.3 *Prickle1*^{Beetlejuice} mouse line as a model to study human Robinow Syndrome

Our animal study model the *Prickle1*^{Beetlejuice} mouse line contains a missense mutation in *Prickle1*. It has decreased Wnt signaling, and spatio-temporal disruption of HH signaling in the face, the frontal bone and the limbs (Gibbs et al., 2016; Wan et al., 2018). Using immunofluorescence staining and TEM, we confirmed ciliary morphological and length defects in *Prickle1*$^{Bj/Bj}$ embryos at E 10.5. Since the classification of the first ciliopathy in 1984 in Kartagener's Syndrome (Cornillie et al., 1984), many human syndromes have been investigated for ciliary dysfunction. At present, more than 30 human syndromes have been confirmed as ciliopathies while 127 disorders still need to be classified (Baker and Beales, 2009; Reiter and Leroux, 2017). Robinow Syndrome is investigated and grouped in the phenotypic overlap syndromes with possible ciliary pathology (Baker and Beales, 2009). Therefore, based on the phenotypic similarities of our mouse model to human RS, we propose *Prickle1* as a potential candidate in the list of refractory genes for molecular diagnosis of ~70% cases of autosomal dominant RS (White et al., 2018).

6.0 Conclusion and perspectives:

Based on previous findings from published literature, and our observation in the *Prickle1*^{Beetlejuice} mouse line, we propose a model for the role of Prickle1 in ciliogenesis (Figure 27): Prickle1 possibly participates with Dishevelled and Vangl1/2 in the docking and orientation of the basal bodies. After docking, some Prickle1 proteins may remain attached to the Dsh-Vangl1/2 complex whereas some migrate to the basal body and/or the ciliary axoneme to modulate proteins cargoes inside the cilia. In addition, Prickle1 seems to interact with the IFT-B complex to guide axonemal elongation, and with the IFT-A complex to maintain ciliary length. Balanced between those two events may contribute to regulate ciliary length. We need to investigate the mechanism by which Prickle1 enter the cilia and interact with IFT cargoes.

Rescuing the *Beetlejuice* mouse will necessitate a careful control of the HH pathway as a decreased or an increased level impact negatively craniofacial development. More investigation will be needed to assess the effect of Vismodegib in delaying osteogenesis. As osteosclerosis is a dangerous complication of RS because it can obliterate important foramina in the cranial base or elsewhere, it remains essential to explore a therapeutic window targeting the HH pathway in RS.

Although the genetic mutation of our mouse model is different than that of RS-fibroblasts, there are many similarities in the morphological and the ciliary phenotype, and in the perturbation of Gli3 processing. The *Beetlejuice* mouse model can be used to investigate therapeutic interventions by targeting the HH pathway and the crosstalk with the Wnt/PCP signaling. The role of *Prickle1* in ciliogenesis in the MNP mesenchyme of *Prickle1*$^{Bj/Bj}$ and the level of HH signaling in the face will also allow to study the process causing hypertelorism and the widening of the

midface in Robinow Syndrome. Therefore, the *Prickle1*^{Beetlejuice} mutant can fit as a ciliopathic and Robinow Syndrome model.

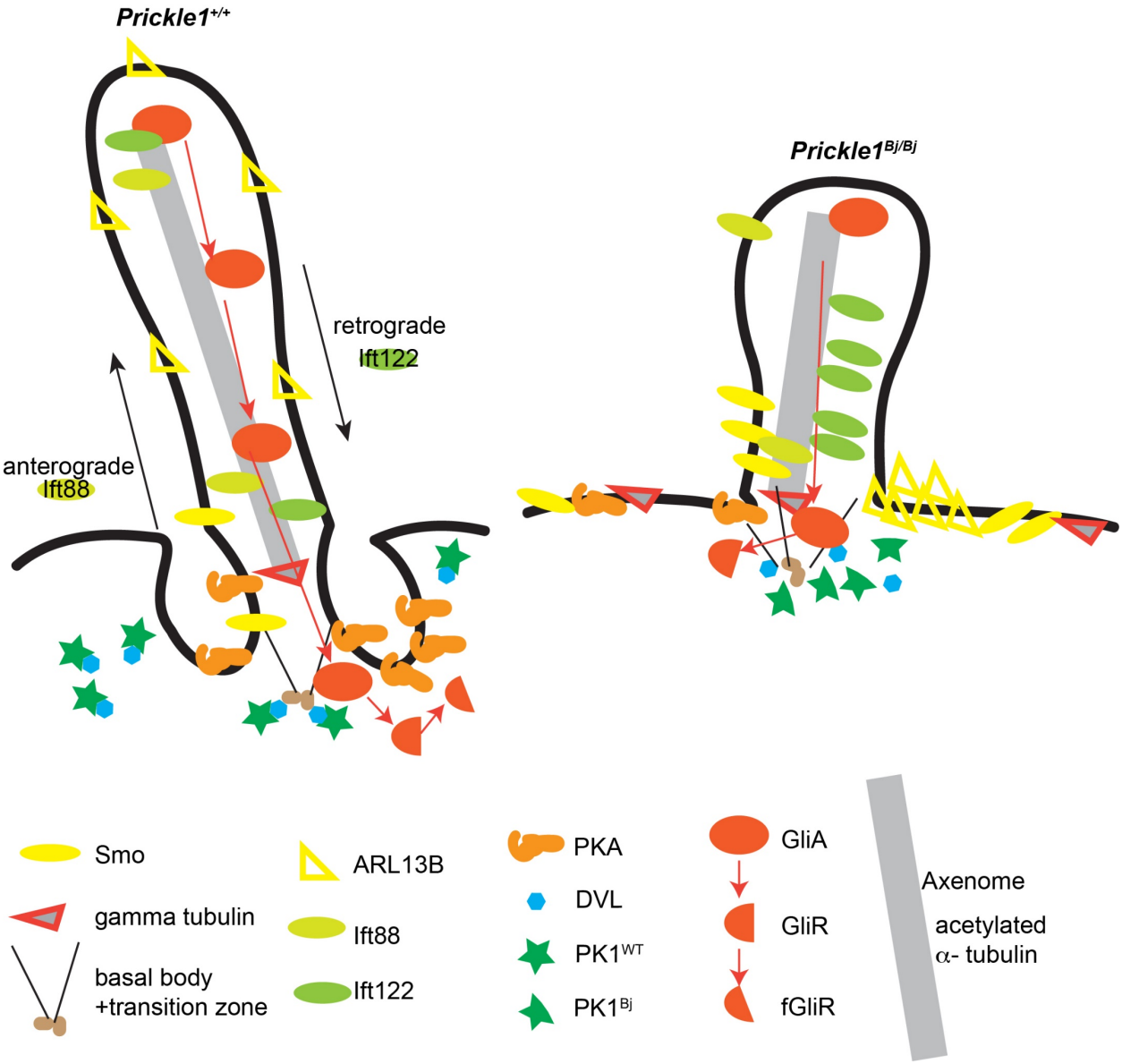

Figure 27: Graphical summary about the intraflagellar transport defect in the *Prickle1*^{Beetlejuice} mouse model.

The missense mutation in the LIM1 domain of Prickle1 in the *Prickle1*$^{Bj/Bj}$ mouse destabilizes Prickle1 and Dishevelled binding. Prickle1 likely participates with the complex Dishevelled and Vangl1/2 to guide the docking of basal bodies. During elongation, Prickle1 possibly modulate cargoes in the anterograde and retrograde trafficking.

When mutated, Prickle1 ciliary membrane and IFT particles, and HH components are mislocalized which cause the swollen or the abnormally elongated morphology.

Bibliography

Abramyan, J., 2019. Hedgehog Signaling and Embryonic Craniofacial Disorders. J Dev Biol 7.

Aditya, S., Rattan, A., 2013. Vismodegib: A smoothened inhibitor for the treatment of advanced basal cell carcinoma. Indian Dermatol Online J 4, 365-368.

Ahsan, K., Singh, N., Rocha, M., Huang, C., Prince, V.E., 2019. Prickle1 is required for EMT and migration of zebrafish cranial neural crest. Dev Biol 448, 16-35.

Algahtani, H., Al-Hakami, F., Al-Shehri, M., Shirah, B., Al-Qahtani, M.H., Abdulkareem, A.A., Naseer, M.I., 2019. A very rare form of autosomal dominant progressive myoclonus epilepsy caused by a novel variant in the PRICKLE1 gene. Seizure 69, 133-139.

Anvarian, Z., Mykytyn, K., Mukhopadhyay, S., Pedersen, L.B., Christensen, S.T., 2019. Cellular signalling by primary cilia in development, organ function and disease. Nat Rev Nephrol 15, 199-219.

Archer, F.L., Wheatley, D.N., 1971. Cilia in cell-cultured fibroblasts. II. Incidence in mitotic and post-mitotic BHK 21-C13 fibroblasts. J Anat 109, 277-292.

Arensdorf, A.M., Dillard, M.E., Menke, J.M., Frank, M.W., Rock, C.O., Ogden, S.K., 2017. Sonic Hedgehog Activates Phospholipase A2 to Enhance Smoothened Ciliary Translocation. Cell Rep 19, 2074-2087.

Athar, M., Li, C., Kim, A.L., Spiegelman, V.S., Bickers, D.R., 2014. Sonic hedgehog signaling in Basal cell nevus syndrome. Cancer Res 74, 4967-4975.

Ayukawa, T., Akiyama, M., Mummery-Widmer, J.L., Stoeger, T., Sasaki, J., Knoblich, J.A., Senoo, H., Sasaki, T., Yamazaki, M., 2014. Dachsous-dependent asymmetric localization of spiny-legs determines planar cell polarity orientation in Drosophila. Cell Rep 8, 610-621.

Bacino, C.A., 1993. ROR2-Related Robinow Syndrome, in: Adam, M.P., Ardinger, H.H., Pagon, R.A., Wallace, S.E., Bean, L.J.H., Stephens, K., Amemiya, A. (Eds.), GeneReviews(®). University of Washington, Seattle

Copyright © 1993-2020, University of Washington, Seattle. GeneReviews is a registered trademark of the University of Washington, Seattle. All rights reserved., Seattle (WA).

Baker, K., Beales, P.L., 2009. Making sense of cilia in disease: the human ciliopathies. Am J Med Genet C Semin Med Genet 151c, 281-295.

Bakshi, A., Chaudhary, S.C., Rana, M., Elmets, C.A., Athar, M., 2017. Basal cell carcinoma pathogenesis and therapy involving hedgehog signaling and beyond. Mol Carcinog 56, 2543-2557.

Bassuk, A.G., Wallace, R.H., Buhr, A., Buller, A.R., Afawi, Z., Shimojo, M., Miyata, S., Chen, S., Gonzalez-Alegre, P., Griesbach, H.L., Wu, S., Nashelsky, M., Vladar, E.K., Antic, D., Ferguson, P.J., Cirak, S., Voit, T., Scott, M.P., Axelrod, J.D., Gurnett, C., Daoud, A.S., Kivity, S., Neufeld, M.Y., Mazarib, A., Straussberg, R., Walid, S., Korczyn, A.D., Slusarski, D.C., Berkovic, S.F., El-Shanti, H.I., 2008. A homozygous mutation in human PRICKLE1 causes an autosomal-recessive progressive myoclonus epilepsy-ataxia syndrome. Am J Hum Genet 83, 572-581.

Basten, S.G., Giles, R.H., 2013. Functional aspects of primary cilia in signaling, cell cycle and tumorigenesis. Cilia 2, 6.

Benmerah, A., 2013. The ciliary pocket. Curr Opin Cell Biol 25, 78-84.

Benmerah, A., 2014. [The ciliary pocket: a rendezvous between the centrosome and vesicular trafficking]. Med Sci (Paris) 30, 962-967.

Bernabé-Rubio, M., Andrés, G., Casares-Arias, J., Fernández-Barrera, J., Rangel, L., Reglero-Real, N., Gershlick, D.C., Fernández, J.J., Millán, J., Correas, I., Miguez, D.G., Alonso, M.A., 2016. Novel role for the midbody in primary ciliogenesis by polarized epithelial cells. J Cell Biol 214, 259-273.
Bertrand, F.E., Angus, C.W., Partis, W.J., Sigounas, G., 2012. Developmental pathways in colon cancer: crosstalk between WNT, BMP, Hedgehog and Notch. Cell Cycle 11, 4344-4351.
Bisgrove, B.W., Yost, H.J., 2006. The roles of cilia in developmental disorders and disease. Development 133, 4131-4143.
Booms, P., Harth, M., Sader, R., Ghanaati, S., 2015. Vismodegib hedgehog-signaling inhibition and treatment of basal cell carcinomas as well as keratocystic odontogenic tumors in Gorlin syndrome. Ann Maxillofac Surg 5, 14-19.
Bresler, S.C., Padwa, B.L., Granter, S.R., 2016. Nevoid Basal Cell Carcinoma Syndrome (Gorlin Syndrome). Head Neck Pathol 10, 119-124.
Breslin, L., Prosser, S.L., Cuffe, S., Morrison, C.G., 2014. Ciliary abnormalities in senescent human fibroblasts impair proliferative capacity. Cell Cycle 13, 2773-2779.
Briscoe, J., 2006. Agonizing Hedgehog. Nature Chemical Biology 2, 10-11.
Briscoe, J., Therond, P.P., 2013. The mechanisms of Hedgehog signalling and its roles in development and disease. Nat Rev Mol Cell Biol 14, 416-429.
Buisson, J., Chenouard, N., Lagache, T., Blisnick, T., Olivo-Marin, J.C., Bastin, P., 2013. Intraflagellar transport proteins cycle between the flagellum and its base. J Cell Sci 126, 327-338.
Bunn, K.J., Daniel, P., Rosken, H.S., O'Neill, A.C., Cameron-Christie, S.R., Morgan, T., Brunner, H.G., Lai, A., Kunst, H.P., Markie, D.M., Robertson, S.P., 2015. Mutations in DVL1 cause an osteosclerotic form of Robinow syndrome. Am J Hum Genet 96, 623-630.
Bunn, K.J., Lai, A., Al-Ani, A., Farella, M., Craw, S., Robertson, S.P., 2014. An osteosclerotic form of Robinow syndrome. Am J Med Genet A 164a, 2638-2642.
Bush, J.O., Jiang, R., 2012. Palatogenesis: morphogenetic and molecular mechanisms of secondary palate development. Development 139, 231-243.
Butler, M.T., Wallingford, J.B., 2017. Planar cell polarity in development and disease. Nat Rev Mol Cell Biol 18, 375-388.
Cantagrel, V., Silhavy, J.L., Bielas, S.L., Swistun, D., Marsh, S.E., Bertrand, J.Y., Audollent, S., Attié-Bitach, T., Holden, K.R., Dobyns, W.B., Traver, D., Al-Gazali, L., Ali, B.R., Lindner, T.H., Caspary, T., Otto, E.A., Hildebrandt, F., Glass, I.A., Logan, C.V., Johnson, C.A., Bennett, C., Brancati, F., Valente, E.M., Woods, C.G., Gleeson, J.G., 2008. Mutations in the cilia gene ARL13B lead to the classical form of Joubert syndrome. Am J Hum Genet 83, 170-179.
Cao, Y., Park, A., Sun, Z., 2010. Intraflagellar transport proteins are essential for cilia formation and for planar cell polarity. J Am Soc Nephrol 21, 1326-1333.
Cardenas-Rodriguez, M., Badano, J.L., 2009. Ciliary biology: understanding the cellular and genetic basis of human ciliopathies. Am J Med Genet C Semin Med Genet 151c, 263-280.
Carlson, J.C., Anand, D., Butali, A., Buxo, C.J., Christensen, K., Deleyiannis, F., Hecht, J.T., Moreno, L.M., Orioli, I.M., Padilla, C., Shaffer, J.R., Vieira, A.R., Wehby, G.L., Weinberg, S.M., Murray, J.C., Beaty, T.H., Saadi, I., Lachke, S.A., Marazita, M.L., Feingold, E., Leslie, E.J., 2019. A systematic genetic analysis and visualization of phenotypic heterogeneity among orofacial cleft GWAS signals. Genet Epidemiol 43, 704-716.
Caspary, T., Larkins, C.E., Anderson, K.V., 2007. The graded response to Sonic Hedgehog depends on cilia architecture. Dev Cell 12, 767-778.

Cevik, S., Hori, Y., Kaplan, O.I., Kida, K., Toivenon, T., Foley-Fisher, C., Cottell, D., Katada, T., Kontani, K., Blacque, O.E., 2010. Joubert syndrome Arl13b functions at ciliary membranes and stabilizes protein transport in Caenorhabditis elegans. J Cell Biol 188, 953-969.
Chen, M.H., Wilson, C.W., Li, Y.J., Law, K.K., Lu, C.S., Gacayan, R., Zhang, X., Hui, C.C., Chuang, P.T., 2009. Cilium-independent regulation of Gli protein function by Sufu in Hedgehog signaling is evolutionarily conserved. Genes Dev 23, 1910-1928.
Cobourne, M.T., Hardcastle, Z., Sharpe, P.T., 2001. Sonic hedgehog regulates epithelial proliferation and cell survival in the developing tooth germ. J Dent Res 80, 1974-1979.
Corbit, K.C., Aanstad, P., Singla, V., Norman, A.R., Stainier, D.Y., Reiter, J.F., 2005. Vertebrate Smoothened functions at the primary cilium. Nature 437, 1018-1021.
Cornillie, F.J., Lauweryns, J.M., Corbeel, L., 1984. Atypical bronchial cilia in children with recurrent respiratory tract infections. A comparative ultrastructural study. Pathol Res Pract 178, 595-604.
Cortellino, S., Wang, C., Wang, B., Bassi, M.R., Caretti, E., Champeval, D., Calmont, A., Jarnik, M., Burch, J., Zaret, K.S., Larue, L., Bellacosa, A., 2009. Defective ciliogenesis, embryonic lethality and severe impairment of the Sonic Hedgehog pathway caused by inactivation of the mouse complex A intraflagellar transport gene Ift122/Wdr10, partially overlapping with the DNA repair gene Med1/Mbd4. Dev Biol 325, 225-237.
Davenport, J.R., Yoder, B.K., 2005. An incredible decade for the primary cilium: a look at a once-forgotten organelle. Am J Physiol Renal Physiol 289, F1159-1169.
Dawe, H.R., Farr, H., Gull, K., 2007. Centriole/basal body morphogenesis and migration during ciliogenesis in animal cells. J Cell Sci 120, 7-15.
Deane, J.A., Cole, D.G., Seeley, E.S., Diener, D.R., Rosenbaum, J.L., 2001. Localization of intraflagellar transport protein IFT52 identifies basal body transitional fibers as the docking site for IFT particles. Curr Biol 11, 1586-1590.
Dupont, M.A., Humbert, C., Huber, C., Siour, Q., Guerrera, I.C., Jung, V., Christensen, A., Pouliet, A., Garfa-Traoré, M., Nitschké, P., Injeyan, M., Millar, K., Chitayat, D., Shannon, P., Girisha, K.M., Shukla, A., Mechler, C., Lorentzen, E., Benmerah, A., Cormier-Daire, V., Jeanpierre, C., Saunier, S., Delous, M., 2019. Human IFT52 mutations uncover a novel role for the protein in microtubule dynamics and centrosome cohesion. Hum Mol Genet 28, 2720-2737.
Duran, I., Taylor, S.P., Zhang, W., Martin, J., Qureshi, F., Jacques, S.M., Wallerstein, R., Lachman, R.S., Nickerson, D.A., Bamshad, M., Cohn, D.H., Krakow, D., 2017. Mutations in IFT-A satellite core component genes IFT43 and IFT121 produce short rib polydactyly syndrome with distinctive campomelia. Cilia 6, 7.
Dworkin, S., Boglev, Y., Owens, H., Goldie, S.J., 2016. The Role of Sonic Hedgehog in Craniofacial Patterning, Morphogenesis and Cranial Neural Crest Survival. J Dev Biol 4.
Eggenschwiler, J.T., Anderson, K.V., 2007. Cilia and developmental signaling. Annu Rev Cell Dev Biol 23, 345-373.
Ehaideb, S.N., Iyengar, A., Ueda, A., Iacobucci, G.J., Cranston, C., Bassuk, A.G., Gubb, D., Axelrod, J.D., Gunawardena, S., Wu, C.F., Manak, J.R., 2014. prickle modulates microtubule polarity and axonal transport to ameliorate seizures in flies. Proc Natl Acad Sci U S A 111, 11187-11192.
Feuerstein, R., Wang, X., Song, D., Cooke, N.E., Liebhaber, S.A., 1994. The LIM/double zinc-finger motif functions as a protein dimerization domain. Proceedings of the National Academy of Sciences 91, 10655-10659.

Fliegauf, M., Benzing, T., Omran, H., 2007. When cilia go bad: cilia defects and ciliopathies. Nat Rev Mol Cell Biol 8, 880-893.
Frampton, J.E., Basset-Séguin, N., 2018. Vismodegib: A Review in Advanced Basal Cell Carcinoma. Drugs 78, 1145-1156.
Garcia, G., 3rd, Raleigh, D.R., Reiter, J.F., 2018. How the Ciliary Membrane Is Organized Inside-Out to Communicate Outside-In. Curr Biol 28, R421-r434.
Garcia, G., 3rd, Reiter, J.F., 2016. A primer on the mouse basal body. Cilia 5, 17.
Garmon, T., Wittling, M., Nie, S., 2018. MMP14 Regulates Cranial Neural Crest Epithelial-to-Mesenchymal Transition and Migration. Dev Dyn 247, 1083-1092.
Geoffroy, V., Stoetzel, C., Scheidecker, S., Schaefer, E., Perrault, I., Bär, S., Kröll, A., Delbarre, M., Antin, M., Leuvrey, A.S., Henry, C., Blanché, H., Decker, E., Kloth, K., Klaus, G., Mache, C., Martin-Coignard, D., McGinn, S., Boland, A., Deleuze, J.F., Friant, S., Saunier, S., Rozet, J.M., Bergmann, C., Dollfus, H., Muller, J., 2018. Whole-genome sequencing in patients with ciliopathies uncovers a novel recurrent tandem duplication in IFT140. Hum Mutat 39, 983-992.
Gerondopoulos, A., Strutt, H., Stevenson, N.L., Sobajima, T., Levine, T.P., Stephens, D.J., Strutt, D., Barr, F.A., 2019. Planar Cell Polarity Effector Proteins Inturned and Fuzzy Form a Rab23 GEF Complex. Curr Biol 29, 3323-3330.e3328.
Ghossoub, R., Molla-Herman, A., Bastin, P., Benmerah, A., 2011. The ciliary pocket: a once-forgotten membrane domain at the base of cilia. Biol Cell 103, 131-144.
Gibbs, B.C., Damerla, R.R., Vladar, E.K., Chatterjee, B., Wan, Y., Liu, X., Cui, C., Gabriel, G.C., Zahid, M., Yagi, H., Szabo-Rogers, H.L., Suyama, K.L., Axelrod, J.D., Lo, C.W., 2016. Prickle1 mutation causes planar cell polarity and directional cell migration defects associated with cardiac outflow tract anomalies and other structural birth defects. Biol Open 5, 323-335.
Gigante, E.D., Taylor, M.R., Ivanova, A.A., Kahn, R.A., Caspary, T., 2020. ARL13B regulates Sonic hedgehog signaling from outside primary cilia. Elife 9.
Gignac, S.J., Hosseini-Farahabadi, S., Akazawa, T., Schuck, N.J., Fu, K., Richman, J.M., 2019. Robinow syndrome skeletal phenotypes caused by the WNT5AC83S variant are due to dominant interference with chondrogenesis. Hum Mol Genet.
Gilbert, S.P., Guzik-Lendrum, S., Rayment, I., 2018. Kinesin-2 motors: Kinetics and biophysics. The Journal of biological chemistry 293, 4510-4518.
Goetz, S.C., Anderson, K.V., 2010. The primary cilium: a signalling centre during vertebrate development. Nat Rev Genet 11, 331-344.
Goodson, H.V., Jonasson, E.M., 2018. Microtubules and Microtubule-Associated Proteins. Cold Spring Harb Perspect Biol 10.
Graham, R.A., Hop, C.E., Borin, M.T., Lum, B.L., Colburn, D., Chang, I., Shin, Y.G., Malhi, V., Low, J.A., Dresser, M.J., 2012. Single and multiple dose intravenous and oral pharmacokinetics of the hedgehog pathway inhibitor vismodegib in healthy female subjects. Br J Clin Pharmacol 74, 788-796.
Gray, R.S., Abitua, P.B., Wlodarczyk, B.J., Szabo-Rogers, H.L., Blanchard, O., Lee, I., Weiss, G.S., Liu, K.J., Marcotte, E.M., Wallingford, J.B., Finnell, R.H., 2009. The planar cell polarity effector Fuz is essential for targeted membrane trafficking, ciliogenesis and mouse embryonic development. Nat Cell Biol 11, 1225-1232.
Gregory J. Pazour, B.L.D., Yvonne Vucica, E. Scott Seeley, Joel L. Rosenbaum, George B. Witman, and Douglas G. Cole, 2000. Chlamydomonas IFT 88 and Its Mouse Homologue, Polycystic Kidney Disease Gene Tg 737, Are Required for Assembly of Cilia and Flagella. The Journal of Cell Biology 151, 9.

Gubb, D., Green, C., Huen, D., Coulson, D., Johnson, G., Tree, D., Collier, S., Roote, J., 1999. The balance between isoforms of the prickle LIM domain protein is critical for planar polarity in Drosophila imaginal discs. Genes Dev 13, 2315-2327.
Guo, D., Li, M., Zou, B., Gu, X., Yuan, Z., Liu, M., Mao, F., Ouyang, H., Wu, K., Wei, L., Liu, Y., Liu, C., 2019. Ocular surface pathogenesis associated with precocious eyelid opening and necrotic autologous tissue in mouse with disruption of Prickle 1 gene. Exp Eye Res 180, 208-225.
Hammond, N.L., Brookes, K.J., Dixon, M.J., 2018. Ectopic Hedgehog Signaling Causes Cleft Palate and Defective Osteogenesis. J Dent Res 97, 1485-1493.
Hampl, M., Cela, P., Szabo-Rogers, H.L., Kunova Bosakova, M., Dosedelova, H., Krejci, P., Buchtova, M., 2017. Role of Primary Cilia in Odontogenesis. J Dent Res 96, 965-974.
Handa, A., Voss, U., Hammarsjö, A., Grigelioniene, G., Nishimura, G., 2020. Skeletal ciliopathies: a pattern recognition approach. Jpn J Radiol 38, 193-206.
Haycraft, C.J., Banizs, B., Aydin-Son, Y., Zhang, Q., Michaud, E.J., Yoder, B.K., 2005. Gli2 and Gli3 localize to cilia and require the intraflagellar transport protein polaris for processing and function. PLoS Genet 1, e53.
Haycraft, C.J., Serra, R., 2008. Chapter 11 Cilia Involvement in Patterning and Maintenance of the Skeleton, Ciliary Function in Mammalian Development, pp. 303-332.
Heyne, G.W., Melberg, C.G., Doroodchi, P., Parins, K.F., Kietzman, H.W., Everson, J.L., Ansen-Wilson, L.J., Lipinski, R.J., 2015. Definition of critical periods for Hedgehog pathway antagonist-induced holoprosencephaly, cleft lip, and cleft palate. PLoS One 10, e0120517.
Hu, D., Helms, J.A., 1999. The role of sonic hedgehog in normal and abnormal craniofacial morphogenesis. Development 126, 4873-4884.
Huangfu, D., Anderson, K.V., 2006. Signaling from Smo to Ci/Gli: conservation and divergence of Hedgehog pathways from Drosophila to vertebrates. Development 133, 3-14.
Hui, C.C., Angers, S., 2011. Gli proteins in development and disease. Annu Rev Cell Dev Biol 27, 513-537.
Humphries, A.C., Mlodzik, M., 2018. From instruction to output: Wnt/PCP signaling in development and cancer. Curr Opin Cell Biol 51, 110-116.
Inc, G., 2012. ERIVEDGE® (vismodegib) capsule for oral use: US prescribing information.
Jenny, A., Reynolds-Kenneally, J., Das, G., Burnett, M., Mlodzik, M., 2005. Diego and Prickle regulate Frizzled planar cell polarity signalling by competing for Dishevelled binding. Nat Cell Biol 7, 691-697.
Jensen, C.G., Poole, C.A., McGlashan, S.R., Marko, M., Issa, Z.I., Vujcich, K.V., Bowser, S.S., 2004. Ultrastructural, tomographic and confocal imaging of the chondrocyte primary cilium in situ. Cell Biol Int 28, 101-110.
Kadrmas, J.L., Beckerle, M.C., 2004. The LIM domain: from the cytoskeleton to the nucleus. Nat Rev Mol Cell Biol 5, 920-931.
Katoh, M., Katoh, M., 2003. Identification and characterization of human PRICKLE1 and PRICKLE2 genes as well as mouse Prickle1 and Prickle2 genes homologous to Drosophila tissue polarity gene prickle. International journal of molecular medicine 11, 249-256.
Katoh, M., Katoh, M., 2017. Molecular genetics and targeted therapy of WNT-related human diseases (Review). International journal of molecular medicine 40, 587-606.
Kaufman, M.H., 1992. The Atlas of Mouse Development. Elsevier Science.
Kaur, S., McGlashan, S.R., Ward, M.L., 2018. Evidence of primary cilia in the developing rat heart. Cilia 7, 4.

Keeling, J., Tsiokas, L., Maskey, D., 2016. Cellular Mechanisms of Ciliary Length Control. Cells 5.
Kiseleva, A.A., Korobeynikov, V.A., Nikonova, A.S., Zhang, P., Makhov, P., Deneka, A.Y., Einarson, M.B., Serebriiskii, I.G., Liu, H., Peterson, J.R., Golemis, E.A., 2019. Unexpected Activities in Regulating Ciliation Contribute to Off-target Effects of Targeted Drugs. Clinical Cancer Research 25, 4179-4193.
Komiya, Y., Habas, R., 2008. Wnt signal transduction pathways. Organogenesis 4, 68-75.
Kumar, S., Reynolds, K., Ji, Y., Gu, R., Rai, S., Zhou, C.J., 2019. Impaired neurodevelopmental pathways in autism spectrum disorder: a review of signaling mechanisms and crosstalk. J Neurodev Disord 11, 10.
Kunova Bosakova, M., Varecha, M., Hampl, M., Duran, I., Nita, A., Buchtova, M., Dosedelova, H., Machat, R., Xie, Y., Ni, Z., Martin, J.H., Chen, L., Jansen, G., Krakow, D., Krejci, P., 2018. Regulation of ciliary function by fibroblast growth factor signaling identifies FGFR3-related disorders achondroplasia and thanatophoric dysplasia as ciliopathies. Hum Mol Genet 27, 1093-1105.
Kurosaka, H., 2015. The Roles of Hedgehog Signaling in Upper Lip Formation. Biomed Res Int 2015, 901041.
Kurosaka, H., Iulianella, A., Williams, T., Trainor, P.A., 2014. Disrupting hedgehog and WNT signaling interactions promotes cleft lip pathogenesis. J Clin Invest 124, 1660-1671.
Lan, Y., Jiang, R., 2009. Sonic hedgehog signaling regulates reciprocal epithelial-mesenchymal interactions controlling palatal outgrowth. Development 136, 1387-1396.
Larkins, C.E., Aviles, G.D., East, M.P., Kahn, R.A., Caspary, T., 2011. Arl13b regulates ciliogenesis and the dynamic localization of Shh signaling proteins. Mol Biol Cell 22, 4694-4703.
Lattao, R., Kovács, L., Glover, D.M., 2017. The Centrioles, Centrosomes, Basal Bodies, and Cilia of Drosophila melanogaster. Genetics 206, 33-53.
Li, C., Lan, Y., Jiang, R., 2017. Molecular and Cellular Mechanisms of Palate Development. J Dent Res 96, 1184-1191.
Liem, K.F., Jr., Ashe, A., He, M., Satir, P., Moran, J., Beier, D., Wicking, C., Anderson, K.V., 2012. The IFT-A complex regulates Shh signaling through cilia structure and membrane protein trafficking. J Cell Biol 197, 789-800.
Lin, Y.Y., Gubb, D., 2009. Molecular dissection of Drosophila Prickle isoforms distinguishes their essential and overlapping roles in planar cell polarity. Dev Biol 325, 386-399.
Lipinski, R.J., Song, C., Sulik, K.K., Everson, J.L., Gipp, J.J., Yan, D., Bushman, W., Rowland, I.J., 2010. Cleft lip and palate results from Hedgehog signaling antagonism in the mouse: Phenotypic characterization and clinical implications. Birth Defects Res A Clin Mol Teratol 88, 232-240.
Liu, A., Wang, B., Niswander, L.A., 2005. Mouse intraflagellar transport proteins regulate both the activator and repressor functions of Gli transcription factors. Development 132, 3103-3111.
Liu, C., Lin, C., Gao, C., May-Simera, H., Swaroop, A., Li, T., 2014. Null and hypomorph Prickle1 alleles in mice phenocopy human Robinow syndrome and disrupt signaling downstream of Wnt5a. Biol Open 3, 861-870.
Liu, C., Lin, C., Whitaker, D.T., Bakeri, H., Bulgakov, O.V., Liu, P., Lei, J., Dong, L., Li, T., Swaroop, A., 2013. Prickle1 is expressed in distinct cell populations of the central nervous system and contributes to neuronal morphogenesis. Hum Mol Genet 22, 2234-2246.
LoRusso, P.M., Rudin, C.M., Reddy, J.C., Tibes, R., Weiss, G.J., Borad, M.J., Hann, C.L., Brahmer, J.R., Chang, I., Darbonne, W.C., Graham, R.A., Zerivitz, K.L., Low, J.A., Von Hoff,

D.D., 2011. Phase I trial of hedgehog pathway inhibitor vismodegib (GDC-0449) in patients with refractory, locally advanced or metastatic solid tumors. Clin Cancer Res 17, 2502-2511.
Lu, Q., Schafer, D.A., Adler, P.N., 2015. The Drosophila planar polarity gene multiple wing hairs directly regulates the actin cytoskeleton. Development 142, 2478-2486.
Lupi, O., 2007. Correlations between the Sonic Hedgehog pathway and basal cell carcinoma. Int J Dermatol 46, 1113-1117.
Marshall, W.F., 2008. Basal bodies platforms for building cilia. Curr Top Dev Biol 85, 1-22.
Maruthamuthu, V., Aratyn-Schaus, Y., Gardel, M.L., 2010. Conserved F-actin dynamics and force transmission at cell adhesions. Curr Opin Cell Biol 22, 583-588.
Mazzeu, J.F., Pardono, E., Vianna-Morgante, A.M., Richieri-Costa, A., Ae Kim, C., Brunoni, D., Martelli, L., de Andrade, C.E., Colin, G., Otto, P.A., 2007. Clinical characterization of autosomal dominant and recessive variants of Robinow syndrome. Am J Med Genet A 143, 320-325.
McClure-Begley, T.D., Klymkowsky, M.W., 2017. Nuclear roles for cilia-associated proteins. Cilia 6, 8.
Menezes, R., Letra, A., Kim, A.H., Küchler, E.C., Day, A., Tannure, P.N., Gomes da Motta, L., Paiva, K.B., Granjeiro, J.M., Vieira, A.R., 2010. Studies with Wnt genes and nonsyndromic cleft lip and palate. Birth Defects Res A Clin Mol Teratol 88, 995-1000.
Michaud, E.J., Yoder, B.K., 2006. The primary cilium in cell signaling and cancer. Cancer Res 66, 6463-6467.
Mickolajczyk, K.J., Hancock, W.O., 2017. Kinesin Processivity Is Determined by a Kinetic Race from a Vulnerable One-Head-Bound State. Biophysical journal 112, 2615-2623.
Milenkovic, L., Scott, M.P., Rohatgi, R., 2009. Lateral transport of Smoothened from the plasma membrane to the membrane of the cilium. J Cell Biol 187, 365-374.
Mlodzik, M., 2002. Planar cell polarization: do the same mechanisms regulate Drosophila tissue polarity and vertebrate gastrulation? Trends Genet 18, 564-571.
Mohan, R., John, A., 2015. Microtubule-associated proteins as direct crosslinkers of actin filaments and microtubules. IUBMB Life 67, 395-403.
Molla-Herman, A., Ghossoub, R., Blisnick, T., Meunier, A., Serres, C., Silbermann, F., Emmerson, C., Romeo, K., Bourdoncle, P., Schmitt, A., Saunier, S., Spassky, N., Bastin, P., Benmerah, A., 2010. The ciliary pocket: an endocytic membrane domain at the base of primary and motile cilia. J Cell Sci 123, 1785-1795.
Mossaad, A.M., Abdelrahman, M.A., Ibrahim, M.A., Al Ahmady, H.H., 2018. Surgical Management of Facial Features of Robinow Syndrome: A Case Report. Open Access Maced J Med Sci 6, 536-539.
Myklebust, R., Engedal, H., Saetersdal, T.S., Ulstein, M., 1977. Primary 9 + 0 cilia in the embryonic and the adult human heart. Anat Embryol (Berl) 151, 127-139.
Nachury, M.V., Mick, D.U., 2019. Establishing and regulating the composition of cilia for signal transduction. Nat Rev Mol Cell Biol 20, 389-405.
Nanci, A., 2008. Ten Cate'S Oral Histology: Development, Structure & Function (7Th Edition). Elsevier (A Divisionof Reed Elsevier India Pvt. Limited).
Noubissi, F.K., Yedjou, C.G., Spiegelman, V.S., Tchounwou, P.B., 2018. Cross-Talk between Wnt and Hh Signaling Pathways in the Pathology of Basal Cell Carcinoma. Int J Environ Res Public Health 15.
Okuda, H., Miyata, S., Mori, Y., Tohyama, M., 2007. Mouse Prickle1 and Prickle2 are expressed in postmitotic neurons and promote neurite outgrowth. FEBS Lett 581, 4754-4760.

Oteiza, P., Köppen, M., Krieg, M., Pulgar, E., Farias, C., Melo, C., Preibisch, S., Müller, D., Tada, M., Hartel, S., Heisenberg, C.P., Concha, M.L., 2010. Planar cell polarity signalling regulates cell adhesion properties in progenitors of the zebrafish laterality organ. Development 137, 3459-3468.
Park, T.J., Mitchell, B.J., Abitua, P.B., Kintner, C., Wallingford, J.B., 2008. Dishevelled controls apical docking and planar polarization of basal bodies in ciliated epithelial cells. Nat Genet 40, 871-879.
Patton, M., Afzal, A.J., 2002. Robinow syndrome. Journal of medical genetics 39, 305-310.
Pazour, G.J., Dickert, B.L., Vucica, Y., Seeley, E.S., Rosenbaum, J.L., Witman, G.B., Cole, D.G., 2000. Chlamydomonas IFT88 and its mouse homologue, polycystic kidney disease gene tg737, are required for assembly of cilia and flagella. J Cell Biol 151, 709-718.
Pazour, G.J., Wilkerson, C.G., Witman, G.B., 1998. A dynein light chain is essential for the retrograde particle movement of intraflagellar transport (IFT). J Cell Biol 141, 979-992.
Pedersen, L.B., Veland, I.R., Schroder, J.M., Christensen, S.T., 2008. Assembly of primary cilia. Dev Dyn 237, 1993-2006.
Perdomo, D., Bonhivers, M., Robinson, D.R., 2016. The Trypanosome Flagellar Pocket Collar and Its Ring Forming Protein-TbBILBO1. Cells 5.
Person, A.D., Beiraghi, S., Sieben, C.M., Hermanson, S., Neumann, A.N., Robu, M.E., Schleiffarth, J.R., Billington, C.J., Jr., van Bokhoven, H., Hoogeboom, J.M., Mazzeu, J.F., Petryk, A., Schimmenti, L.A., Brunner, H.G., Ekker, S.C., Lohr, J.L., 2010. WNT5A mutations in patients with autosomal dominant Robinow syndrome. Dev Dyn 239, 327-337.
Prevo, B., Scholey, J.M., Peterman, E.J.G., 2017. Intraflagellar transport: mechanisms of motor action, cooperation, and cargo delivery. Febs j 284, 2905-2931.
Proctor, A.E., Thompson, L.A., O'Bryant, C.L., 2014. Vismodegib: an inhibitor of the Hedgehog signaling pathway in the treatment of basal cell carcinoma. Ann Pharmacother 48, 99-106.
Qin, J., Lin, Y., Norman, R.X., Ko, H.W., Eggenschwiler, J.T., 2011. Intraflagellar transport protein 122 antagonizes Sonic Hedgehog signaling and controls ciliary localization of pathway components. Proc Natl Acad Sci U S A 108, 1456-1461.
Reiter, J.F., Leroux, M.R., 2017. Genes and molecular pathways underpinning ciliopathies. Nat Rev Mol Cell Biol 18, 533-547.
Reynolds, K., Kumari, P., Sepulveda Rincon, L., Gu, R., Ji, Y., Kumar, S., Zhou, C.J., 2019. Wnt signaling in orofacial clefts: crosstalk, pathogenesis and models. Dis Model Mech 12.
Roberts, A.J., 2018. Emerging mechanisms of dynein transport in the cytoplasm versus the cilium. Biochem Soc Trans 46, 967-982.
Robinow, M., Beemer, F.A., 1990. New syndrome. American Journal of Medical Genetics 36, 375-375.
Robinow, M., Silverman, F.N., Smith, H.D., 1969. A newly recognized dwarfing syndrome. Am J Dis Child 117, 645-651.
Rohatgi, R., Milenkovic, L., Scott, M.P., 2007. Patched1 regulates hedgehog signaling at the primary cilium. Science 317, 372-376.
Rohatgi, R., Snell, W.J., 2010. The ciliary membrane. Curr Opin Cell Biol 22, 541-546.
Roifman, M., Brunner, H., Lohr, J., Mazzeu, J., Chitayat, D., 1993. Autosomal Dominant Robinow Syndrome, in: Adam, M.P., Ardinger, H.H., Pagon, R.A., Wallace, S.E., Bean, L.J.H., Stephens, K., Amemiya, A. (Eds.), GeneReviews((R)). University of Washington, Seattle
University of Washington, Seattle. GeneReviews is a registered trademark of the University of Washington, Seattle. All rights reserved., Seattle (WA).

Sadler, T.W., 2012. Langman's Medical Embryology. Wolters Kluwer Health/Lippincott Williams & Wilkins.
Satir, P., 2017. CILIA: before and after. Cilia 6, 1.
Satir, P., Christensen, S.T., 2007. Overview of structure and function of mammalian cilia. Annu Rev Physiol 69, 377-400.
Satir, P., Christensen, S.T., 2008. Structure and function of mammalian cilia. Histochem Cell Biol 129, 687-693.
Satishchandra, P., Sinha, S., 2010. Progressive myoclonic epilepsy. Neurol India 58, 514-522.
Schliwa, M., Woehlke, G., 2003. Molecular motors. Nature 422, 759-765.
Schock, E.N., Struve, J.N., Chang, C.F., Williams, T.J., Snedeker, J., Attia, A.C., Stottmann, R.W., Brugmann, S.A., 2017. A tissue-specific role for intraflagellar transport genes during craniofacial development. PLoS One 12, e0174206.
Schrick, J.J., Onuchic, L.F., Reeders, S.T., Korenberg, J., Chen, X.N., Moyer, J.H., Wilkinson, J.E., Woychik, R.P., 1995. Characterization of the human homologue of the mouse Tg737 candidate polycystic kidney disease gene. Hum Mol Genet 4, 559-567.
Schwabe, G.C., Trepczik, B., Suring, K., Brieske, N., Tucker, A.S., Sharpe, P.T., Minami, Y., Mundlos, S., 2004. Ror2 knockout mouse as a model for the developmental pathology of autosomal recessive Robinow syndrome. Dev Dyn 229, 400-410.
Sekulic, A., Migden, M.R., Lewis, K., Hainsworth, J.D., Solomon, J.A., Yoo, S., Arron, S.T., Friedlander, P.A., Marmur, E., Rudin, C.M., Chang, A.L., Dirix, L., Hou, J., Yue, H., Hauschild, A., 2015. Pivotal ERIVANCE basal cell carcinoma (BCC) study: 12-month update of efficacy and safety of vismodegib in advanced BCC. J Am Acad Dermatol 72, 1021-1026.e1028.
Sekulic, A., Migden, M.R., Oro, A.E., Dirix, L., Lewis, K.D., Hainsworth, J.D., Solomon, J.A., Yoo, S., Arron, S.T., Friedlander, P.A., Marmur, E., Rudin, C.M., Chang, A.L., Low, J.A., Mackey, H.M., Yauch, R.L., Graham, R.A., Reddy, J.C., Hauschild, A., 2012. Efficacy and safety of vismodegib in advanced basal-cell carcinoma. N Engl J Med 366, 2171-2179.
Shprintzen, R.J., Goldberg, R.B., Saenger, P., Sidoti, E.J., 1982. Male-to-male transmission of Robinow's syndrome. Its occurrence in association with cleft lip and cleft palate. Am J Dis Child 136, 594-597.
Shulman, J.M., Perrimon, N., Axelrod, J.D., 1998. Frizzled signaling and the developmental control of cell polarity. Trends Genet 14, 452-458.
Simons, M., Gloy, J., Ganner, A., Bullerkotte, A., Bashkurov, M., Krönig, C., Schermer, B., Benzing, T., Cabello, O.A., Jenny, A., Mlodzik, M., Polok, B., Driever, W., Obara, T., Walz, G., 2005. Inversin, the gene product mutated in nephronophthisis type II, functions as a molecular switch between Wnt signaling pathways. Nat Genet 37, 537-543.
Simons, M., Mlodzik, M., 2008. Planar cell polarity signaling: from fly development to human disease. Annu Rev Genet 42, 517-540.
Singh, B.N., Fu, J., Srivastava, R.K., Shankar, S., 2011. Hedgehog signaling antagonist GDC-0449 (Vismodegib) inhibits pancreatic cancer stem cell characteristics: molecular mechanisms. PLoS One 6, e27306.
Sinha, S., Chen, J.K., 2006. Purmorphamine activates the Hedgehog pathway by targeting Smoothened. Nature Chemical Biology 2, 29-30.
Sorokin, S., 1962. Centrioles and the formation of rudimentary cilia by fibroblasts and smooth muscle cells. J Cell Biol 15, 363-377.
Srivastava, S., Ramsbottom, S.A., Molinari, E., Alkanderi, S., Filby, A., White, K., Henry, C., Saunier, S., Miles, C.G., Sayer, J.A., 2017. A human patient-derived cellular model of Joubert

syndrome reveals ciliary defects which can be rescued with targeted therapies. Hum Mol Genet 26, 4657-4667.
Sweede, M., Ankem, G., Chutvirasakul, B., Azurmendi, H.F., Chbeir, S., Watkins, J., Helm, R.F., Finkielstein, C.V., Capelluto, D.G., 2008. Structural and membrane binding properties of the prickle PET domain. Biochemistry 47, 13524-13536.
Takahara, M., Katoh, Y., Nakamura, K., Hirano, T., Sugawa, M., Tsurumi, Y., Nakayama, K., 2018. Ciliopathy-associated mutations of IFT122 impair ciliary protein trafficking but not ciliogenesis. Hum Mol Genet 27, 516-528.
Takei, R., Katoh, Y., Nakayama, K., 2018. Robust interaction of IFT70 with IFT52-IFT88 in the IFT-B complex is required for ciliogenesis. Biol Open 7.
Takeuchi, S., Takeda, K., Oishi, I., Nomi, M., Ikeya, M., Itoh, K., Tamura, S., Ueda, T., Hatta, T., Otani, H., Terashima, T., Takada, S., Yamamura, H., Akira, S., Minami, Y., 2000. Mouse Ror2 receptor tyrosine kinase is required for the heart development and limb formation. Genes Cells 5, 71-78.
Tao, H., Suzuki, M., Kiyonari, H., Abe, T., Sasaoka, T., Ueno, N., 2009. Mouse prickle1, the homolog of a PCP gene, is essential for epiblast apical-basal polarity. Proc Natl Acad Sci U S A 106, 14426-14431.
Tempé, D., Casas, M., Karaz, S., Blanchet-Tournier, M.F., Concordet, J.P., 2006. Multisite protein kinase A and glycogen synthase kinase 3beta phosphorylation leads to Gli3 ubiquitination by SCFbetaTrCP. Mol Cell Biol 26, 4316-4326.
Tian, H., Feng, J., Li, J., Ho, T.V., Yuan, Y., Liu, Y., Brindopke, F., Figueiredo, J.C., Magee, W., 3rd, Sanchez-Lara, P.A., Chai, Y., 2017. Intraflagellar transport 88 (IFT88) is crucial for craniofacial development in mice and is a candidate gene for human cleft lip and palate. Hum Mol Genet 26, 860-872.
Tissir, F., Goffinet, A.M., 2006. Expression of planar cell polarity genes during development of the mouse CNS. Eur J Neurosci 23, 597-607.
Todd, B.P., Bassuk, A.G., 2018. A de novo mutation in PRICKLE1 associated with myoclonic epilepsy and autism spectrum disorder. J Neurogenet 32, 313-315.
Tuma, R., 2004. Pericentrin pivotal in primary cilia. J Cell Biol 166, 607.
Verhey, K.J., Dishinger, J., Kee, H.L., 2011. Kinesin motors and primary cilia. Biochem Soc Trans 39, 1120-1125.
Vinson, C.R., Conover, S., Adler, P.N., 1989. A Drosophila tissue polarity locus encodes a protein containing seven potential transmembrane domains. Nature 338, 263-264.
Von Hoff, D.D., LoRusso, P.M., Rudin, C.M., Reddy, J.C., Yauch, R.L., Tibes, R., Weiss, G.J., Borad, M.J., Hann, C.L., Brahmer, J.R., Mackey, H.M., Lum, B.L., Darbonne, W.C., Marsters, J.C., Jr., de Sauvage, F.J., Low, J.A., 2009. Inhibition of the hedgehog pathway in advanced basal-cell carcinoma. N Engl J Med 361, 1164-1172.
Walczak-Sztulpa, J., Eggenschwiler, J., Osborn, D., Brown, D.A., Emma, F., Klingenberg, C., Hennekam, R.C., Torre, G., Garshasbi, M., Tzschach, A., Szczepanska, M., Krawczynski, M., Zachwieja, J., Zwolinska, D., Beales, P.L., Ropers, H.H., Latos-Bielenska, A., Kuss, A.W., 2010. Cranioectodermal Dysplasia, Sensenbrenner syndrome, is a ciliopathy caused by mutations in the IFT122 gene. Am J Hum Genet 86, 949-956.
Wallingford, J.B., Mitchell, B., 2011. Strange as it may seem: the many links between Wnt signaling, planar cell polarity, and cilia. Genes Dev 25, 201-213.
Wan, Y., Lantz, B., Cusack, B.J., Szabo-Rogers, H.L., 2018. Prickle1 regulates differentiation of frontal bone osteoblasts. Sci Rep 8, 18021.

Wang, B., Fallon, J.F., Beachy, P.A., 2000. Hedgehog-regulated processing of Gli3 produces an anterior/posterior repressor gradient in the developing vertebrate limb. Cell 100, 423-434.
Wang, C., Pan, Y., Wang, B., 2010. Suppressor of fused and Spop regulate the stability, processing and function of Gli2 and Gli3 full-length activators but not their repressors. Development 137, 2001-2009.
Wang, L., Dynlacht, B.D., 2018. The regulation of cilium assembly and disassembly in development and disease. Development 145.
Watt, F.M., 2004. Unexpected Hedgehog-Wnt interactions in epithelial differentiation. Trends Mol Med 10, 577-580.
Wen, X., Lai, C.K., Evangelista, M., Hongo, J.A., de Sauvage, F.J., Scales, S.J., 2010. Kinetics of hedgehog-dependent full-length Gli3 accumulation in primary cilia and subsequent degradation. Mol Cell Biol 30, 1910-1922.
Wheatley, D.N., 1972. Cilia in cell-cultured fibroblasts. IV. Variation within the mouse 3T6 fibroblastic cell line. J Anat 113, 83-93.
White, J., Mazzeu, J.F., Hoischen, A., Jhangiani, S.N., Gambin, T., Alcino, M.C., Penney, S., Saraiva, J.M., Hove, H., Skovby, F., Kayserili, H., Estrella, E., Vulto-van Silfhout, A.T., Steehouwer, M., Muzny, D.M., Sutton, V.R., Gibbs, R.A., Baylor-Hopkins Center for Mendelian, G., Lupski, J.R., Brunner, H.G., van Bon, B.W., Carvalho, C.M., 2015. DVL1 frameshift mutations clustering in the penultimate exon cause autosomal-dominant Robinow syndrome. Am J Hum Genet 96, 612-622.
White, J.J., Mazzeu, J.F., Coban-Akdemir, Z., Bayram, Y., Bahrambeigi, V., Hoischen, A., van Bon, B.W.M., Gezdirici, A., Gulec, E.Y., Ramond, F., Touraine, R., Thevenon, J., Shinawi, M., Beaver, E., Heeley, J., Hoover-Fong, J., Durmaz, C.D., Karabulut, H.G., Marzioglu-Ozdemir, E., Cayir, A., Duz, M.B., Seven, M., Price, S., Ferreira, B.M., Vianna-Morgante, A.M., Ellard, S., Parrish, A., Stals, K., Flores-Daboub, J., Jhangiani, S.N., Gibbs, R.A., Brunner, H.G., Sutton, V.R., Lupski, J.R., Carvalho, C.M.B., 2018. WNT Signaling Perturbations Underlie the Genetic Heterogeneity of Robinow Syndrome. Am J Hum Genet 102, 27-43.
White, J.J., Mazzeu, J.F., Hoischen, A., Bayram, Y., Withers, M., Gezdirici, A., Kimonis, V., Steehouwer, M., Jhangiani, S.N., Muzny, D.M., Gibbs, R.A., van Bon, B.W.M., Sutton, V.R., Lupski, J.R., Brunner, H.G., Carvalho, C.M.B., 2016. DVL3 Alleles Resulting in a -1 Frameshift of the Last Exon Mediate Autosomal-Dominant Robinow Syndrome. Am J Hum Genet 98, 553-561.
Wilson, N.H., Stoeckli, E.T., 2012. Sonic Hedgehog regulates Wnt activity during neural circuit formation. Vitam Horm 88, 173-209.
Wingfield, J.L., Mengoni, I., Bomberger, H., Jiang, Y.Y., Walsh, J.D., Brown, J.M., Picariello, T., Cochran, D.A., Zhu, B., Pan, J., Eggenschwiler, J., Gaertig, J., Witman, G.B., Kner, P., Lechtreck, K., 2017. IFT trains in different stages of assembly queue at the ciliary base for consecutive release into the cilium. Elife 6.
Wong, L.L., Adler, P.N., 1993. Tissue polarity genes of Drosophila regulate the subcellular location for prehair initiation in pupal wing cells. J Cell Biol 123, 209-221.
Wu, X., Ding, S., Ding, Q., Gray, N.S., Schultz, P.G., 2002. A small molecule with osteogenesis-inducing activity in multipotent mesenchymal progenitor cells. J Am Chem Soc 124, 14520-14521.
Yamaguchi, T.P., Bradley, A., McMahon, A.P., Jones, S., 1999. A Wnt5a pathway underlies outgrowth of multiple structures in the vertebrate embryo. Development 126, 1211-1223.
Yang, H., Cong, W.N., Yoon, J.S., Egan, J.M., 2015. Vismodegib, an antagonist of hedgehog signaling, directly alters taste molecular signaling in taste buds. Cancer Med 4, 245-252.

Yang, T., Bassuk, A.G., Fritzsch, B., 2013. Prickle1 stunts limb growth through alteration of cell polarity and gene expression. Dev Dyn 242, 1293-1306.
Yang, T., Jia, Z., Bryant-Pike, W., Chandrasekhar, A., Murray, J.C., Fritzsch, B., Bassuk, A.G., 2014. Analysis of PRICKLE1 in human cleft palate and mouse development demonstrates rare and common variants involved in human malformations. Mol Genet Genomic Med 2, 138-151.
Yang, Y., Mlodzik, M., 2015. Wnt-Frizzled/planar cell polarity signaling: cellular orientation by facing the wind (Wnt). Annu Rev Cell Dev Biol 31, 623-646.
Zeng, H., Hoover, A.N., Liu, A., 2010. PCP effector gene Inturned is an important regulator of cilia formation and embryonic development in mammals. Dev Biol 339, 418-428.
Zhang, C., Zhang, S., Sun, Y., 2019. Expression of IFT140 During Bone Development. J Histochem Cytochem 67, 723-734.
Zhang, S., Wang, C., Xie, C., Lai, Y., Wu, D., Gan, G., Chen, W., 2017. Disruption of Hedgehog Signaling by Vismodegib Leads to Cleft Palate and Delayed Osteogenesis in Experimental Design. J Craniofac Surg 28, 1607-1614.
Zhang, W., Taylor, S.P., Nevarez, L., Lachman, R.S., Nickerson, D.A., Bamshad, M., Krakow, D., Cohn, D.H., 2016. IFT52 mutations destabilize anterograde complex assembly, disrupt ciliogenesis and result in short rib polydactyly syndrome. Hum Mol Genet 25, 4012-4020.
Zilkha-Falb, R., Gurevich, M., Hanael, E., Achiron, A., 2017. Prickle1 as positive regulator of oligodendrocyte differentiation. Neuroscience 364, 107-121.
National Organization for Rare Disorders, Robinow Syndrome, 2017, Available from: https://rarediseases.org/rare-diseases/robinow-syndrome/. Consulted on May 20, 2020.